Supporting Information

Diastereoselective Formation of Homochiral Flexible Perylene Bisimide Cyclophanes and their Hybrids with Fullerenes

Iris Solymosi,[a]# Swathi Krishna,[b]# Edurne Nuin,[c] Harald Maid,[a] Barbara Scholz,[a] Dirk M. Guldi,[b] M. Eugenia Pérez-Ojeda*[a] and Andreas Hirsch*[a]

[a] I. Solymosi, H. Maid, B. Scholz, Dr. M. E. Pérez-Ojeda, Prof. Dr. A. Hirsch
Department of Chemistry and Pharmacy
Friedrich-Alexander-University Erlangen-Nuremberg
Nikolaus-Fiebiger-Straße 10
91058 Erlangen (Germany)
E-mail: eugenia.perez-ojeda@fau.de, andreas.hirsch@fau.de

[b] S. Krishna, Prof. Dr. D. M. Guldi
Department of Chemistry and Pharmacy
Friedrich-Alexander-University Erlangen-Nuremberg
Egerlandstraße 3
91058 Erlangen (Germany)
E-mail: dirk.guldi@fau.de

[c] Dr. E. Nuin
Instituto de Ciencia Molecular (ICMol)
Universidad de Valencia
Catedrático José Beltrán 2
Paterna 46980 (Spain)

# These authors contributed equally

Table of contents

1. Materials and Methods

General: All chemicals and HPLC solvents were purchased from chemical suppliers and were used as received without further purification. C_{60} (99.0%) was purchased from IoLiTec nanomaterials. All analytical-reagent grade solvents were purified by distillation with a rotary evaporator. Reactions were monitored by thin layer chromatography on silica gel 60 F254 0.2 mm on aluminium foil (Merck). Detection of the compounds was accomplished by means of a UV-lamp (254 nm or 366 nm). For column chromatography silica gel 60 M (230 - 400 mesh ASTM, 0.04 - 0.063 mm) from Marcherey-Nagel & Co. KG was used. Size exclusion chromatography was performed with polystyrene gel of the type S-X1 with a dry mesh size of 28-74 μ, marketed by Bio-Rad Laboratories.

UV/Vis-NIR Spectroscopy:

UV-vis absorption spectroscopy was performed using UV WinLab software on PerkinElmer Lambda 2 dual beam absorption spectrophotometer, with a scan rate of 480 nm/min. The samples were measured in a 10 mm×10 mm quartz cuvette.

Fluorescence Spectroscopy:

Steady-state emission spectra were obtained using Horiba Jobin Yvon FluoroMax-3 emission spectrometer, with a slit width of 3 nm and an integration time of 0.1 s in the wavelength range of 525 – 850 nm. The data were processed in FluorEssence software. The samples were measured in a 10 mm×10 mm quartz cuvette. Quantum yields of the samples were calculated following the relative method using Rhodamine B in ethanol ($\phi = 0.70$) as reference. $^1O_2$ quantum yield measurements were performed on FluoroLog3 spectrometer (Horiba) with Symphony II detector in the NIR detection range. The samples were purged with oxygen for 20 -30 mins. Quantum yields were calculated using C_{60} in air-equilibrated toluene ($\Phi_\Delta^{ref} = 0.98 \pm 0.05$) as reference.

Spectroelectrochemistry:

Spectroelectrochemistry was performed using a PGSTAT101 Autolab potentiostat and AvaSpec spectrometer. A three-electrode setup comprising a Pt-gauze as working electrode, a Pt-wire as counter electrode and a silver wire as a reference electrode was used. 0.1 M tetrabutylammonium hexafluorophosphate was used as supporting electrolyte. The data were recorded with NOVA 1.10 software.

Transient absorption spectroscopy:

Femtosecond and nanosecond transient absorption spectroscopy measurements were performed using the pump/probe systems HELIOS (0 to 5500 ps) and EOS (1 ns to 350 μs) from Ultrafast Systems.

The laser source was CPA2101 and 2110 Ti:Sapphire amplifier (775 nm output, 1 kHz repetition rate, 150 fs pulse width; 500 nJ excitation laser energy) from Clark-MXR Inc. The desired excitation pulse of 550 nm was generated with NOPA. The white light for the femtosecond experiments was generated using a Sapphire crystal. The white light for the nanosecond transient measurements came from a supercontinuum laser source (2 kHz repetition rate, 1 ns pulsewidth). Samples were taken in 2 x 10 mm optical glass cuvettes and purged with argon for 20 min. Optical densities (OD) of the samples were around 0.4 at the excitation wavelength. Global analyses of the resulting data were performed with the GloTarAn software.[1]

FTIR-ATR Spectroscopy: The FTIR-ATR spectra were obtained on a Bruker Tensor 27, Pike MIRacleTM ATR, Pike Technologies as well as on a ThermoFisher Scientific Nicolet iS5. The spectra were measured as pure solids or liquids and absorptions are given in wavenumbers $\tilde{\nu}$ (cm^{-1}).

Analytical HPLC: Analytical HPLC was carried out in a LC20-AT prominence liquid chromatograph, SHIMADZU CORPORATION, Analytical Instruments Division, Kyoto, Japan using a Nucleosil Column (EC250/4 Nucleosil 100-5) from Macherey-Nagel and 150 uL injection volume. Before the injection, small aliquots of the reaction mixture (0.2 mL) were filtered through silica to avoid the possible blocking of the employed column due to the polymers formed in the reaction mixture. All chromatograms were processed with SHIMADZU LabSolution software and exported as ASCII files. The chromatograms are depicted at a wavelength of λ = 280 nm or λ = 530 nm and the following solvent gradient was used: CH_2Cl_2:ethyl acetate:MeOH 1:0:0 → 75:20:5.

NMR Spectroscopy: NMR spectra were recorded on a BRUKER Avance 600 (^{1}H: 600 MHz, ^{13}C: 151 MHz), BRUKER Avance 500 (^{1}H: 500 MHz, ^{13}C: 125 MHz), BRUKER Avance 400 (^{1}H: 400 MHz, ^{13}C: 101 MHz) spectrometers. Chemical shifts are given in ppm, referenced to residual solvent signals and reported relative to external $SiMe_4$. Chloroform-d1 (99.8%) and 1,1,2,2-tetrachloroethane-d2 (99.5%) were purchased from Sigma Aldrich and were used as received without further purification. The resonance multiplicities are indicated as s (singlet), d (doublet), t (triplet) and m (multiplet).

Mass spectrometry: Spectra were recorded on BRUKER microTOF II focus (BRUKER Daltonik GmbH) and SHIMADZU Axima Confidence maXis 4G instruments (Nitrogen UV laser, 50 Hz, 337 nm). MALDI-TOF HRMS were recorded on a Bruker UltrafleXtreme TOF/TOF and trans-2-[3-(4-tert-butylphenyl)-2-methyl-propenylidene]malonitrile (DCTB) and 2,5-dihydroxy-benzoic acid (DHB) were used as matrices. The APPI mass spectra were obtained on Bruker maXis 4G TOF-mass spectrometer. ESI mass spectra were recorded on BRUKER microTOF II focus ESI-TOF spectrometer.

2. Synthesis

Synthesis of cyclophane **P2**

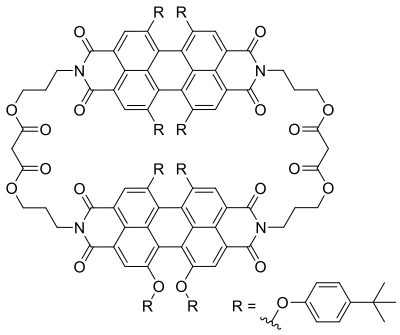

P2

Experiment F: Pyridine anhydrous (18.7 mg, 19.2 µL, 237 µmol, 4 eq.) was added to a solution of compound **1** (130 mg, 118 µmol, 2 eq.) and tetrathiafulvalene (12.5 mg, 61.1 µmol, 97% purity, 1 eq.) in CH_2Cl_2 anhydrous (225 mL). To the stirred reaction mixture, malonyl dichloride (17.2 mg, 11.9 µL, 122 µmol, 97% purity, 2 eq.) in CH_2Cl_2 anhydrous (5 mL) was added with an automatic syringe pump within 3 h. After 29 h, 47 h and 51 h the previously described addition of malonyl dichloride was repeated three times. In total the solution was stirred at rt for 3 d. Afterwards, the solvent was removed under vacuum without drying completely and the crude product solution was separated by size exclusion chromatography (Biobeads S-X1, dry mesh size: 28-74 µ, CH_2Cl_2). The fractions containing compound **P2** (as indicated by TLC) were purified by column chromatography (SiO_2, CH_2Cl_2:ethyl acetate, 1:0 -> 99:1). The mixed fractions containing compound **P2** were further purified by column chromatography (SiO_2, CH_2Cl_2:ethyl acetate, 1:0 -> 90:10) to obtain **P2** (11.2 mg, 4.80 µmol, 8.1%) as dark purple solid.

TLC (Hexane:ethyl acetate, 3:1): R_f = 0.22.

^{1}H NMR (500 MHz, $C_2D_2Cl_4$, 90 °C): δ = 7.84 (s, 8H, CH_{PBI}), 7.16 – 7.10 (m, 16H, C$H_{phenoxy}$), 6.75 – 6.66 (m, 16H, C$H_{phenoxy}$), 4.19 – 4.08 (m, 8H, CH_2), 4.07 – 3.90 (m, 8H, CH_2), 3.21 (bs, 4H, OCCH_2CO), 2.01 – 1.82 (m, 8H, CH_2), 1.26 ppm (s, 72H, CH_3).

^{13}C NMR (126 MHz, $C_2D_2Cl_4$, 90 °C): δ = 166.30 (4C, O-*C*=*O*), 163.08 (8C, N-*C*=O), 155.91 (8C, *C*-O), 153.33 (8C, $C_{phenoxy}$-O), 147.56 (8C, $C_{phenoxy}$), 132.77 (4C, C_{PBI}), 126.60 (16C, H$C_{phenoxy}$), 122.24 (8C, C_{PBI}), 120.69 (8C, C_{PBI}), 120.19 (8C, HC_{PBI}), 119.55 (16C, H$C_{phenoxy}$), 119.44 (4C, C_{PBI}), 63.65 (4C, CH_2), 42.12 (2C, O=CCH_2C=O), 38.04 (4C, CH_2), 34.48 (8C, $C(CH_3)_3$), 31.70 (24C, CH_3), 27.46 ppm (4C, CH_2).

HRMS (APPI): *m/z* calcd for $[C_{146}H_{140}N_4O_{24}]^+$ 2332.9852, found: 2332.9897.

IR (ATR, rt): $\tilde{\nu}$ = 2958, 2924, 2853, 1732, 1694, 1659, 1584, 1505, 1459, 1292, 1260, 1217, 1152, 1091, 1016, 799, 745, 700 cm^{-1}.

UV-vis (CH_2Cl_2): ε (λ_{max}) = 18143 (536), 15833 (576) $M^{-1}\cdot cm^{-1}$ (nm).

Synthesis of cyclophane **P3**

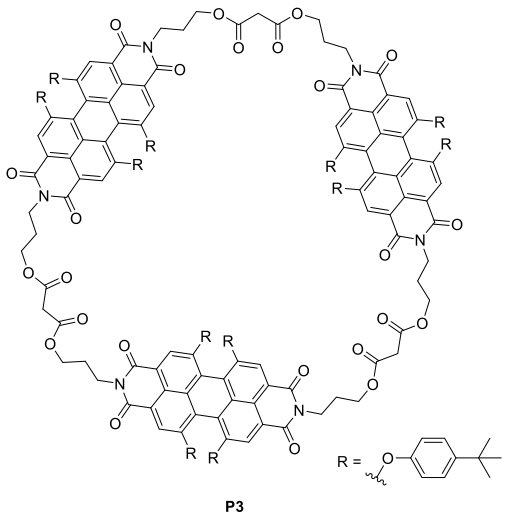

P3

Pyridine anhydrous (28.8 mg, 29.5 µL, 364 µmol, 2 eq.) was added to a solution of compound **1** (200 mg, 182 µmol, 1 eq.) in CH_2Cl_2 anhydrous (250 mL). Malonyl dichloride (25.6 mg, 17.7 µL, 182 µmol, 1 eq.) in CH_2Cl_2 anhydrous (24 mL) was added dropwise with a dropping funnel. The solution was stirred at rt for 5 d. Afterwards, the solvent was removed under vacuum without drying completely and the crude product solution was separated by size exclusion chromatography (Biobeads S-X1, dry mesh size: 28-74 µ, CH_2Cl_2). The fractions containing **P3** (as indicated by TLC) were purified by column chromatography (SiO_2, CH_2Cl_2:ethyl acetate:methanol, 1:0:0 -> 6:0:1) to yield compound **P3** (7.29 mg, 2.08 µmol, 3.4%) as purple solid.

TLC (Hexane:ethyl acetate, 3:1): R_f = 0.17.

^{1}H NMR (500 MHz, $C_2D_2Cl_4$, 60 °C): δ = 8.11 (s, 12H, CH_{PBI}), 7.14 – 7.10 (m, 24H, C$H_{phenoxy}$), 6.77 – 6.72 (m, 24H, C$H_{phenoxy}$), 4.11 – 4.05 (m, 24H, CH_2), 3.20 (s, 6H, OCCH_2CO), 1.98 – 1.91 (m, 12H, CH_2), 1.18 ppm (s, 108H, CH_3).

^{13}C NMR (126 MHz, $C_2D_2Cl_4$, 60 °C): δ = 166.55 (6C, O-*C*=*O*), 163.55 (12C, N-*C*=O), 156.20 (12C, *C*-O), 153.07 (12C, $C_{phenoxy}$-O), 147.62 (12C, $C_{phenoxy}$), 133.14 (6C, C_{PBI}), 126.81 (24C, H$C_{phenoxy}$), 122.45 (12C, C_{PBI}), 120.97 (12C, C_{PBI}), 120.24 (12C, C_{PBI}), 119.66 (6C, C_{PBI}), 119.50 (24C, H$C_{phenoxy}$), 63.83 (6C, CH_2), 41.55 (3C, O=CCH_2C=O), 37.86 (6C, CH_2), 34.47 (12C, $C(CH_3)_3$), 31.68 (36C, CH_3), 27.60 ppm (6C, CH_2).

HRMS (MALDI-TOF, dctb): *m/z* calcd for $[C_{219}H_{210}N_6O_{36}]^+$ 3499.4781, found: 3499.4762.

IR (ATR, rt): $\tilde{\nu}$ = 2965, 2364, 2343, 1753, 1699, 1662, 1589, 1505, 1440, 1412, 1288, 1217, 1174, 697, 668, 643, 633 cm^{-1}.

UV-vis (CH_2Cl_2): ε (λ_{max}) = 75823 (539), 104860 (579) $M^{-1}\cdot cm^{-1}$ (nm).

Synthesis of cyclophane **P4**

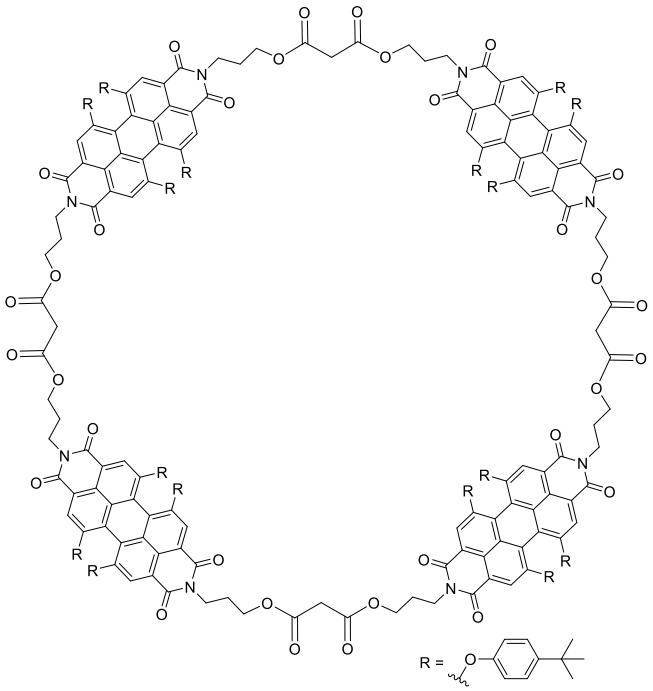

P4

The reaction conditions and the purification by size exclusion and column chromatography are as described for compound **P3**. The fraction containing most of compound **P4** (as indicated by TLC) was further purified by preparative TLC (CH_2Cl_2:ethyl acetate 98:2) and subsequently purified by column chromatography (SiO_2, hexane:ethyl acetate:CH_2Cl_2, 4:1:0 -> 0:1:9) to yield **P4** (2.70 mg, 578 nmol, 1.3%) as purple solid.

TLC (Hexane:ethyl acetate, 3:1): R_f = 0.10.

^{1}H NMR (400 MHz, $CDCl_3$, rt): δ = 8.08 (s, 16H, CH_{PBI}), 7.19 – 7.15 (m, 32H, C$H_{phenoxy}$), 6.78 – 6.72 (m, 32H, C$H_{phenoxy}$), 4.19 – 4.09 (m, 32H, CH_2), 3.31 (bs, 8H, OCCH_2CO), 1.99 – 1.94 (m, 16H, CH_2), 1.26 ppm (s, 144H, CH_3).

DEPTQ NMR (151 MHz, $CDCl_3$, rt): δ = 166.55 (8C, O-*C*=*O*), 163.33 (16C, N-*C*=O), 155.95 (16C, *C*-O), 153.03 (16C, $C_{phenoxy}$-O), 147.30 (16C, $C_{phenoxy}$), 132.88 (8C, C_{PBI}), 126.71 (32C, H$C_{phenoxy}$), 122.24 (16C, C_{PBI}), 120.68 (16C, C_{PBI}), 120.10 (16C, HC_{PBI}), 119.48 (8C, C_{PBI}), 119.37 (32C, H$C_{phenoxy}$), 63.49 (8C, CH_2), 41.54 (4C, O=CCH_2C=O), 37.66 (8C, CH_2), 34.48 (16C, $C(CH_3)_3$), 31.59 (48C, CH_3), 27.33 ppm (8C, CH_2).

HRMS (MALDI-TOF, dctb): *m/z* calcd for $[C_{292}H_{280}N_8O_{48}]^+$ 4665.9710, found: 4665.9701.

IR (ATR, rt): $\tilde{\nu}$ = 2957, 2920, 2851, 1738, 1697, 1657, 1587, 1503, 1409, 1338, 1288, 1217, 1171, 1015, 887, 837, 802 cm^{-1}.

UV-vis (CH_2Cl_2): ε (λ_{max}) = 58960 (540), 71264 (580) $M^{-1}\cdot cm^{-1}$ (nm).

Synthesis of model compound **P1**

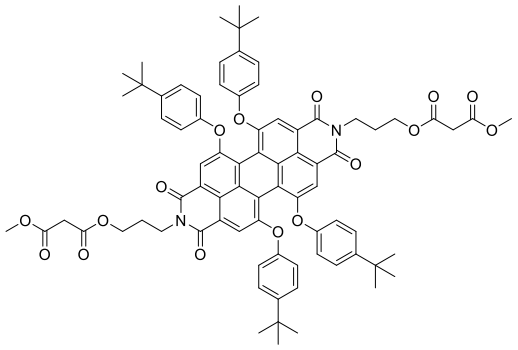

P1

To a solution of **1** (200 mg, 0.1819 mmol, 1 eq.) in anhydrous CH_2Cl_2 (100 mL) pyridine (122.3 mg, 1.546 mmol, 8.5 eq.) was added under inert atmosphere. The mixture was cooled in an ice bath for 10 min. Methyl malonyl chloride (99.3 mg, 728 µmol, 97% purity, 4 eq.) was added dropwise over 5 min. The reaction was warmed to rt and stirred overnight. The crude was washed with aq. HCl (40 mL), water (40 mL) and two times with brine (2x 40 mL). The combined organic layers were dried over $MgSO_4$ and the solvent was removed under vacuum. The solid was rotated onto SiO_2 and purified by column chromatography three times (SiO_2, 1. CH_2Cl_2:EA 100:0 -> 98:2, 2. CH_2Cl_2:EA 100:0 -> 97:3, 3. CH_2Cl_2:Hex:THF 80:40:0 -> 80:20:5) to yield PBI **P1** (140.2 mg, 108 µmol, 59%) as a purple solid.

TLC (CH_2Cl_2:ethyl acetate 98:2): R_f = 0.71.

^{1}H NMR (400 MHz, $CDCl_3$, rt): δ = 8.22 (s, 4H, CH_{PBI}), 7.25 – 7.21 (m, 8H, C$H_{phenoxy}$), 6.84 – 6.80 (m, 8H, C$H_{phenoxy}$), 4.23 (t, J= 6.4 Hz, 8H, NCH_2/OCH_2), 3.70 (s, 6H, OCH_3), 3.36 (s, 4H, COCH_2CO), 2.10 – 2.02 (m, 4H, CH_2), 1.29 ppm (s, 36H, CH_3).

^{13}C NMR (101 MHz, $CDCl_3$, rt): δ = 167.03 (2C, O-*C*=O), 166.59 (2C, O-*C*=O), 163.54 (4C, N-*C*=O), 156.15 (4C, *C*-O), 153.00 (4C, $C_{phenoxy}$-O), 147.52 (4C, $C_{phenoxy}$), 133.06 (2C, C_{PBI}), 126.84 (2, 8C, H$C_{phenoxy}$), 122.41 (4C, C_{PBI}), 120.78 (4C, C_{PBI}), 120.14 (4C, HC_{PBI}), 119.59 (2C, C_{PBI}), 119.46 (8C, H$C_{phenoxy}$), 63.55 (2C, O-*C*H_2), 52.65 (2C, O-*C*H_3), 41.41 (2C, CO*C*CO), 37.69 (2C, N-*C*H_2), 34.53 (4C, *C*(CH_3)$_3$), 31.60 (12C, *C*H_3), 27.41 ppm (2C, *C*H_2).

HRMS (MALDI-TOF, dctb): *m/z* calcd for $[C_{78}H_{78}N_2O_{16}]^+$ 1298.5346, found: 1298.5364.

IR (ATR, rt): $\tilde{\nu}$ = 2958, 2928, 2866, 1757, 1737, 1693, 1655, 1585, 1504, 1437, 1412, 1358, 1337, 1311, 1287, 1217, 1170 cm^{-1}.

UV-vis (DCM): ε (λ_{max}) = 24 823 (541), 40 558 (580) $M^{-1}\cdot cm^{-1}$ (nm).

Synthesis of model compound **P1F2$_{Et}$**

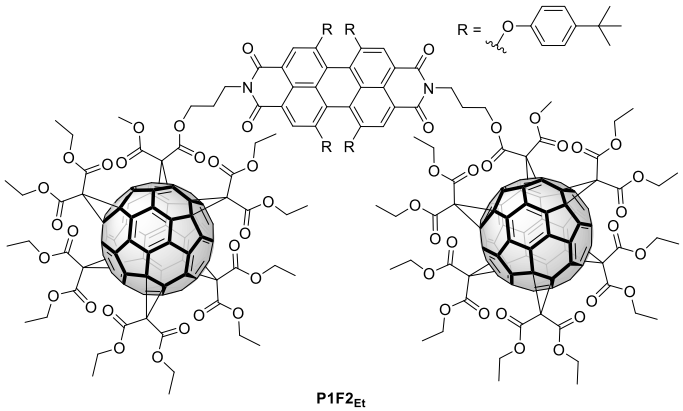

Pentakisadduct **F$_{Et}$** (34.9 mg, 23.1 µmol, 3 eq.) was dissolved in CH_2Cl_2 anhydrous (15 mL) together with PBI derivative **P1** (10.0 mg, 7.70 µmol, 1 eq.) and CBr_4 (5.62 mg, 16.9 µmol, 2.2 eq.). After stirring at rt for 15 min under inert atmosphere, P_1-*t*Bu (4.09 mg, 4.35 µL, 17.5 µmol, 97% purity, 2.2 eq.) was added and the mixture was stirred for additional 30 min. Then the solvent was removed under vacuum without drying completely and the crude was plug-filtered (SiO_2, CH_2Cl_2:ethyl acetate:methanol, 1:0:0 -> 95:0:5). After purification by column chromatography (SiO_2, CH_2Cl_2:ethyl acetate, 1:0 -> 95:5) model compound **P1F2$_{Et}$** (20.7 mg, 4.79 µmol, 62%) was obtained as purple solid.

TLC (CH_2Cl_2:ethyl acetate, 99:1): R_f = 0.18.

^{1}H NMR (400 MHz, $CDCl_3$, rt): δ = 8.21 (s, 4H, CH_{PBI}), 7.25 – 7.21 (m, 8H, C$H_{phenoxy}$), 6.86 – 6.78 (m, 8H, C$H_{phenoxy}$), 4.32 (m, 40H, CH_2 / 4H, CH_2), 4.26 – 4.19 (m, 4H, CH_2), 3.87 (s, 6H, OCH_3), 2.16 – 2.04 (m, 4H, CH_2), 1.36 – 1.27 ppm (m, 60H, CH_3 / 36H, CH_3).

^{13}C NMR (151 MHz, $CDCl_3$, rt): δ = 164.37 (2C, O-*C*=O), 163.99, 163.98, 163.96, 163.93, 163.91, 163.85 (22C, *C*O), 163.46 (4C, N-*C*=O), 156.10 (4C, *C*-O), 153.01 (4C, $C_{phenoxy}$-O), 147.44 (4C, $C_{phenoxy}$), 146.05, 145.99, 145.97, 145.93, 145.91, 145.84, 145.82, 145.77, 141.34, 141.32, 141.30, 141.27, 141.21, 141.00 (96C, C_{60}-sp^2), 133.07 (2C, C_{PBI}), 126.82 (8C, H$C_{phenoxy}$), 122.43 (4C, C_{PBI}), 120.79 (4C, C_{PBI}), 120.14 (4C, HC_{PBI}), 119.63 (2C, C_{PBI}), 119.45 (8C, H$C_{phenoxy}$), 69.22, 69.21, 69.20, 69.18, 69.17 (24C, C_{60}-sp^3), 64.96 (2C, O-CH_2), 62.99, 62.96 (20C, CH_2), 53.95 (2C, CH_3), 53.57, 45.53, 45.49, 45.29 (12C, CO*C*CO), 37.54 (2C, NCH_2), 34.53 (4C, *C*(CH_3)$_3$), 31.61 (12C, CH_3), 27.49 (2C, CH_2), 14.28, 14.20 ppm (20C, CH_3).

HRMS (MALDI-TOF, dctb): *m/z* calcd for $[C_{268}H_{174}N_2NaO_{56}]^+$ 4338.0721, found: 4338.0825.

IR (ATR, rt): ṽ [cm^{-1}] = 2957, 2922, 2851, 1744, 1697, 1260, 1209, 1173, 1076, 1040, 1015, 802, 729, 714 cm^{-1}.

UV-vis (CH_2Cl_2): ε (λ_{max}) = 23374 (541), 38138 (580) $M^{-1}\cdot cm^{-1}$ (nm).

Synthesis of functional hybrid **P2F2$_{Et}$**

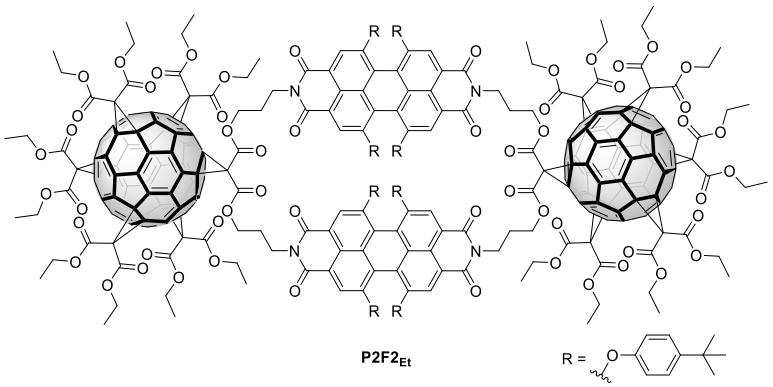

Cyclophane **P2** (5.00 mg, 2.14 µmol, 1 eq.), pentakisadduct **F$_{Et}$** (9.71 mg, 6.42 µmol, 3 eq.) and CBr_4 (1.56 mg, 4.71 µmol, 2.2 eq.) were dissolved in CH_2Cl_2 anhydrous (4.20 mL) under inert atmosphere. The solution was stirred for 10 min at rt. P_1-*t*Bu (1.14 mg, 1.21 µL, 4.86 µmol, 97% purity, 2.2 eq.) was added and the mixture was stirred at rt. After 40 min more pentakisadduct **F$_{Et}$** (4.86 mg, 3.21 µmol, 1.5 eq.) was added. After stirring overnight CBr_4 (780 µg, 2.36 µmol, 1.1 eq.) and P_1-*t*Bu (570 µg, 1.21 µL, 2.43 µmol, 97% purity, 1.1 eq.) dissolved in CH_2Cl_2 anhydrous (1.00 mL) were added to complete the reaction. The solution was directly purified by column chromatography (SiO_2, CH_2Cl_2:ethyl acetate, 1:0 -> 90:10) to obtain cyclophane fullerene adduct **P2F2$_{Et}$** (8.00 mg, 1.49 µmol, 70%) as purple solid.

TLC (CH_2Cl_2:ethyl acetate, 99.8:0.2): R_f = 0.12.

^{1}H NMR (400 MHz, $C_2D_2Cl_4$, 90 °C): δ = 7.82 (s, 8H, C*H*$_{PBI}$), 7.15 – 7.10 (m, 16H, C*H*$_{phenoxy}$), 6.77 – 6.64 (m, 16H, C*H*$_{phenoxy}$), 4.43 – 4.25 (m, 8H, C*H*$_2$ / 40H, C*H*$_2$), 4.15 – 4.03 (m, 8H, C*H*$_2$), 2.13 – 1.95 (m, 8H, C*H*$_2$), 1.31 – 1.25 ppm (m, 72H, C*H*$_3$ / 60H, C*H*$_3$).

^{13}C NMR (101 MHz, $C_2D_2Cl_4$, 90 °C): δ = 163.95, 163.92, 163.87, 163.83 (24C, *C*O), 162.98 (8C, N-*C*=O), 153.45 (8C, *C*$_{phenoxy}$-O), 147.54 (8C, *C*$_{phenoxy}$), 146.03, 145.98, 145.94, 145.92, 145.89, 145.84, 141.49, 141.45, 141.41, 141.40, 141.39, 141.35 (96C, C_{60}-sp^2), 132.65 (4C, *C*$_{PBI}$), 126.57 (16C, H*C*$_{phenoxy}$), 122.22 (8C, *C*$_{PBI}$), 120.57 (8C, *C*$_{PBI}$), 120.40 (8C, H*C*$_{PBI}$), 119.61 (16C, H*C*$_{phenoxy}$), 119.37 (4C, *C*$_{PBI}$), 69.78, 69.56 (24C, C_{60}-sp^3), 64.88 (4C, O-*C*H$_2$), 63.22, 63.21 (20C, *C*H$_2$), 46.12, 46.07 (12C, CO*C*CO), 34.48 (8C, *C*(CH$_3$)$_3$), 31.70 (24C, *C*H$_3$), 27.48 (4C, *C*H$_2$), 14.21 ppm (20C, *C*H$_3$).

HRMS (MALDI-TOF, dctb): *m/z* calcd for $[C_{336}H_{236}N_4O_{64}]^+$ 5349.5330, found: 5349.5487.

IR (ATR, rt): $\tilde{\nu}$ = 2959, 2926, 2867, 2854, 1743, 1698, 1660, 1589, 1505, 1263, 1206, 1171, 1076, 1012, 713, 528 cm^{-1}.

UV-vis (CH_2Cl_2): ε (λ_{max}) = 82483 (537), 62564 (575) M^{-1}·cm^{-1} (nm).

Synthesis of functional hybrid **P2F2$_{TEG}$**

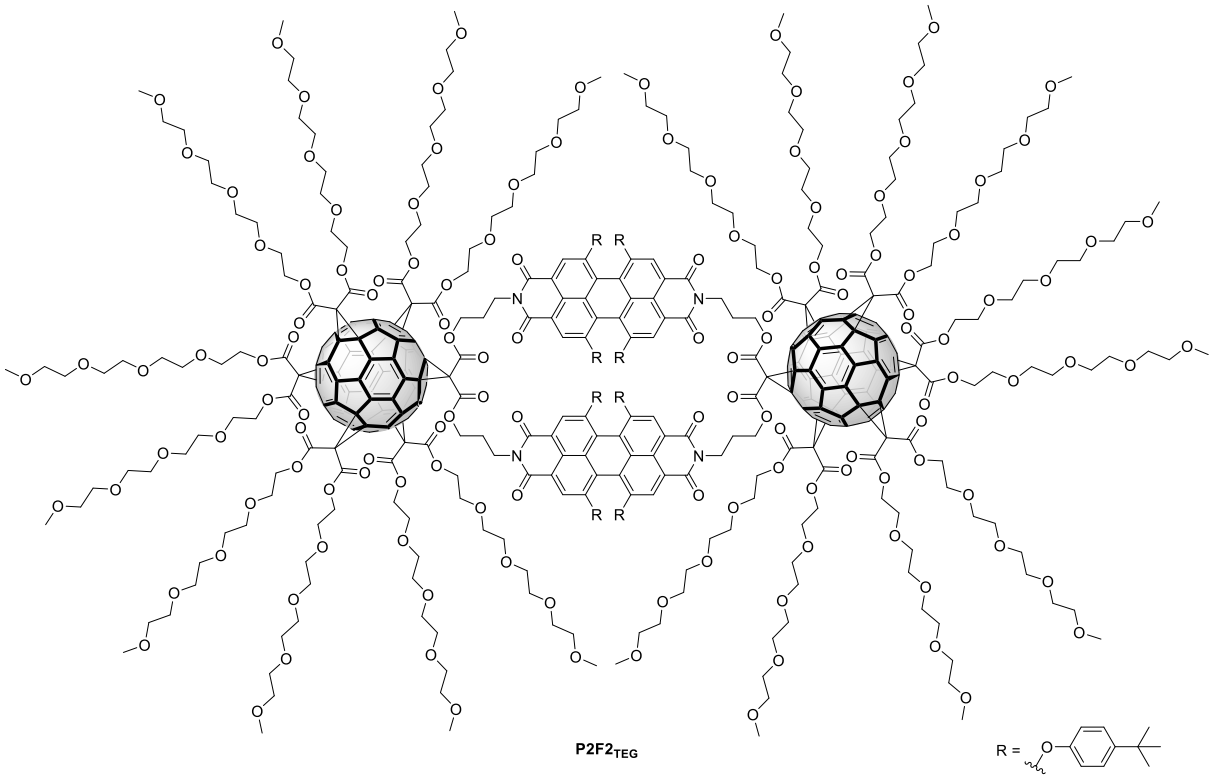

Cyclophane **P2** (5.00 mg, 2.14 µmol, 1 eq.), pentakisadduct **F$_{TEG}$** (20.1 mg, 6.42 µmol, 3 eq.) and CBr_4 (1.56 mg, 4.71 µmol, 2.2 eq.) were dissolved in CH_2Cl_2 anhydrous (4.20 mL). P_1-*t*Bu (1.14 mg, 1.21 µL, 4.86 µmol, 97% purity, 2.2 eq.) was added and the mixture was stirred at rt under inert atmosphere. After 21 h, CBr_4 (780 µg, 2.36 µmol, 1.1 eq.) and P_1-*t*Bu (570 µg, 605 nL, 2.43 µmol, 97% purity, 1.1 eq.) were added to the mixture and stirred for additional 4 d. The process was repeated together with pentakisadduct **F$_{TEG}$** (10.1 mg, 3.21 µmol, 1.5 eq.) and the reaction mixture was stirred for another 6 d. The crude mixture was directly purified by column chromatography (SiO_2, CH_2Cl_2:toluene:methanol, 100:60:15). The mixed fractions containing **P2F2$_{TEG}$** were further purified by four fold column chromatography (SiO_2, 1. CH_2Cl_2:toluene:methanol, 100:60:12 -> 100:60:15, 2. CH_2Cl_2:toluene:methanol, 100:60:8 -> 90:70:25, 3. CH_2Cl_2:toluene:methanol, 90:70:15 -> 100:60:20, 4. CH_2Cl_2:toluene:methanol, 100:60:8 -> 100:60:12). The combined pure fractions yielded cyclophane fullerene adduct **P2F2$_{TEG}$** (5.00 mg, 582 nmol, 27%) as purple viscous oil.

TLC (CH_2Cl_2:toluene:methanol, 100:60:12): R_f = 0.12

^{1}H NMR (500 MHz, $C_2D_2Cl_4$, 110 °C): δ = 7.82 (s, 8H, CH_{PBI}), 7.21 – 7.06 (m, 16H, C$H_{phenoxy}$), 6.83 – 6.60 (m, 16H, C$H_{phenoxy}$), 4.51 – 4.23 (m, 8H, CH_2 / 40H, COOCH_2), 4.16 – 4.06 (m, 8H, CH_2), 3.84 – 3.37 (m, 280H, OCH_2), 3.36 – 3.23 (m, 60H, OCH_3), 2.14 – 2.04 (m, 8H, CH_2), 1.28 ppm (s, 72H, CH_3).

DEPTQ NMR (126 MHz, $C_2D_2Cl_4$, 110 °C): δ = 163.72, 163.68, 163.65, 163.58 (24C, *C*O), 162.93 (8C, N-*C*=O), 155.81 (8C, *C*-O), 153.50 (8C, $C_{phenoxy}$-O), 147.59 (8C, $C_{phenoxy}$), 146.03, 145.99, 145.97, 145.92, 141.33 (96C, C_{60}-sp^2), 132.67 (4C, C_{PBI}), 126.54 (16C, H$C_{phenoxy}$), 122.31 (8C, C_{PBI}), 120.59 (8C, C_{PBI}), 120.40

(8C, HC_{PBI}), 119.62 (16C, H$C_{phenoxy}$), 119.41 (4C, C_{PBI}), 72.28, 70.93, 70.89, 70.83, 70.81, 70.64, 68.76 (140C, OCH_2), 69.54 (24C, C_{60}-sp^3), 66.21 (20C, OCH_2), 58.89 (20C, OCH_3), 53.60, 46.01, 45.99 (12C, CO*C*CO), 34.47 (8C, *C*$(CH_3)_3$), 31.68 ppm (24C, *C*H_3).

HRMS (ESI): *m/z* calcd for $[C_{476}H_{516}N_4Na_4O_{144}]^{4+}$ 2170.8187, found: 2170.8206.

IR (ATR, rt): $\tilde{\nu}$ = 2953, 2920, 2868, 2853, 1742, 1698, 1505, 1350, 1282, 1258, 1214, 1171, 1093, 1025, 1016, 942, 872, 841, 803, 714, 551, 528 cm^{-1}.

UV-vis (CH_2Cl_2): ε (λ_{max}) = 76456 (537), 57932 (575) $M^{-1}\cdot cm^{-1}$ (nm).

Synthesis of side product **P2F1$_{TEG}$**

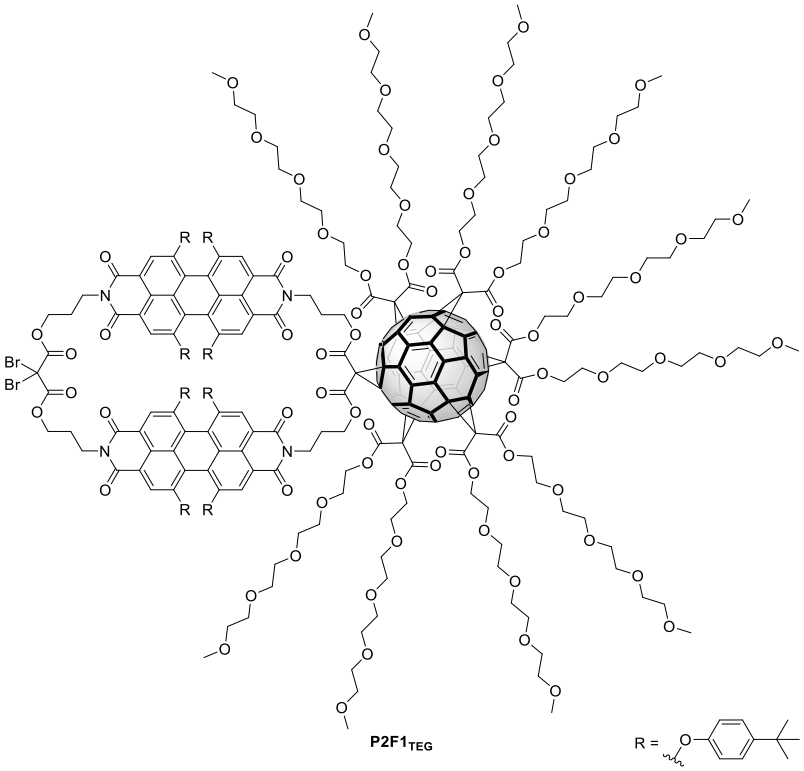

Cyclophane **P2** (5.00 mg, 2.14 µmol, 1 eq.), pentakisadduct **F$_{TEG}$** (20.1 mg, 6.42 µmol, 3 eq.) and CBr_4 (1.56 mg, 4.71 µmol, 2.2 eq.) were dissolved in CH_2Cl_2 anhydrous (4.20 mL). P_1-*t*Bu (1.14 mg, 1.21 µL, 4.86 µmol, 97% purity, 2.2 eq.) was added and the mixture was stirred at rt under inert atmosphere. After 80 min, another portion of CBr_4 (2.2 eq.) and P_1-*t*Bu (2.2 eq.) were added and the mixture was stirred for additional 100 min. The crude solution was directly purified by column chromatography (SiO_2, CH_2Cl_2:toluene:methanol, 100:60:12 -> 100:60:20) to obtain compound **P2F1$_{TEG}$** (4.50 mg, 800 nmol, 37%) as purple viscous oil.

TLC (CH_2Cl_2:toluene:methanol, 100:60:12): R_f = 0.19

^{1}H NMR (500 MHz, $C_2D_2Cl_4$, 110 °C): δ = 7.84 (s, 4H, CH_{PBI}), 7.80 (s, 4H, CH_{PBI}), 7.18 – 7.10 (m, 16H, C$H_{phenoxy}$), 6.76 – 6.65 (m, 16H, C$H_{phenoxy}$), 4.50 – 4.28 (m, 8H, CH_2 / 20H, COOCH_2), 4.16 – 4.05 (m, 8H,

CH_2), 3.75 – 3.43 (m, 140H, OCH_2), 3.34 – 3.25 (m, 30H, OCH_3), 2.12 – 1.98 (m, 8H, CH_2), 1.28 ppm (s, 72H, CH_3).

DEPTQ NMR (126 MHz, $C_2D_2Cl_4$, 100 °C): δ = 163.70, 163.67, 163.32, 163.30, 162.99, 162.94 (14C, *C*O), 155.84, 155.82 (8C, *C*-O), 153.45, 153.41 (8C, $C_{phenoxy}$-O), 147.62, 147.60, 147.58 (8C, $C_{phenoxy}$), 146.10, 146.04, 146.00, 145.97, 145.94, 141.33, 141.31 (48C, C_{60}-sp^2), 132.74, 132.65 (4C, C_{PBI}), 126.58 (16C, H$C_{phenoxy}$), 122.17 (8C, C_{PBI}), 120.66 (8C, C_{PBI}), 120.37 (8C, HC_{PBI}), 119.60 (16C, H$C_{phenoxy}$), 119.36 (4C, C_{PBI}), 72.26, 72.24, 70.91, 70.89, 70.87, 70.85, 70.81, 70.80, 70.77, 70.63, 70.61, 68.75 (70C, O*C*H_2), 69.53 (12C, C_{60}-sp^3), 66.22 (10C, OCH_2), 65.09, 65.07, 65.05 (4C, *C*H_2), 58.91 (10C, O*C*H_3), 46.17, 45.92 (12C, CO*C*CO), 37.49, 37.47, 37.44 (4C, *C*H_2), 34.48 (8C, *C*$(CH_3)_3$), 31.67 (24C, *C*H_3), 27.34, 27.32, 27.30 ppm (4C, *C*H_2).

HRMS (ESI): *m/z* calcd for $[C_{311}H_{326}Br_2N_4Na_2O_{84}]^{2+}$ 2831.9756, found: 2831.9770.

IR (ATR, rt): $\tilde{\nu}$ = 2953, 2919, 2868, 2853, 1742, 1698, 1659, 1591, 1343, 1284, 1266, 1212, 1172, 1104, 1038, 1025, 1013, 945, 902, 873, 839, 822, 803, 715, 554, 528 cm^{-1}.

UV-vis (CH_2Cl_2): ε (λ_{max}) = 78287 (537), 60178 (575) $M^{-1}\cdot cm^{-1}$ (nm).

3. HPLC chromatograms

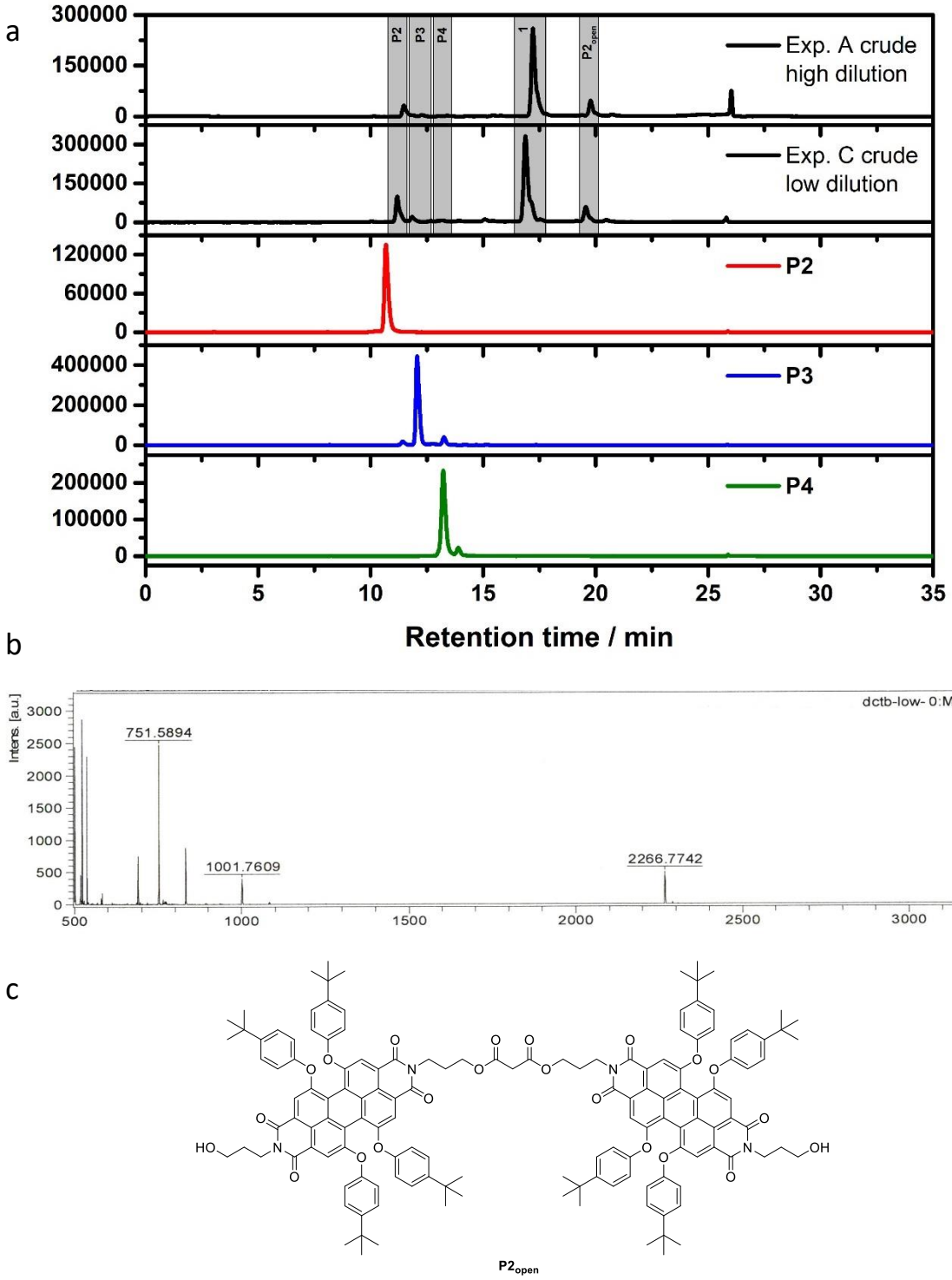

Figure S1. a) HPLC chromatograms of the crude mixtures of experiment A and C as well as the macrocycles **P2**, **P3** and **P4** analysed at a wavelength of 530 nm. b) Corresponding MALDI MS spectrum of **P2$_{open}$**. c) Chemical structure of **P2$_{open}$** with a retention time of approximately 20 min.

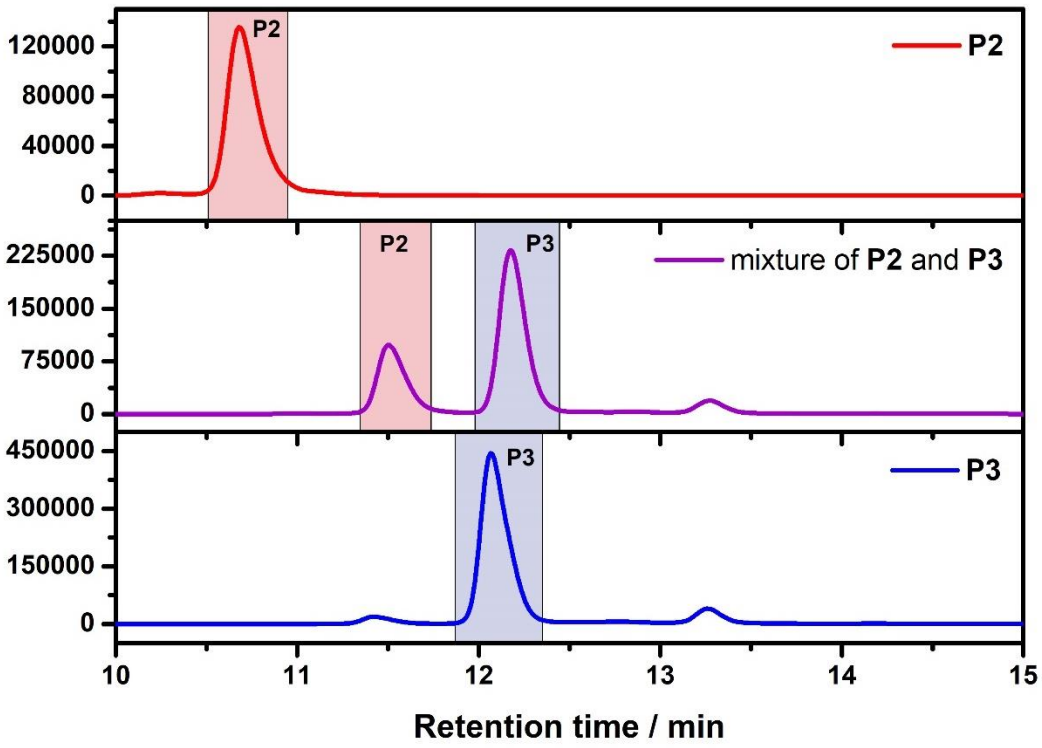

Figure S2. Comparison of the HPLC chromatograms of **P2** (top), **P3** (bottom) and a mixture of both cyclophanes (middle). The retention time of pure **P2** is less than the retention times of the two-membered ring in the different crude mixtures or in a mixture of only **P2** and **P3** (middle). It can be concluded that **P2** interacts with other molecules, which leads to a delay in the retention time.

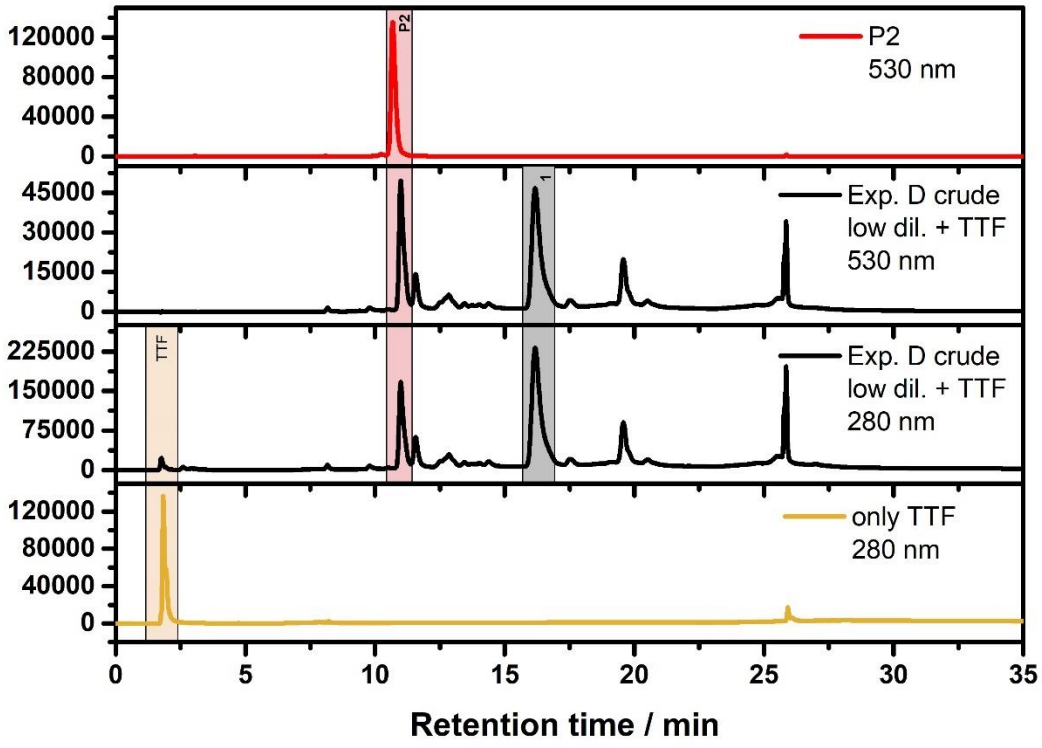

Figure S3. Comparison of the HPLC chromatograms of the crude mixture of experiment D evaluated both in the absorption region of **P2** (530 nm) and TTF (280 nm)**.**

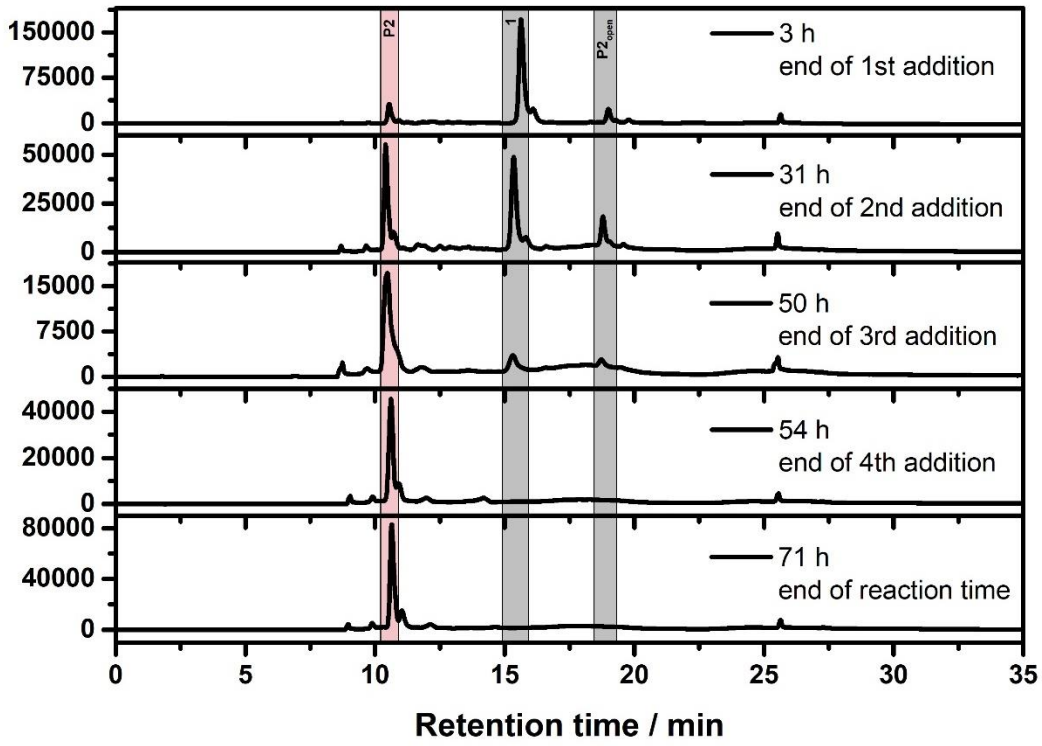

Figure S4. HPLC chromatograms of the crude mixture of experiment E at different times analysed at a wavelength of 530 nm.

4. Temperature-dependent ^{1}H NMR spectra

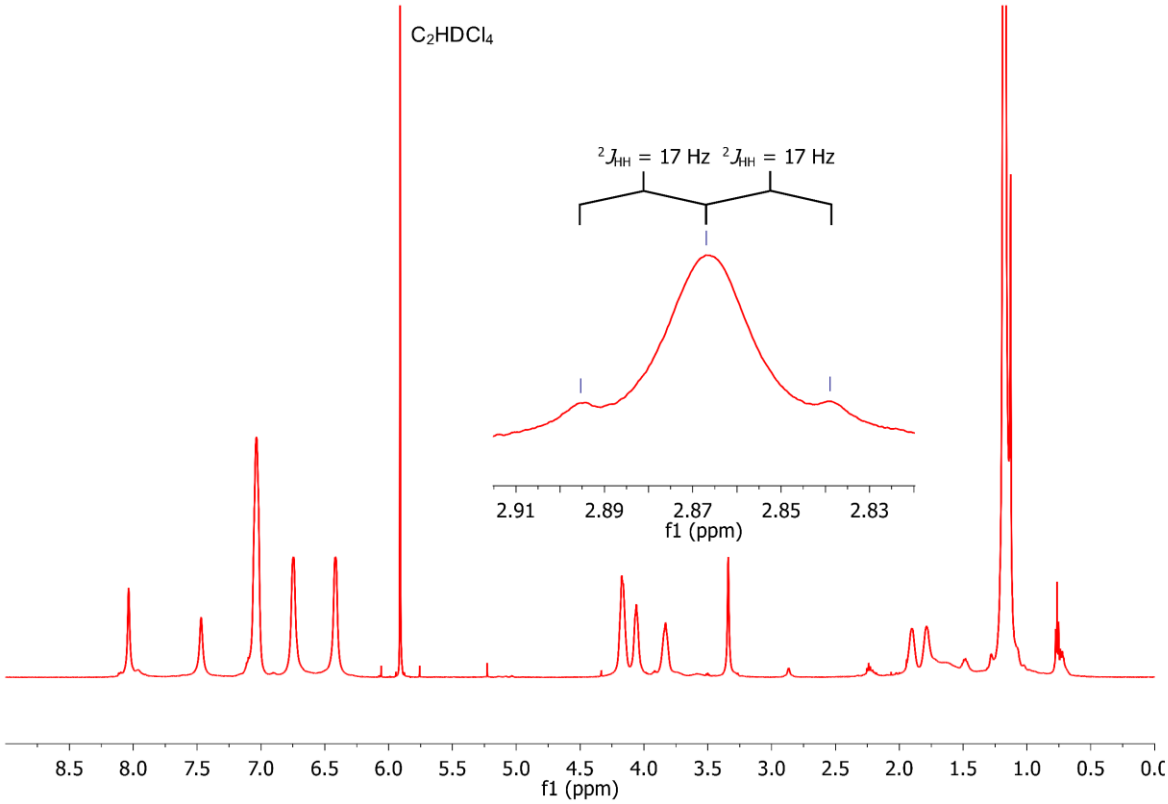

Figure S5. ^{1}H NMR (600 MHz) spectrum of **P2** in $C_2D_2Cl_4$ at -5 °C, enlarged at 2.87 ppm with labelled peaks in Hz.

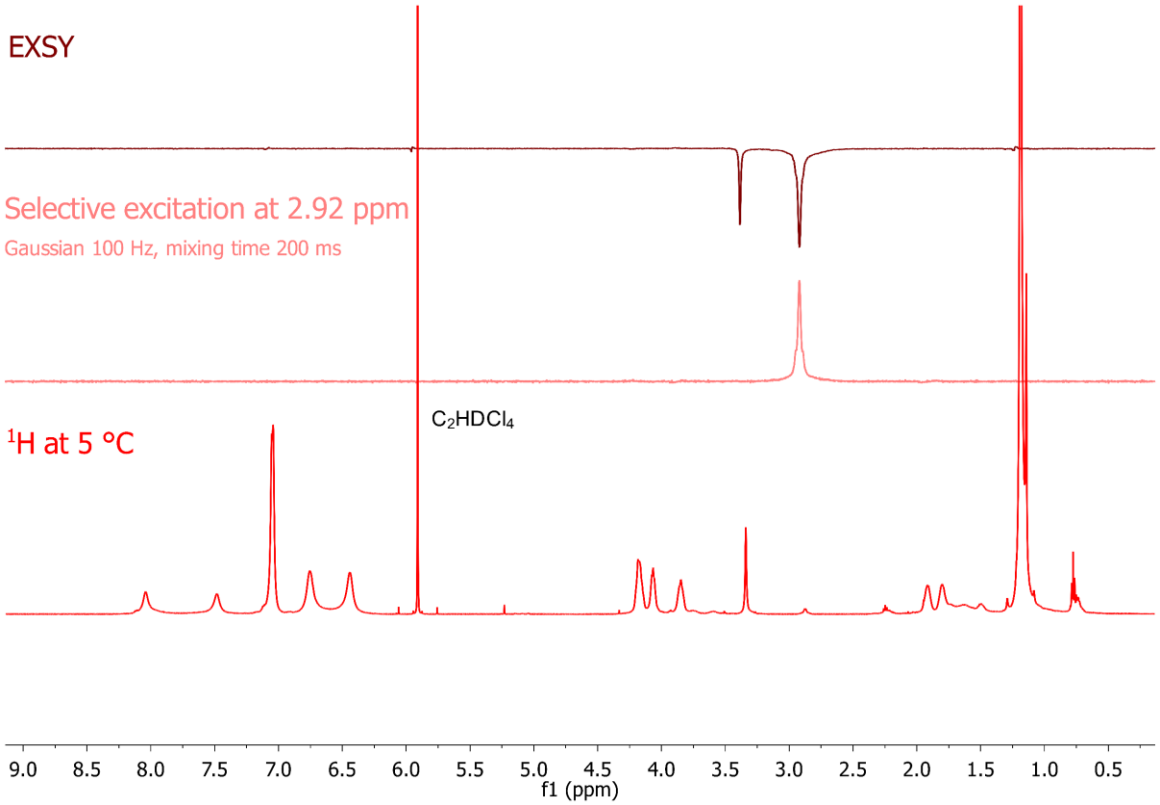

Figure S6. ^{1}H and EXSY (600 MHz) NMR spectra of **P2** in $C_2D_2Cl_4$ at 5 °C showing the selective excitation at 2.92 ppm.

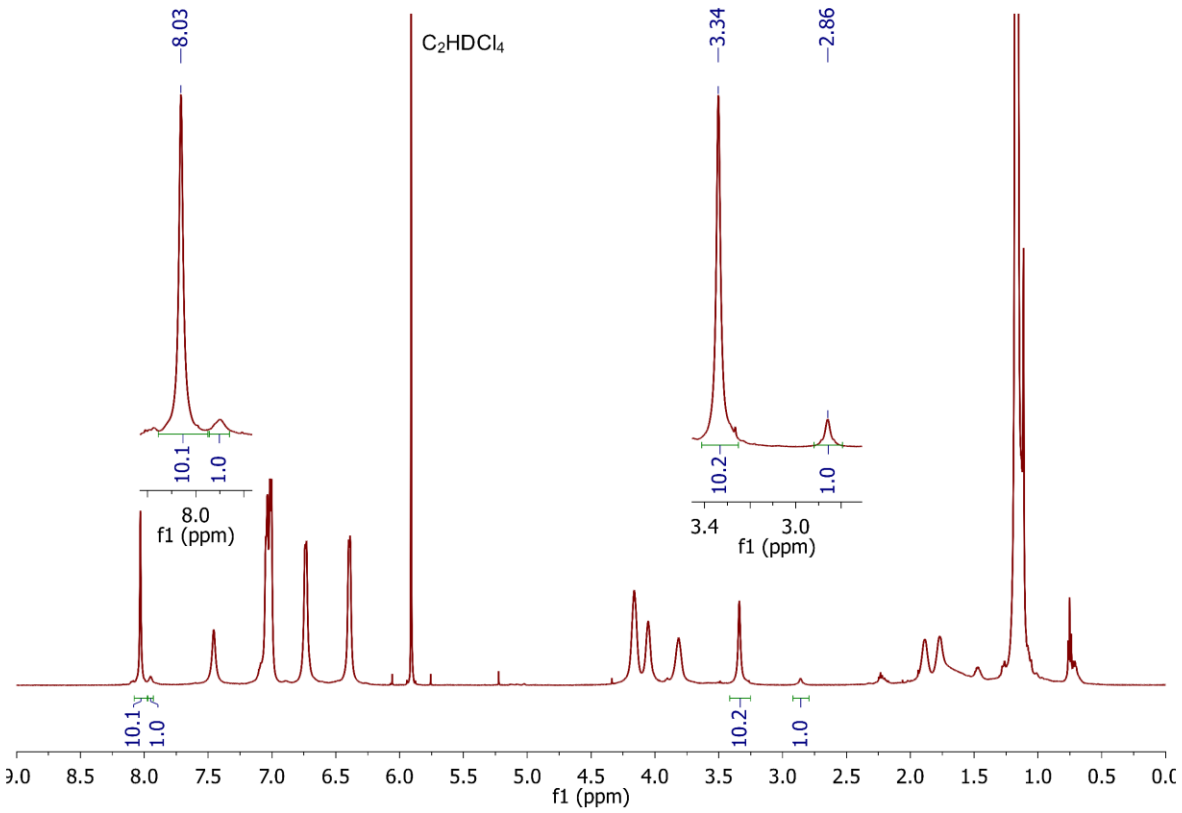

Figure S7. ^{1}H (600 MHz) NMR spectrum of **P2** in $C_2D_2Cl_4$ at -15 °C showing the ratio of (*P*,*P*)/(*M*,*M*) : (*P*,*M*)/(*M*,*P*) of 10:1.

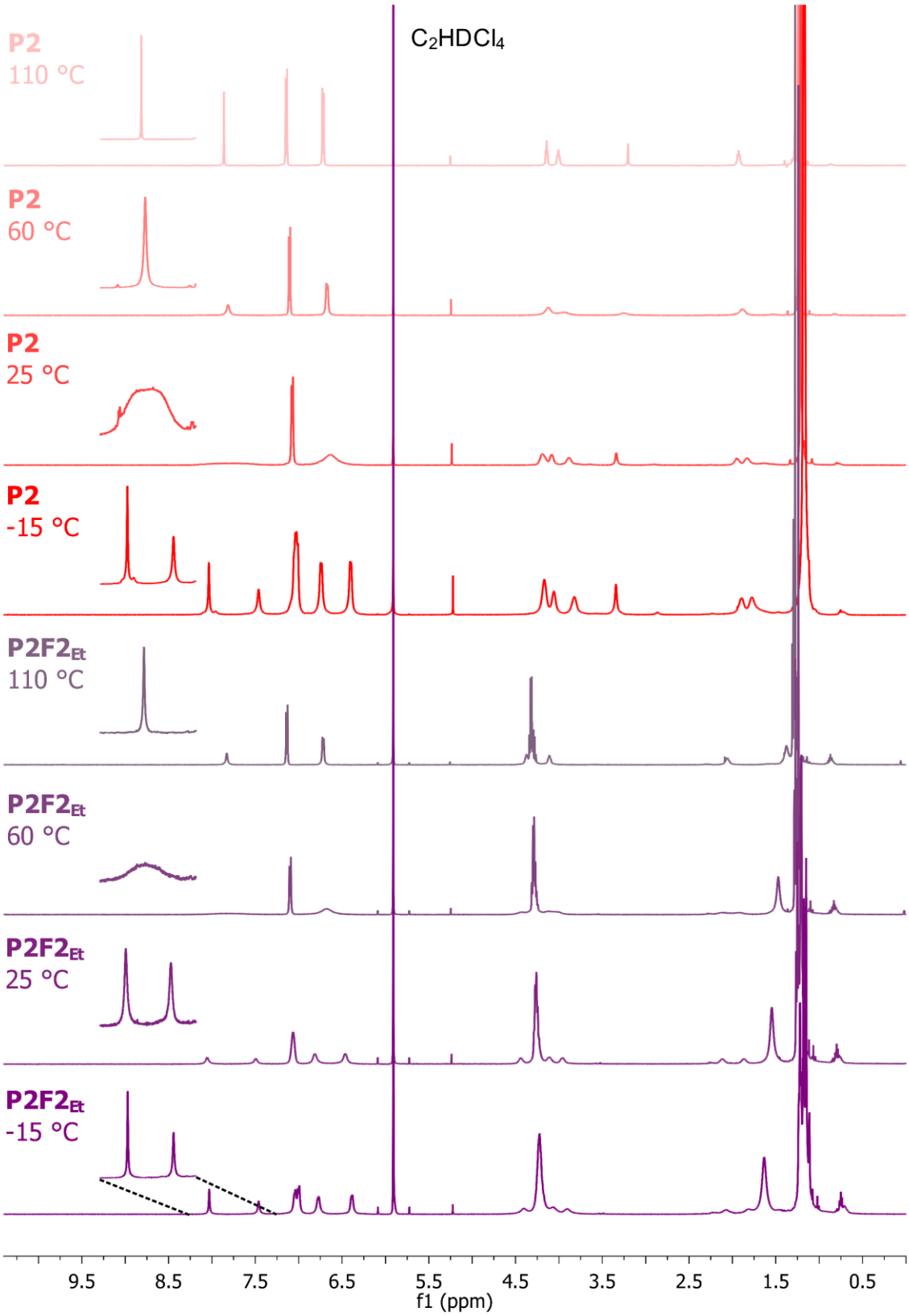

Figure S8. Temperature-dependent ^{1}H (500 MHz) NMR spectra of **P2** and **P2F2$_{Et}$** dissolved in $C_2D_2Cl_4$.

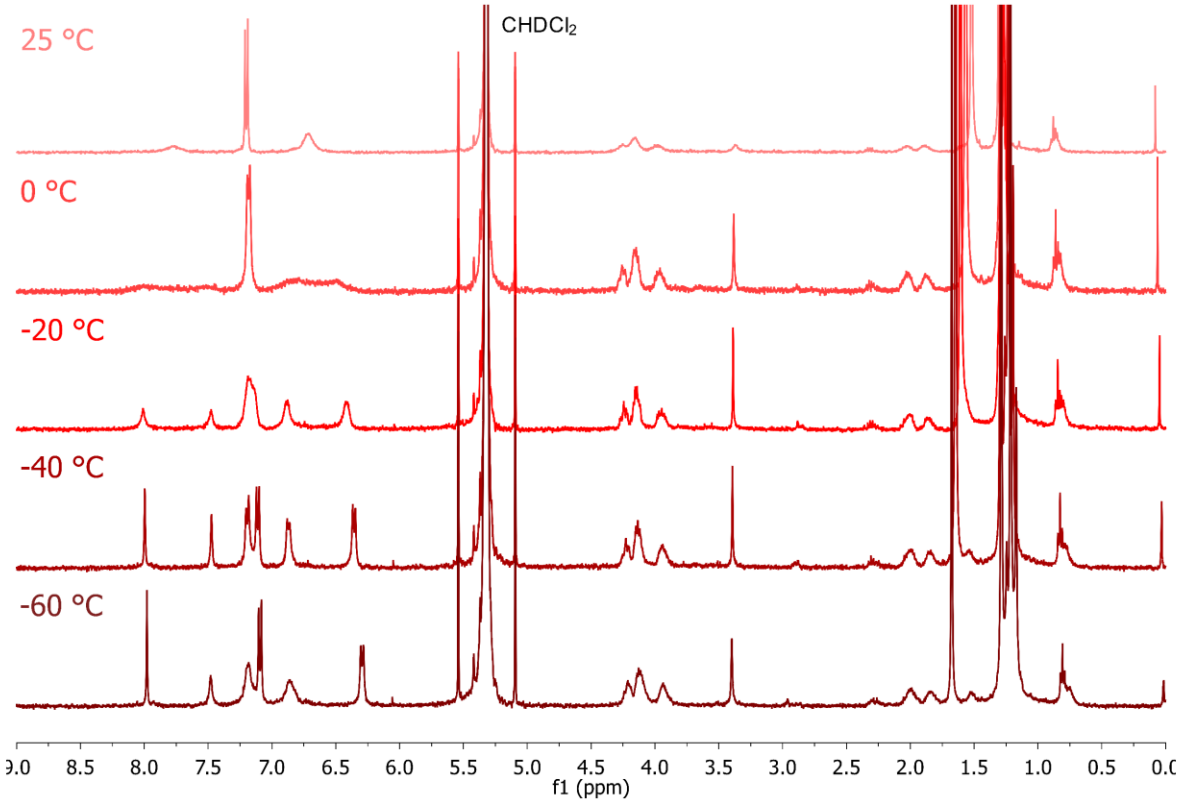

Figure S9. Temperature-dependent ^{1}H (400 MHz) NMR spectra of **P2** dissolved in CD_2Cl_2.

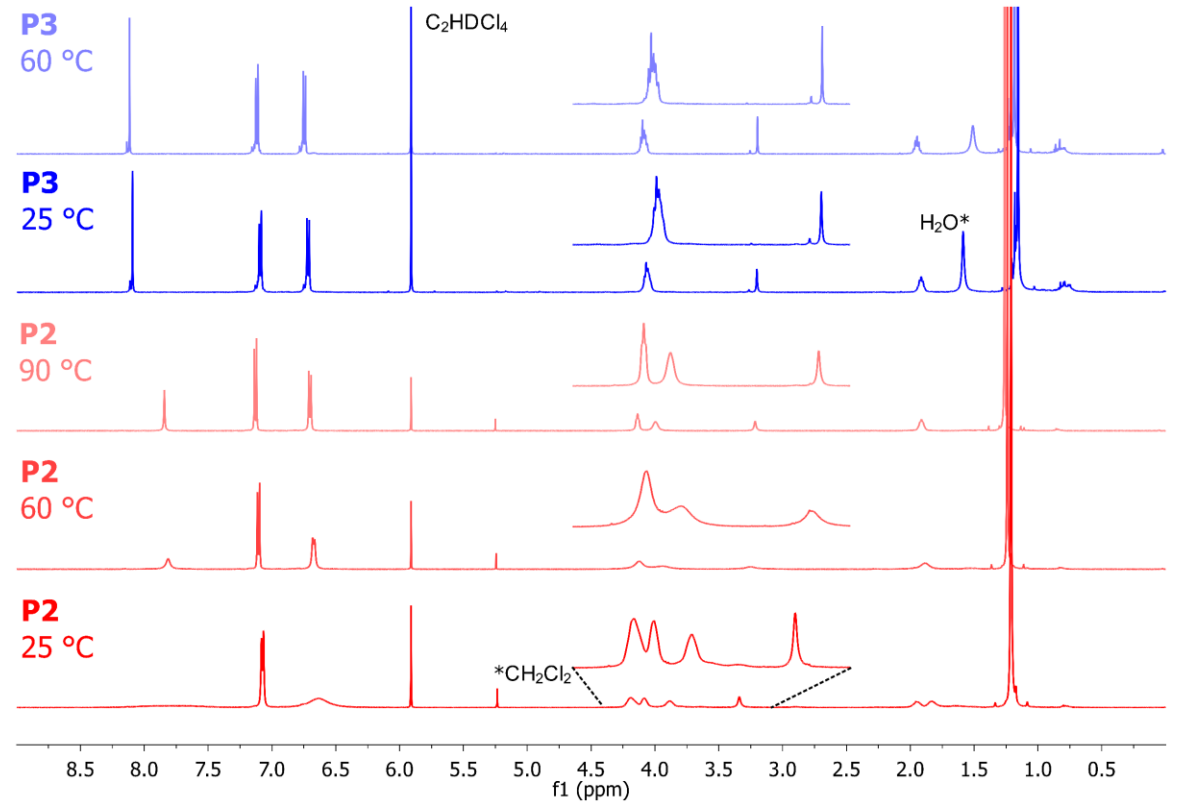

Figure S10. Temperature-dependent ^{1}H (500 MHz) NMR spectra of **P2** and **P3** in $C_2D_2Cl_4$.

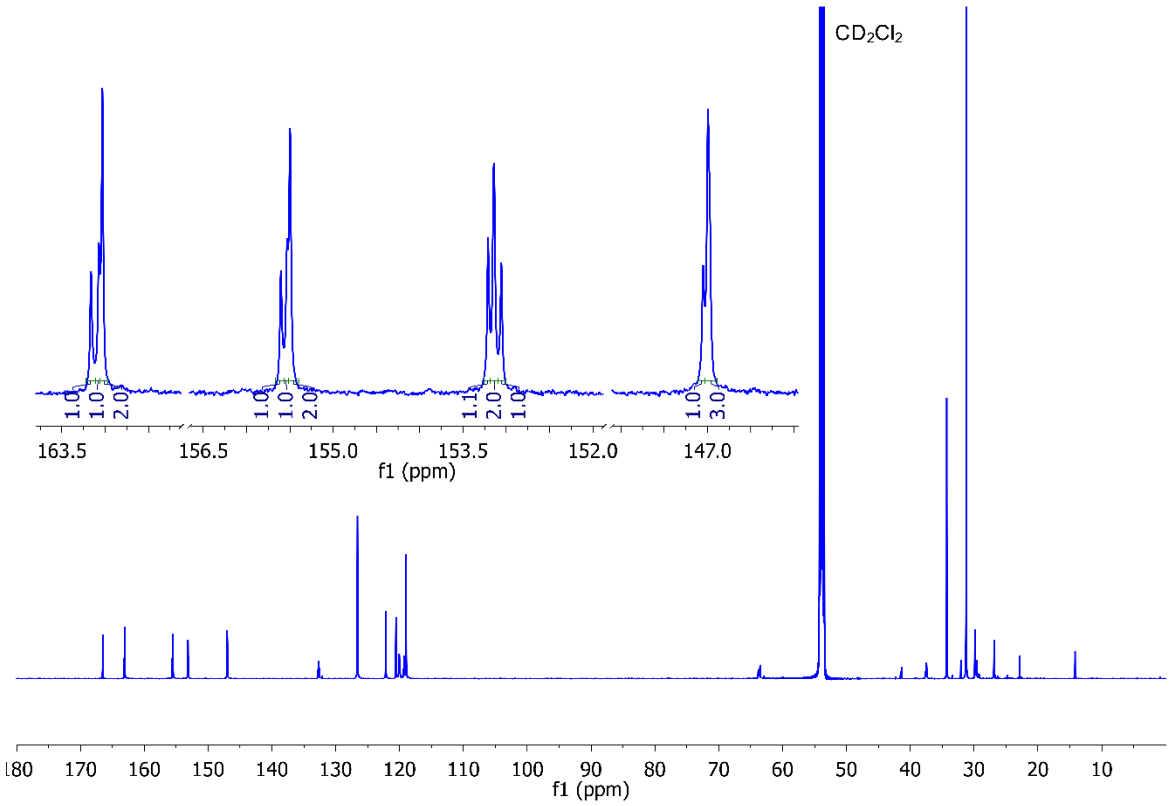

Figure S11. ^{13}C (600 MHz) NMR spectrum of **P3** dissolved in CD_2Cl_2 recorded at -20 °C.

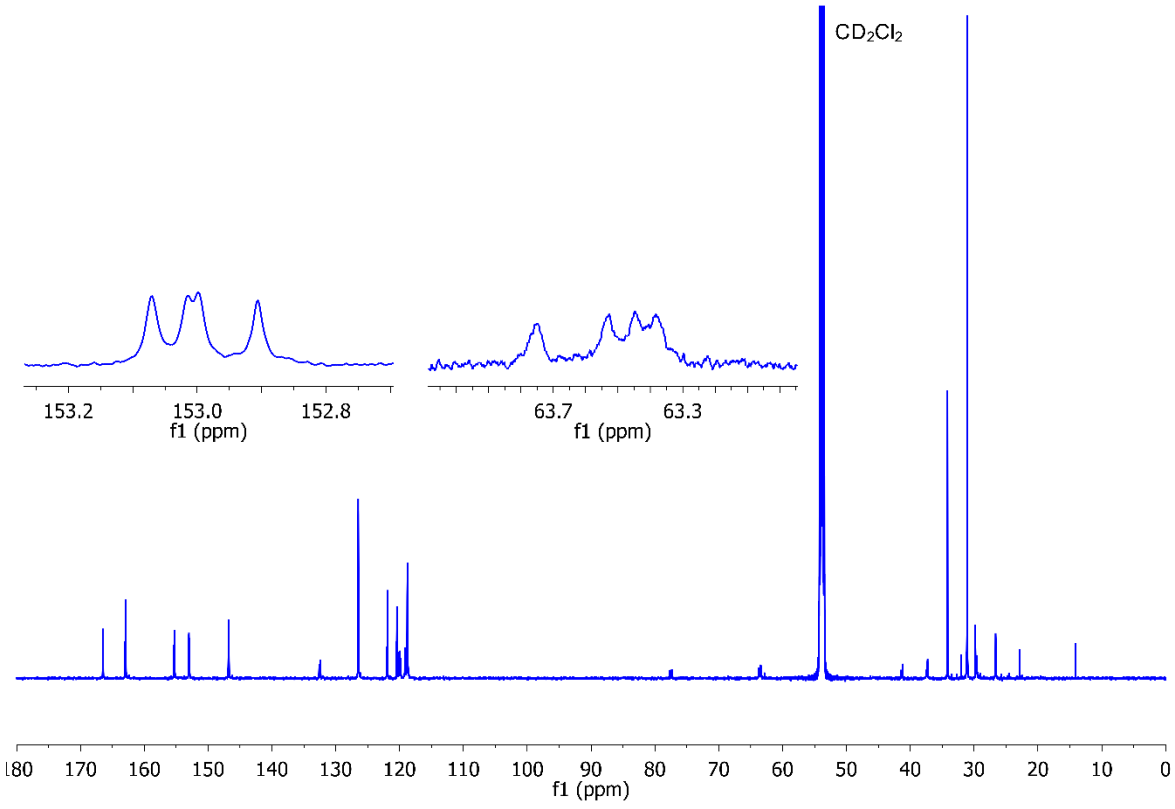

Figure S12. ^{13}C (600 MHz) NMR spectrum of **P3** dissolved in CD_2Cl_2 recorded at -38 °C.

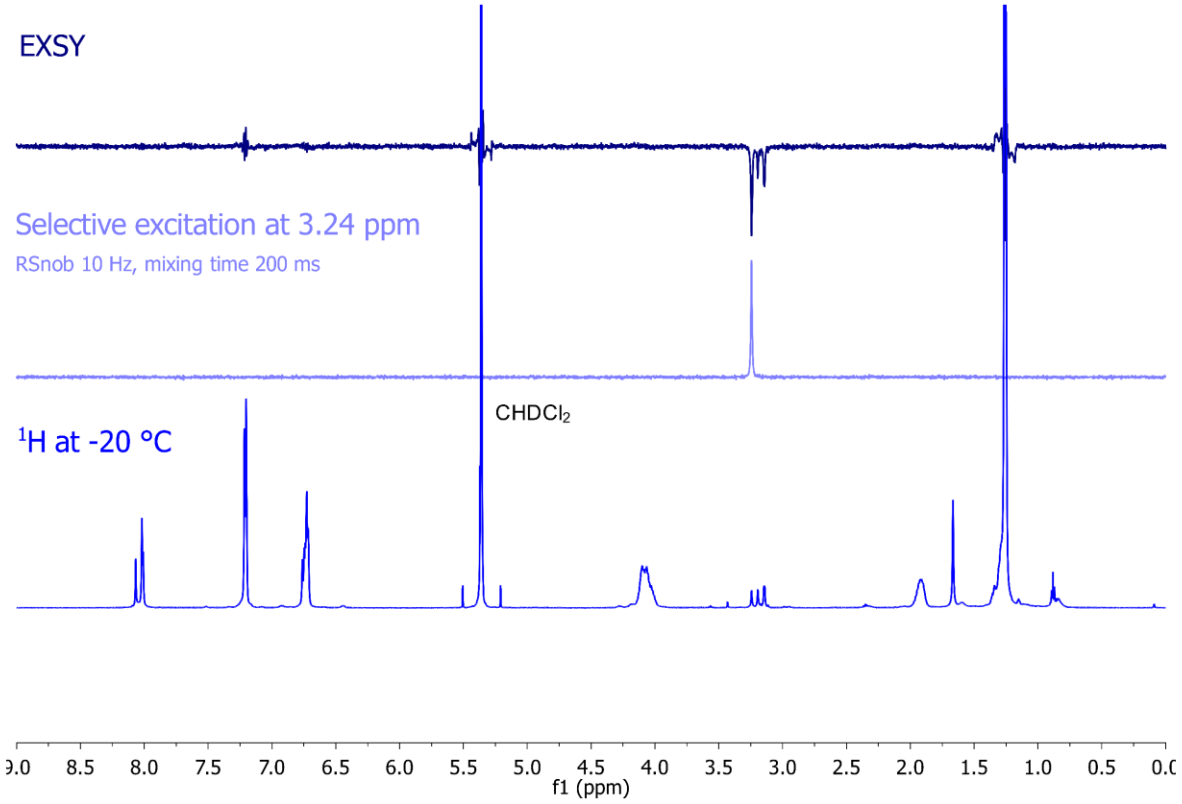

Figure S13. ^{1}H and EXSY (600 MHz) NMR spectra of **P3** in CD_2Cl_2 at -20 °C showing the selective excitation at 3.24 ppm.

5. Calculation of the activation energy $\Delta G^{\ddagger}$

To calculate the activation energy $\Delta G^{\ddagger}$ the following equation was used[2]:

$$\Delta G^{\ddagger} = RT_C \cdot ln\left(\frac{RT_C\sqrt{2}}{\pi N_A h|\nu_A - \nu_B|}\right)$$

$\Delta G^{\ddagger}$: activation energy for conformational interconversion; R: universal gas constant; N_A: Avogadro constant, h: Planck's constant, ν: chemical shift

Table S1. Summary of the coalescence temperature and the difference in frequencies for the calculation of the activation energy.

Compound	Solvent	T_c [K]	$\lvert\nu_A - \nu_B\rvert$ [Hz] at T [K]	$\Delta G^{\ddagger}$ [kJ/mol]
P2	CD_2Cl_2	273	205.45 at 233	52.77
P2	$C_2D_2Cl_4$	298	291.21 at 248	56.95
P2F2$_{Et}$	CD_2Cl_2	292	29.27 at 253	61.33
P2F2$_{Et}$	$C_2D_2Cl_4$	333	283.83 at 268	64.02

6. NMR spectra

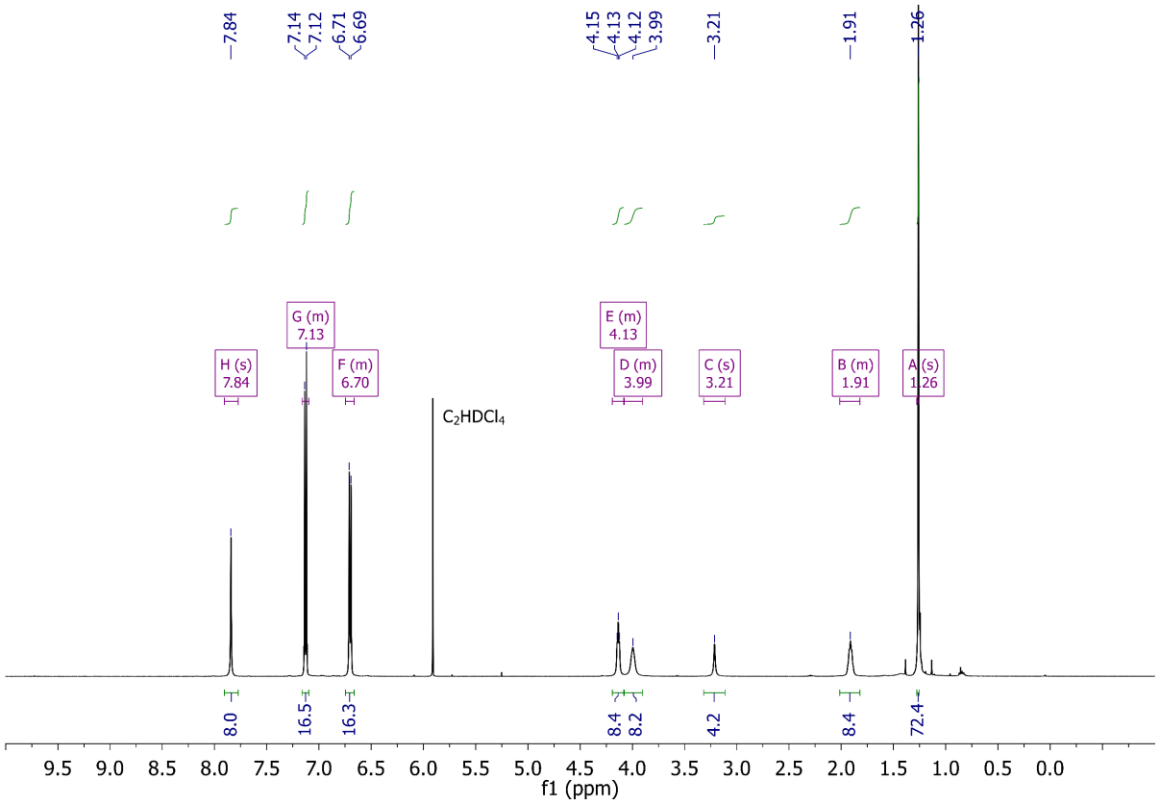

Figure S14. ^{1}H NMR (500 MHz, $C_2D_2Cl_4$, 90 °C) spectrum of macrocycle **P2**.

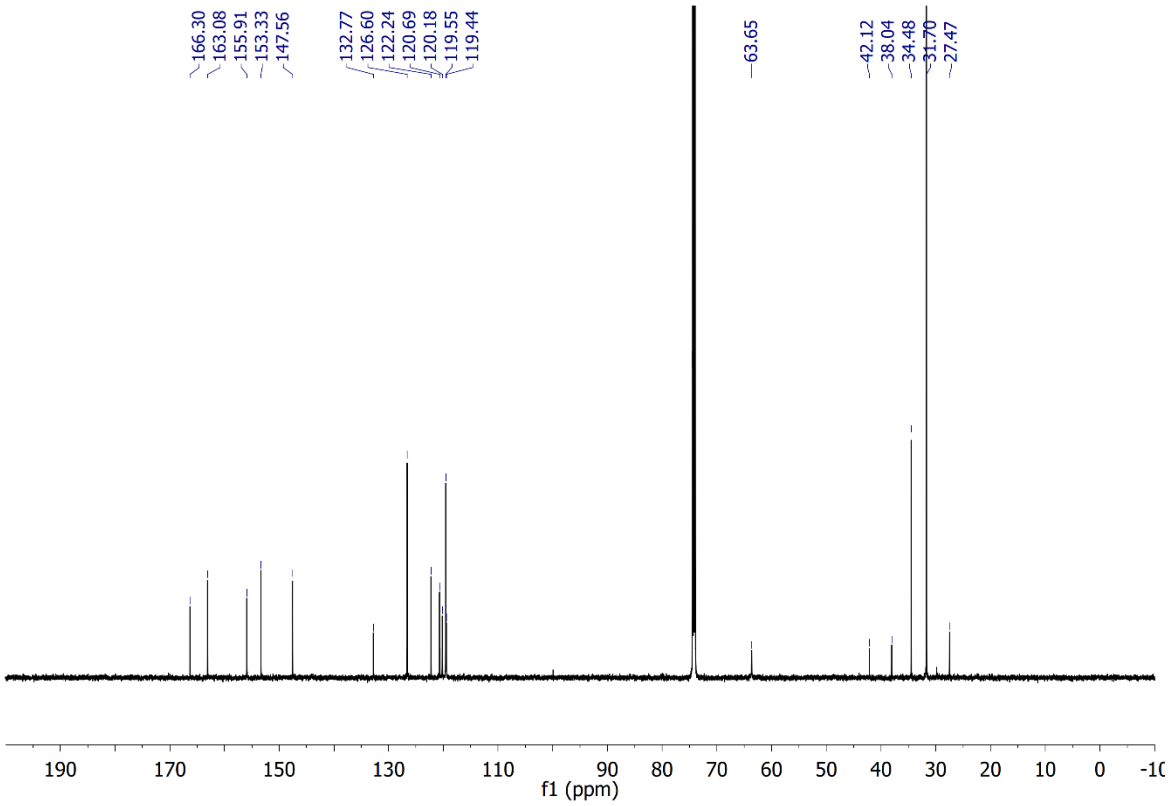

Figure S15. ^{13}C NMR (126 MHz, $C_2D_2Cl_4$, 90 °C) spectrum of macrocycle **P2**.

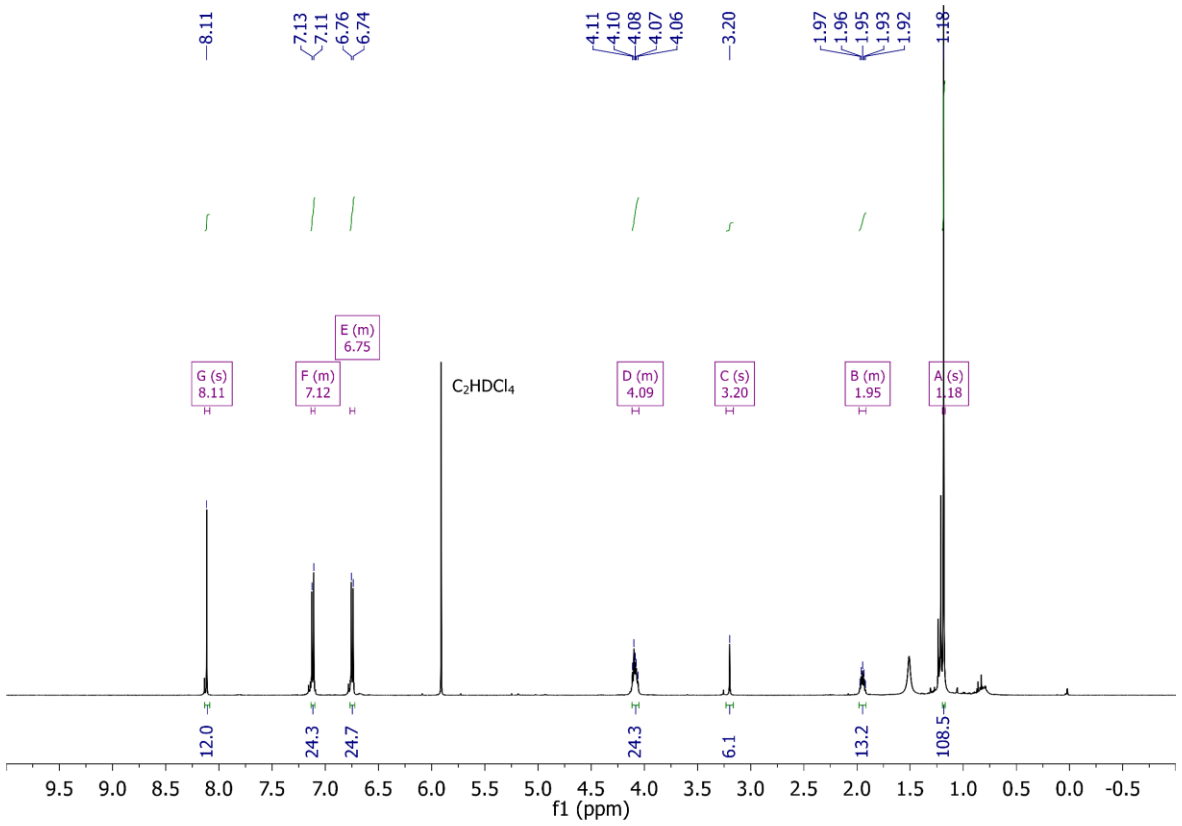

Figure S16. ^{1}H NMR (500 MHz, $C_2D_2Cl_4$, 60 °C) spectrum of macrocycle **P3**.

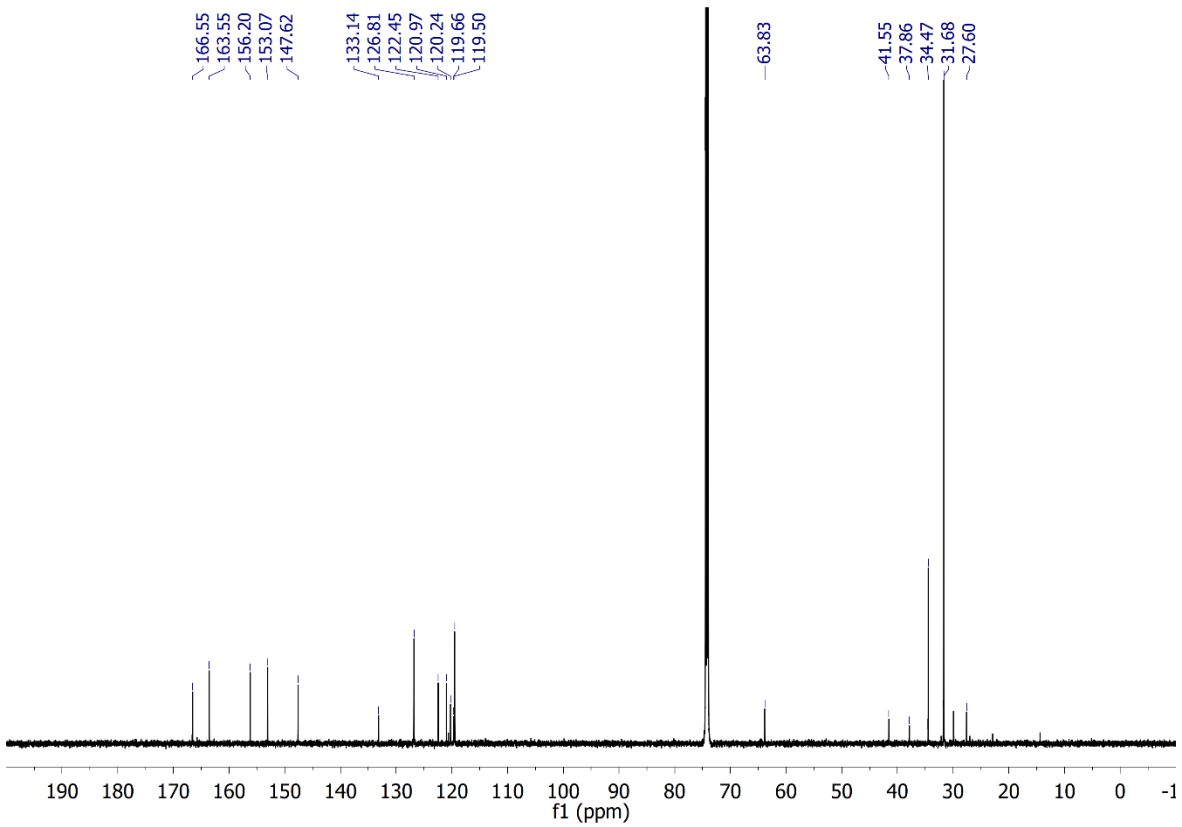

Figure S17. ^{13}C NMR (126 MHz, $C_2D_2Cl_4$, 60 °C) spectrum of macrocycle **P3**.

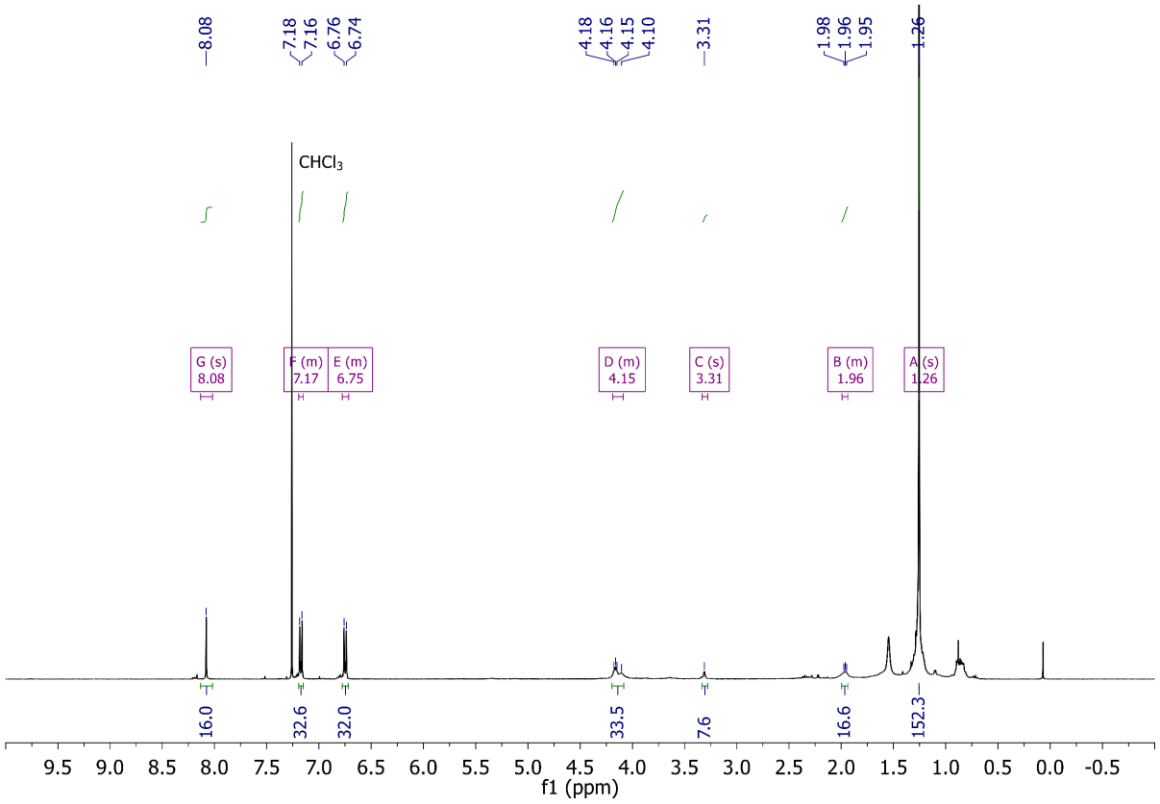

Figure S18. ^{1}H NMR (400 MHz, $CDCl_3$, rt) spectrum of macrocycle **P4**.

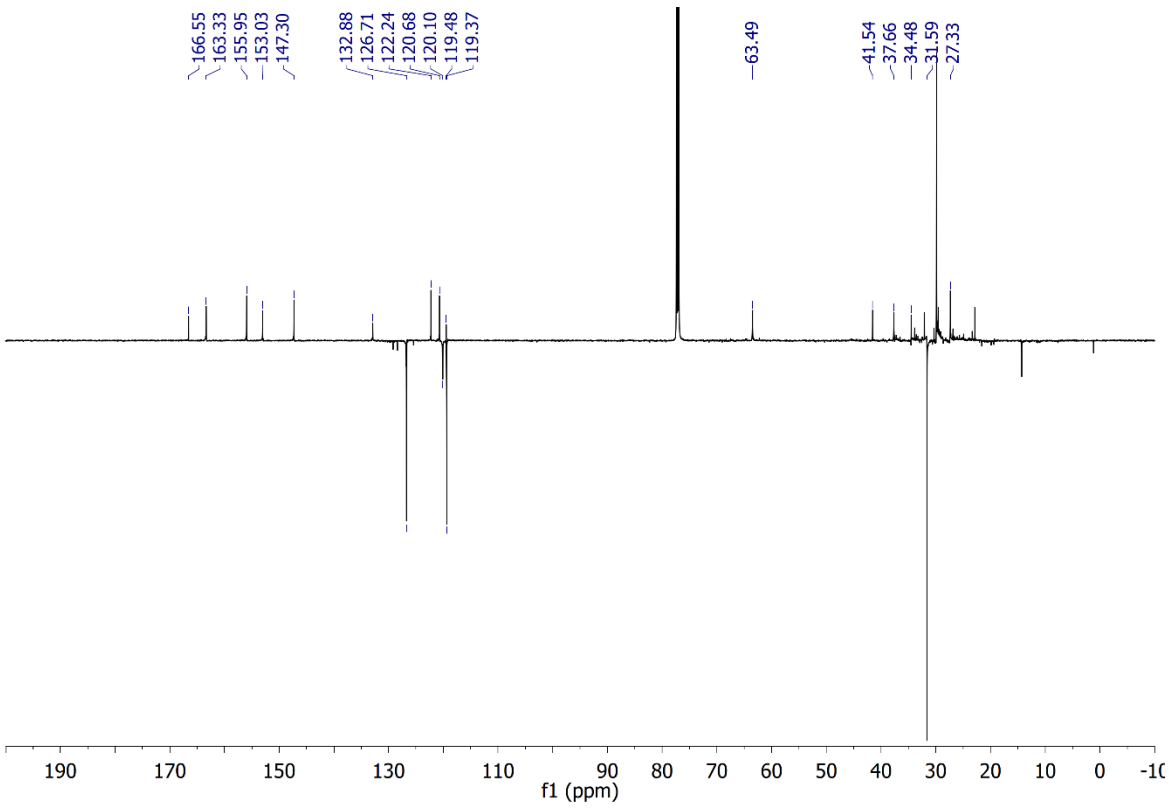

Figure S19. DEPTQ NMR (151 MHz, $CDCl_3$, rt) spectrum of macrocycle **P4**.

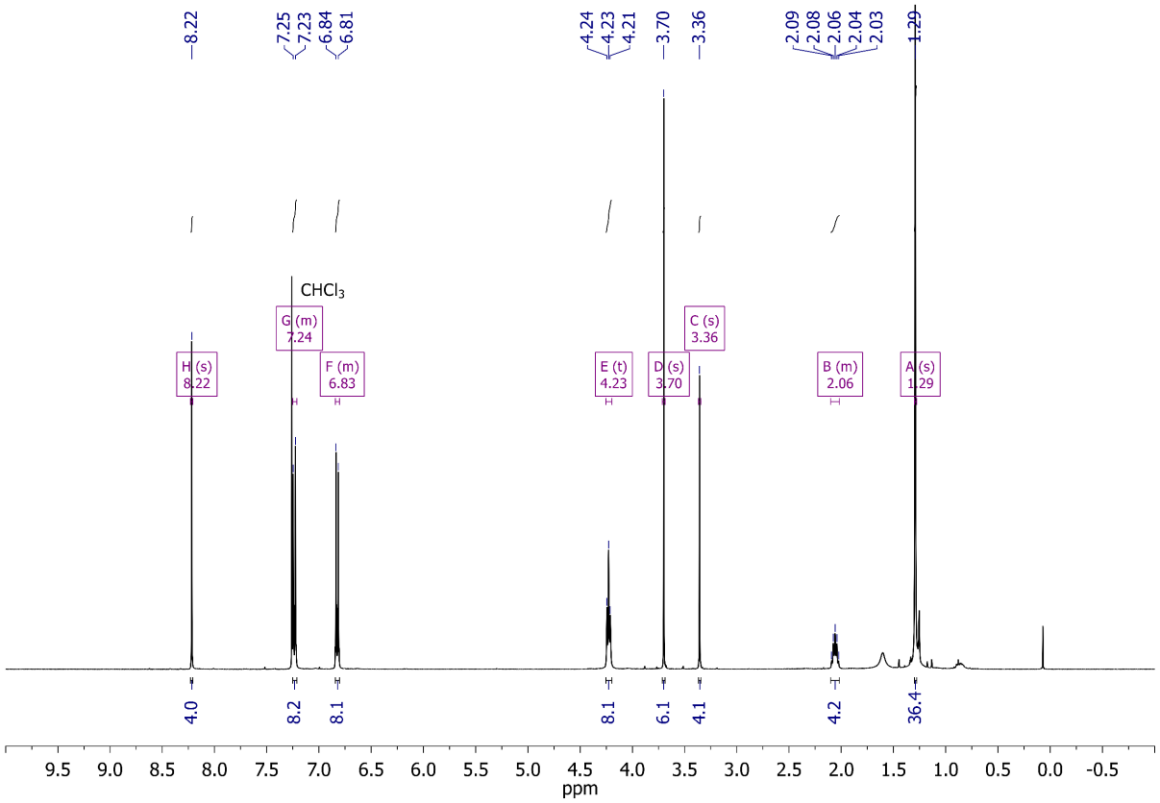

Figure S20. ^{1}H NMR (400 MHz, $CDCl_3$, rt) spectrum of precursor **P1.**

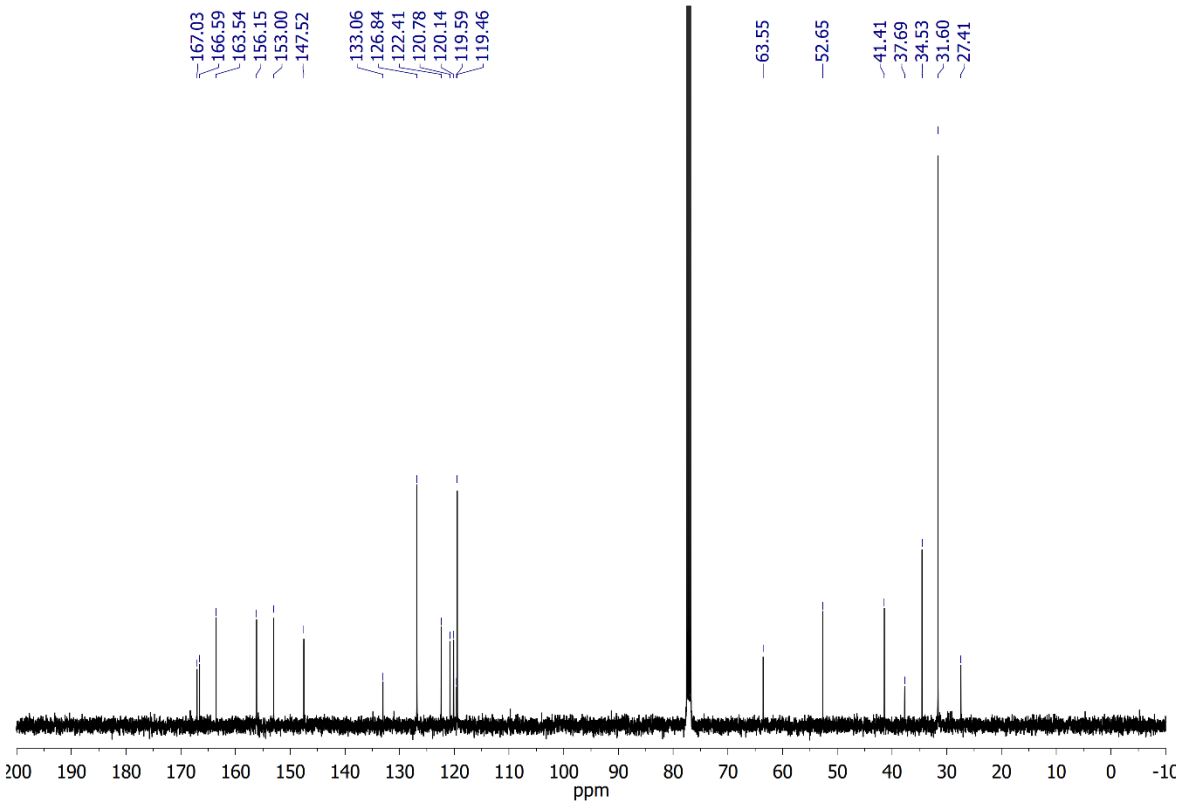

Figure S21. ^{13}C NMR (101 MHz, $CDCl_3$, rt) spectrum of model precursor **P1**.

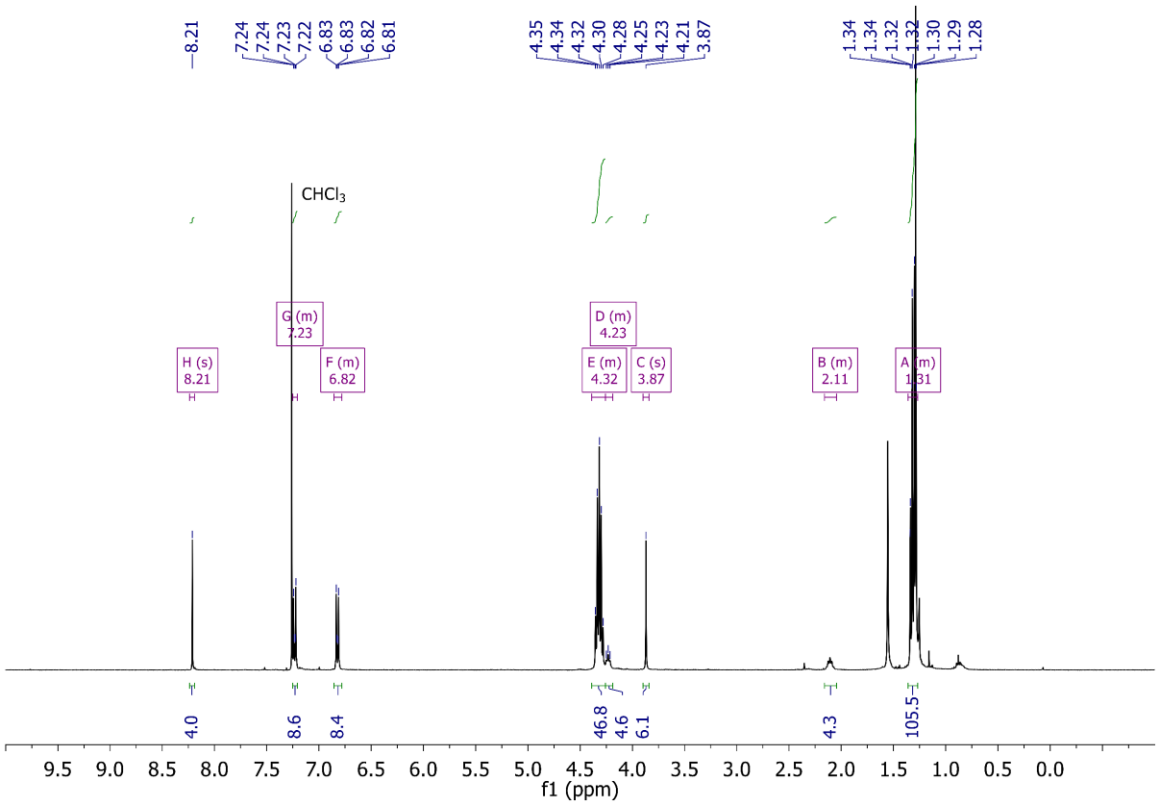

Figure S22. ^{1}H NMR (400 MHz, $CDCl_3$, rt) spectrum of model compound **P1F2$_{Et}$**.

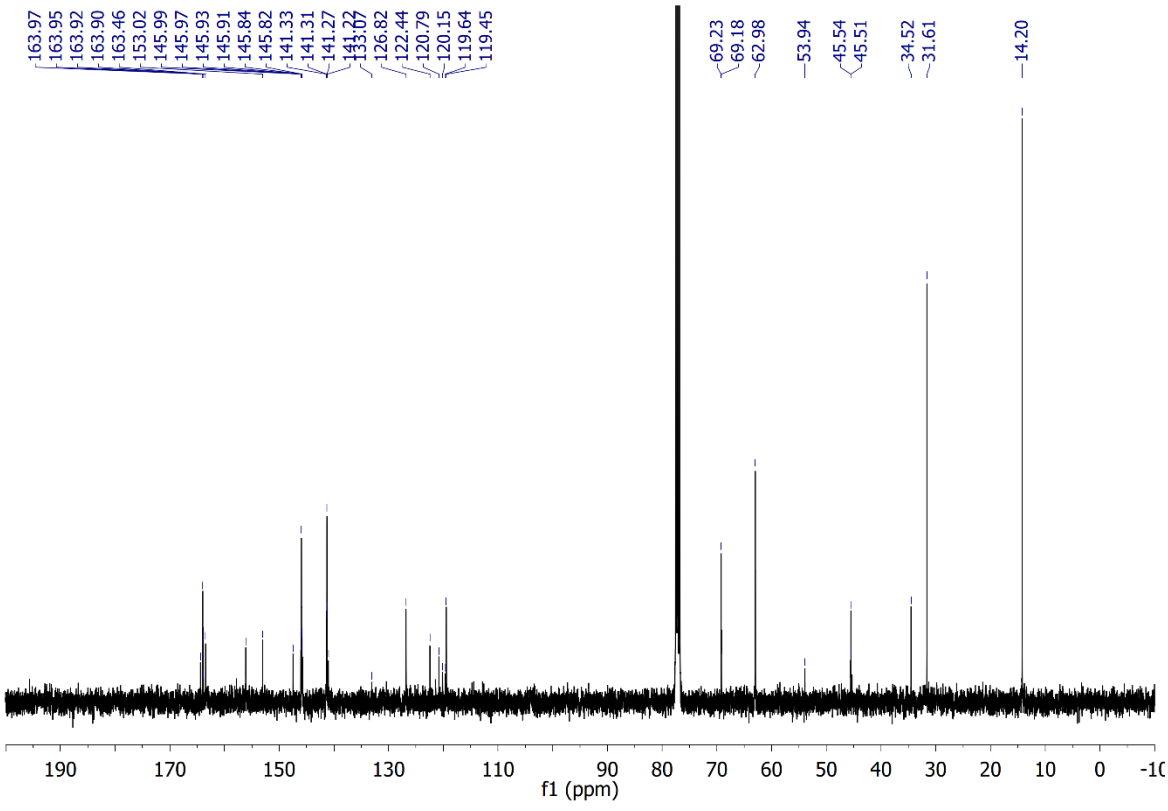

Figure S23. ^{13}C NMR (151 MHz, $CDCl_3$, rt) spectrum of model compound **P1F2$_{Et}$**.

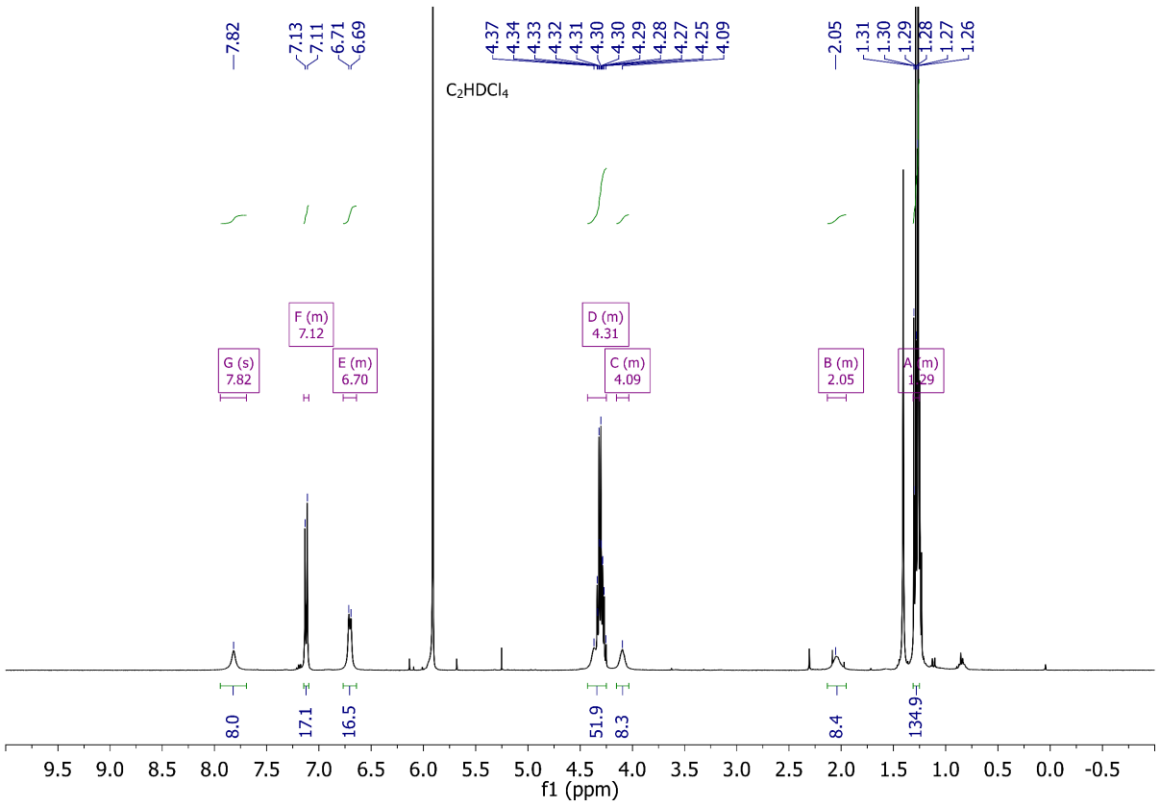

Figure S24. ^{1}H NMR (400 MHz, $C_2D_2Cl_4$, 90 °C) spectrum of the functional hybrid **P2F2$_{Et}$**.

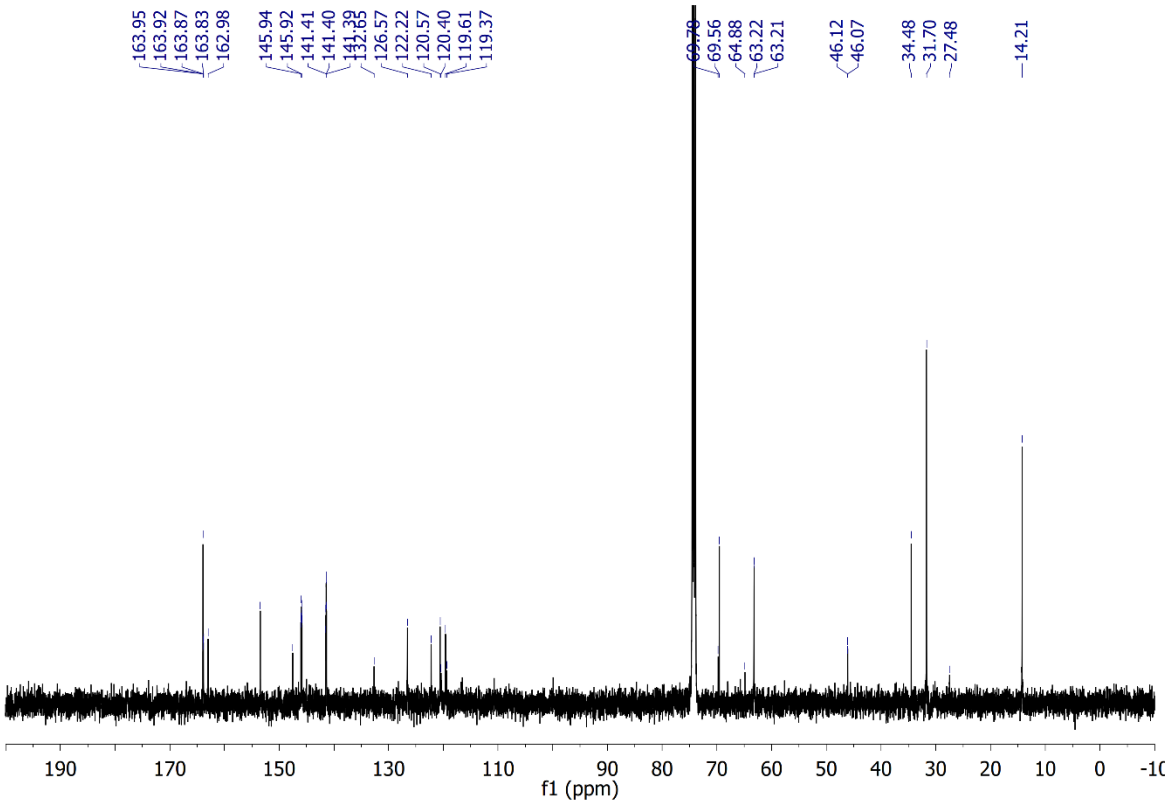

Figure S25. ^{13}C NMR (101 MHz, $C_2D_2Cl_4$, 90 °C) spectrum of the functional hybrid **P2F2$_{Et}$**.

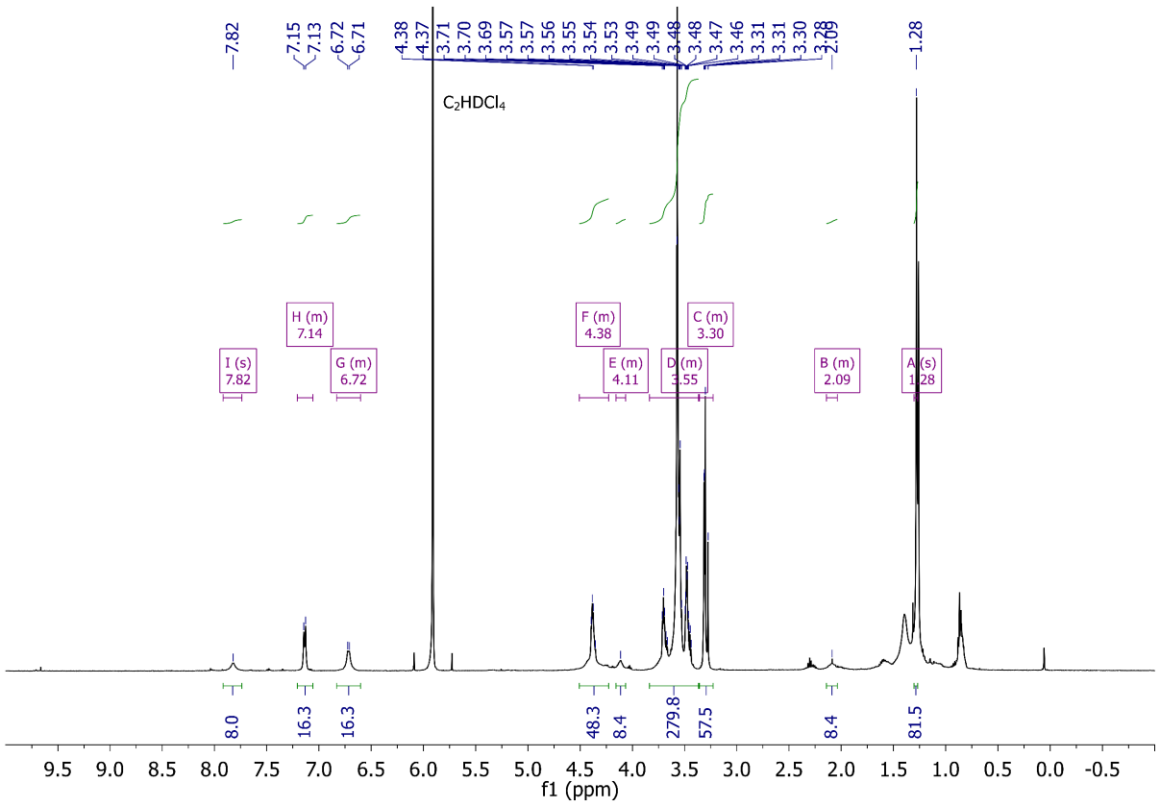

Figure S26. ^{1}H NMR (500 MHz, $C_2D_2Cl_4$, 110 °C) spectrum of the functional hybrid **P2F2$_{TEG}$**.

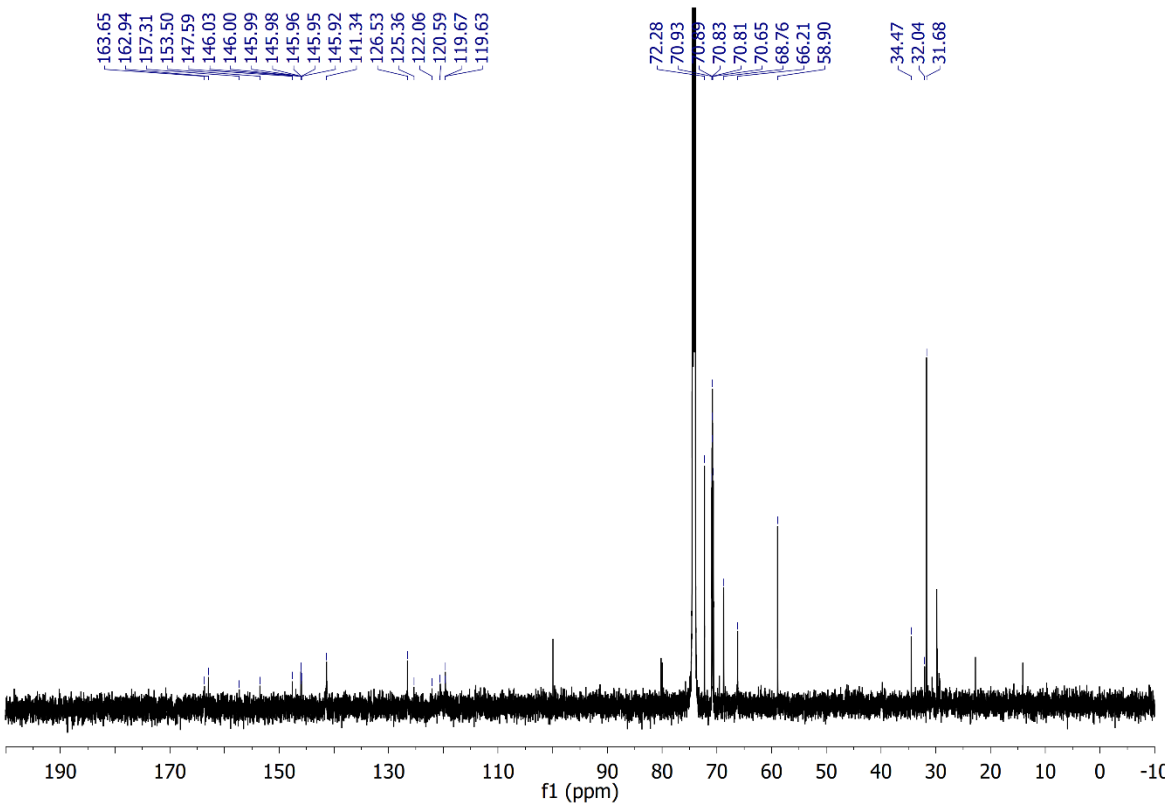

Figure S27. ^{13}C NMR (126 MHz, $C_2D_2Cl_4$, 110 °C) spectrum of the functional hybrid **P2F2$_{TEG}$**.

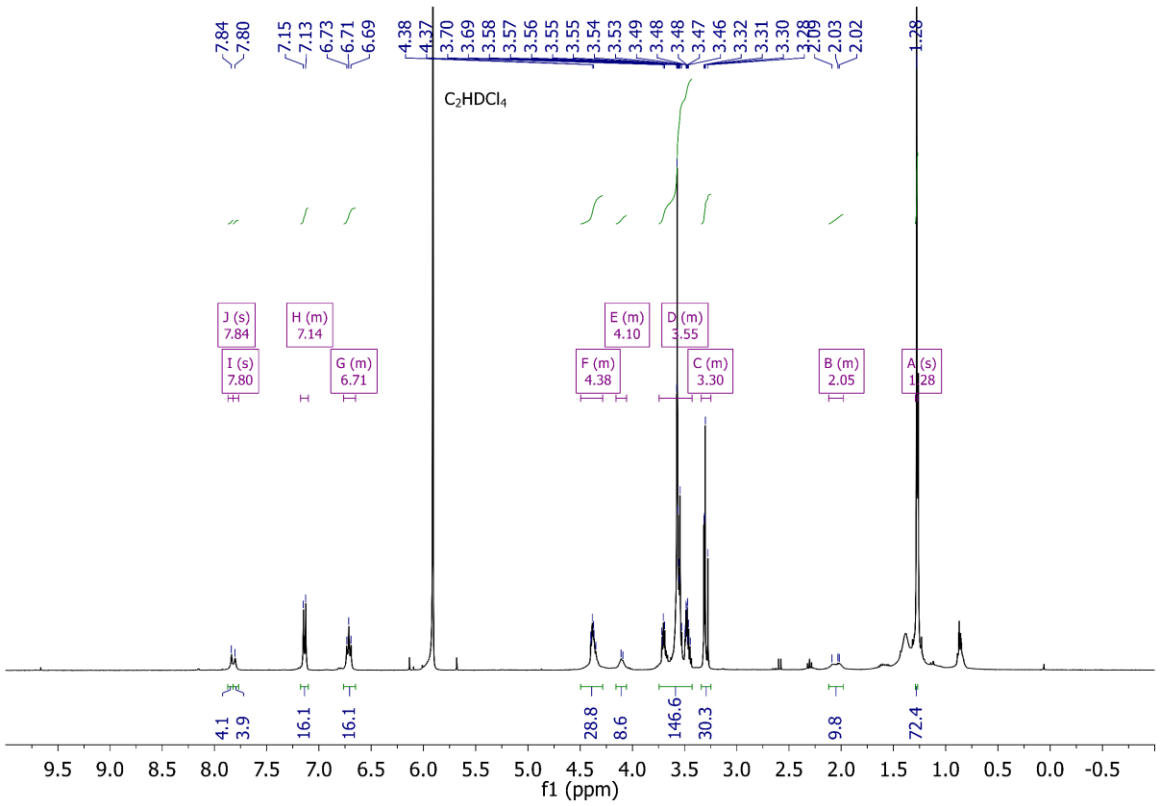

Figure S28. ^{1}H NMR (500 MHz, $C_2D_2Cl_4$, 110 °C) spectrum of the functional hybrid **P2F1$_{TEG}$**.

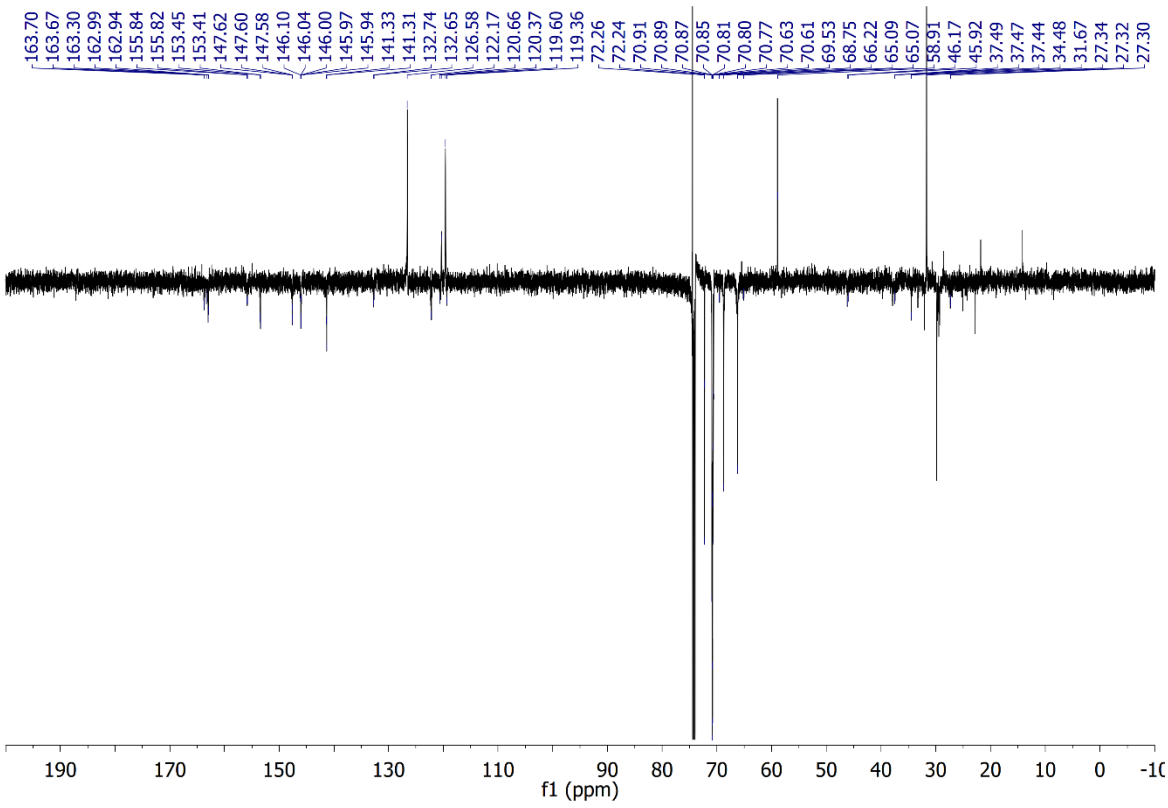

Figure S29. DEPTQ NMR (126 MHz, $C_2D_2Cl_4$, 110 °C) spectrum of the functional hybrid **P2F1$_{TEG}$**.

7. MS spectra

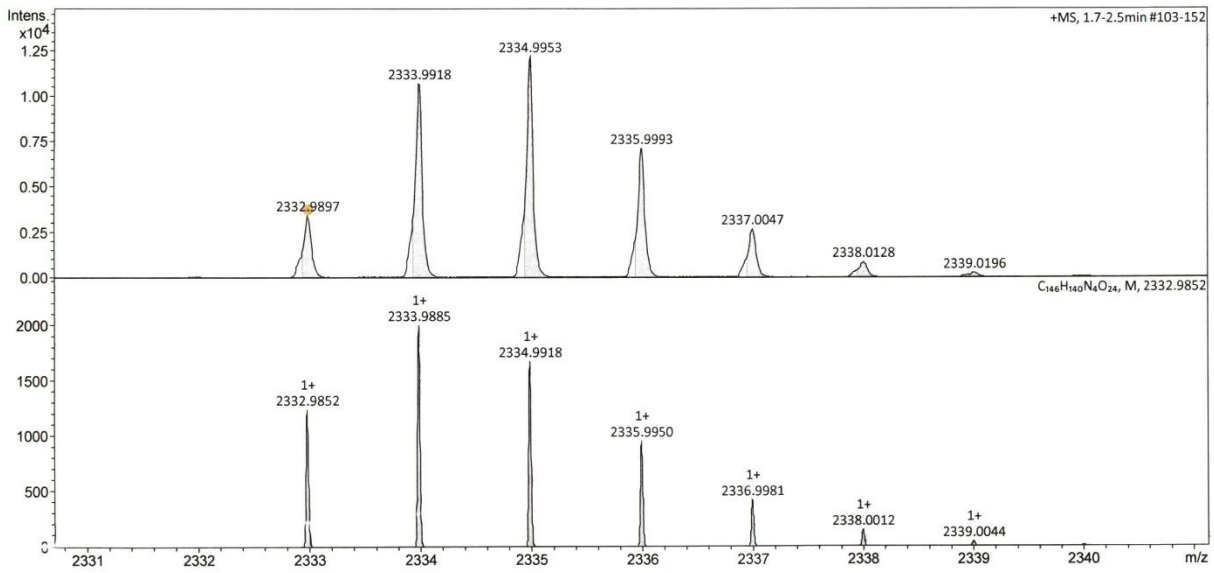

Figure S30. APPI HRMS spectrum of macrocycle **P2**.

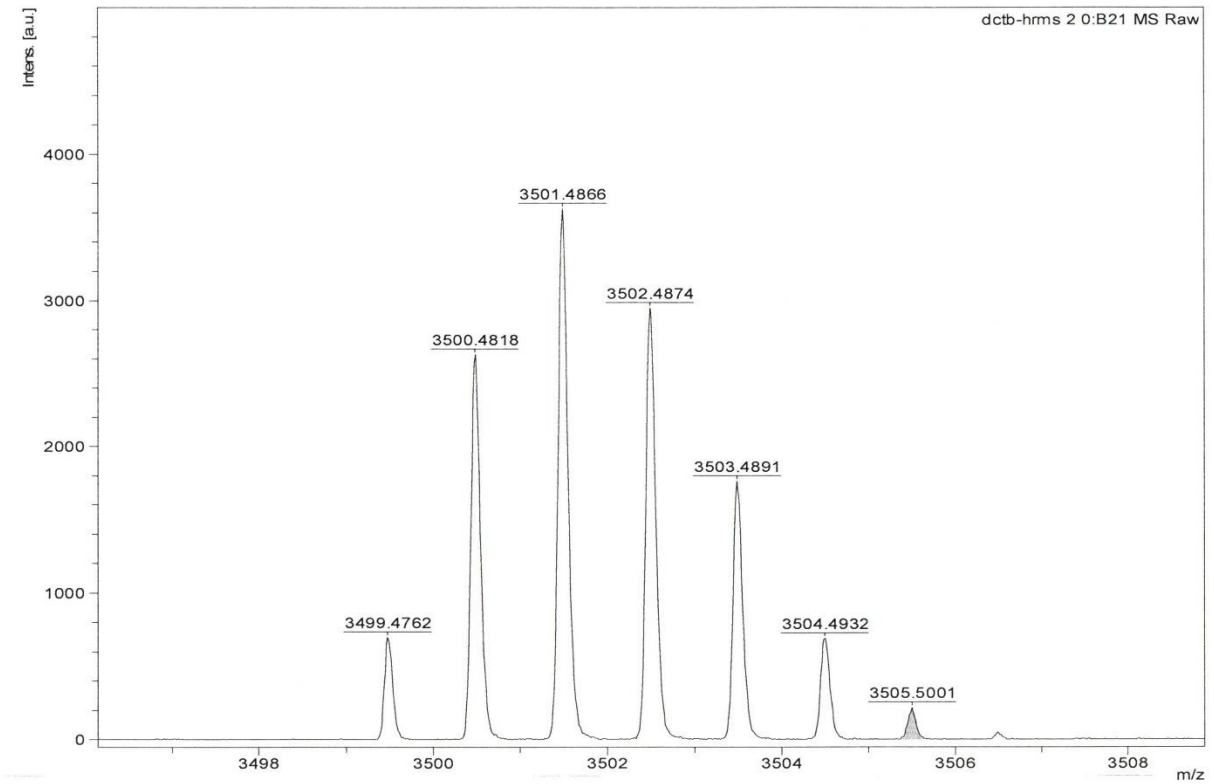

Figure S31. MALDI HRMS spectrum of macrocycle **P3**.

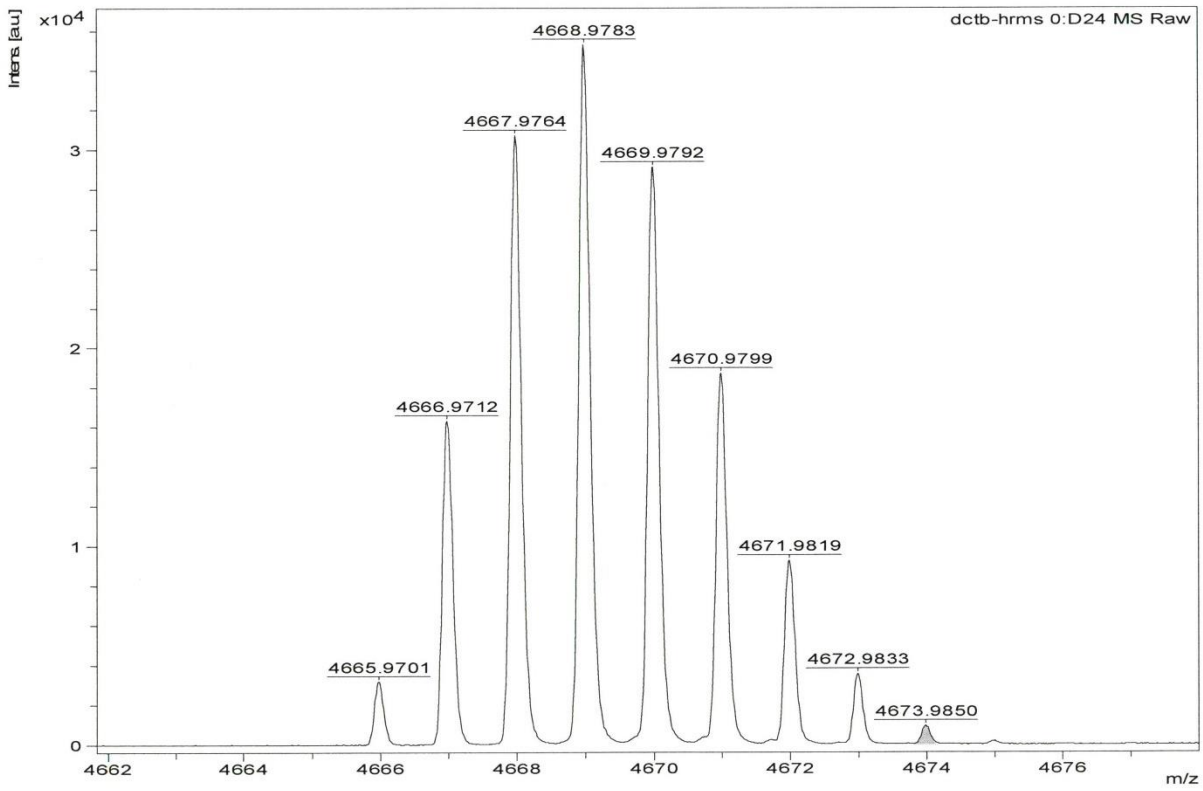

Figure S32. MALDI HRMS spectrum of macrocycle **P4**.

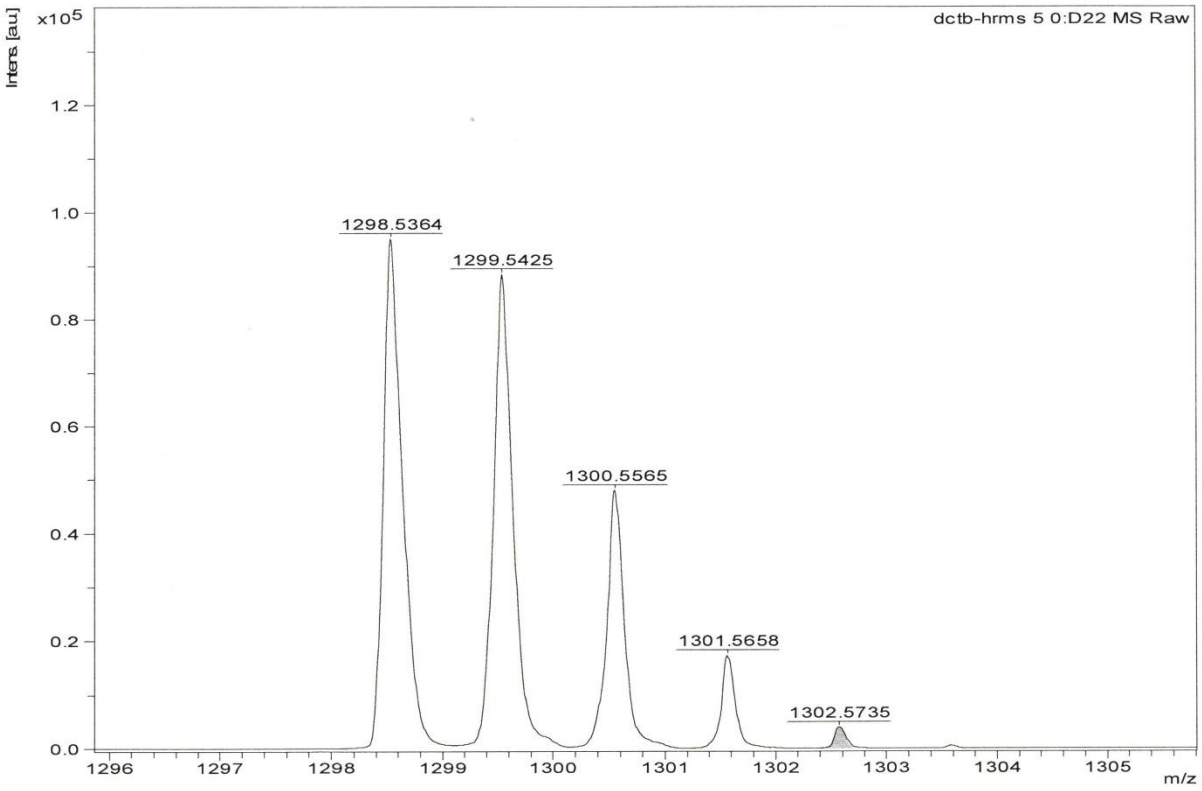

Figure S 33. MALDI HRMS spectrum of precursor **P1**.

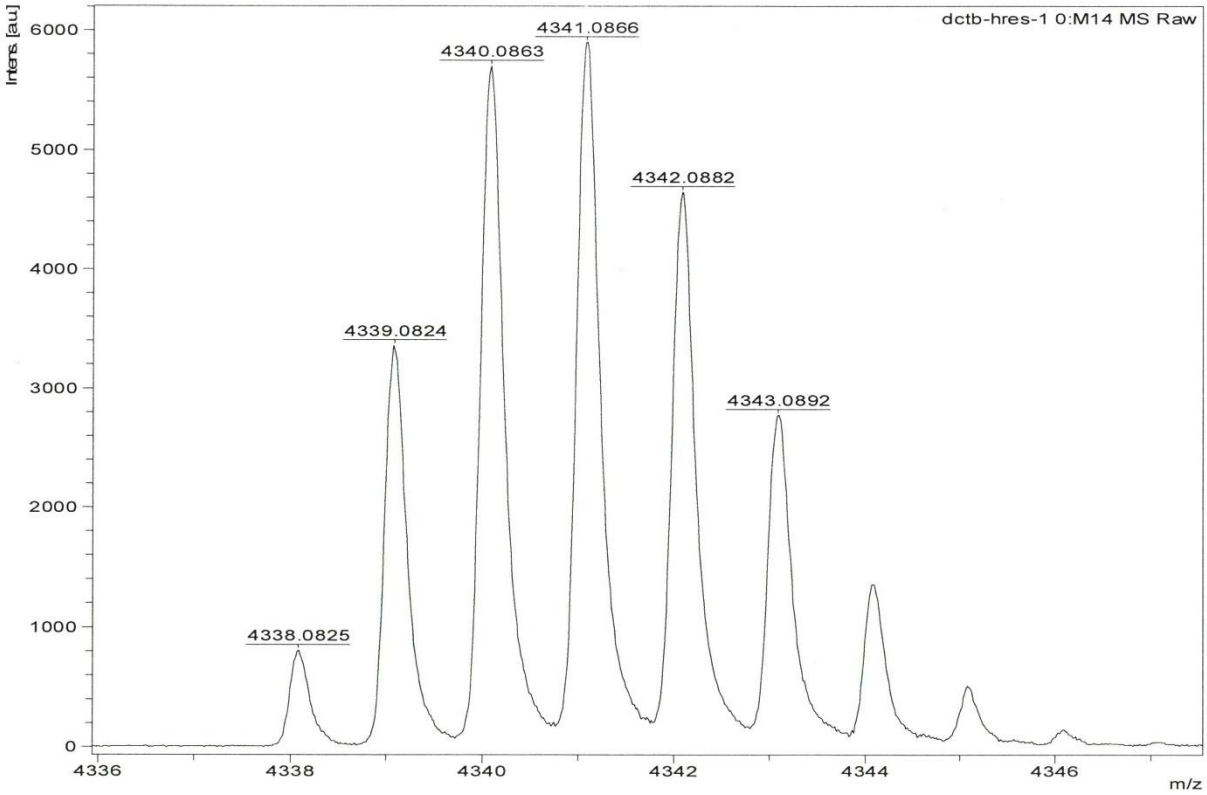

Figure S34. MALDI HRMS spectrum of model compound **P1F2$_{Et}$**.

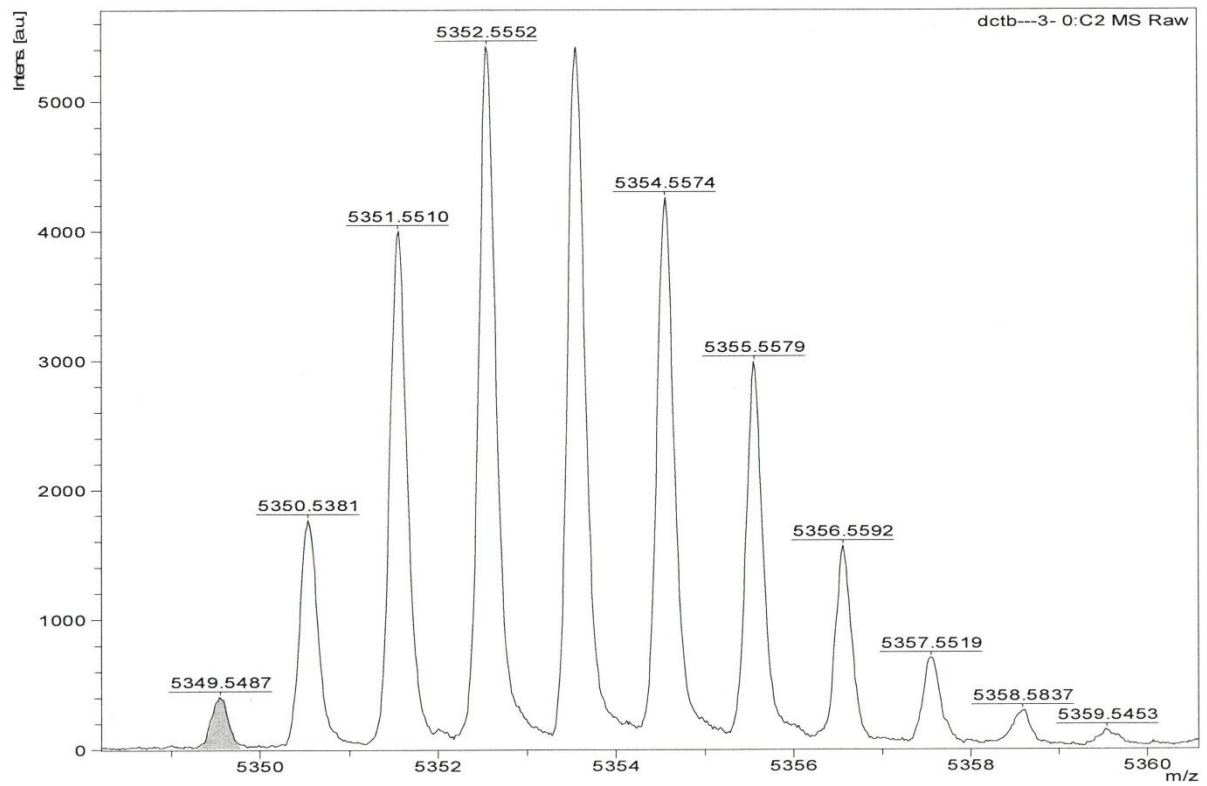

Figure S35. MALDI HRMS spectrum of functional hybrid **P2F2$_{Et}$**.

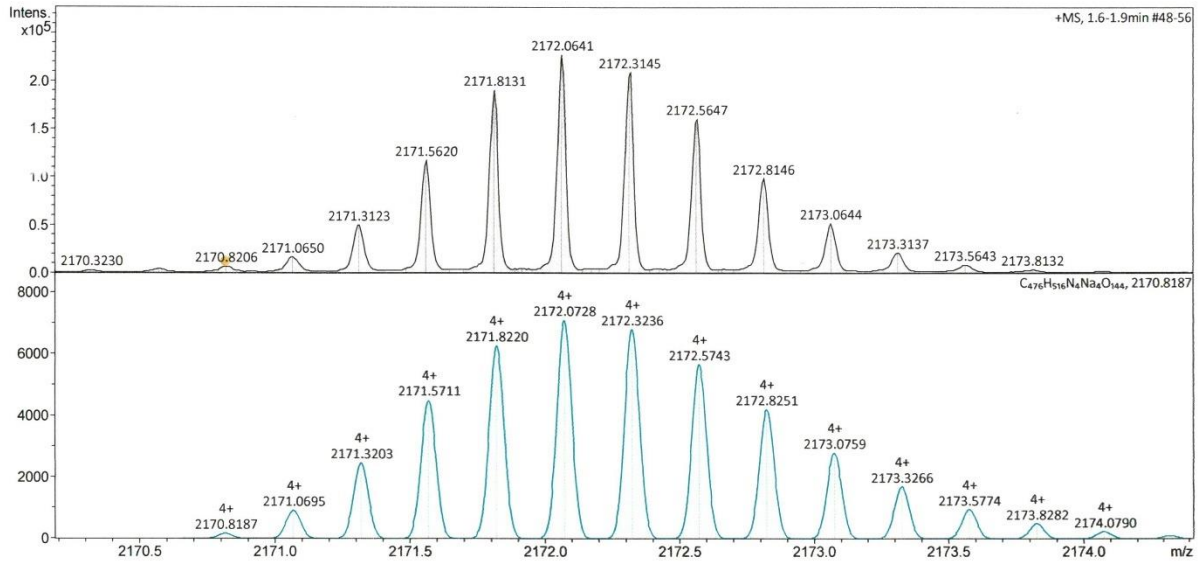

Figure S36. ESI HRMS spectrum of functional hybrid **P2F2$_{TEG}$**.

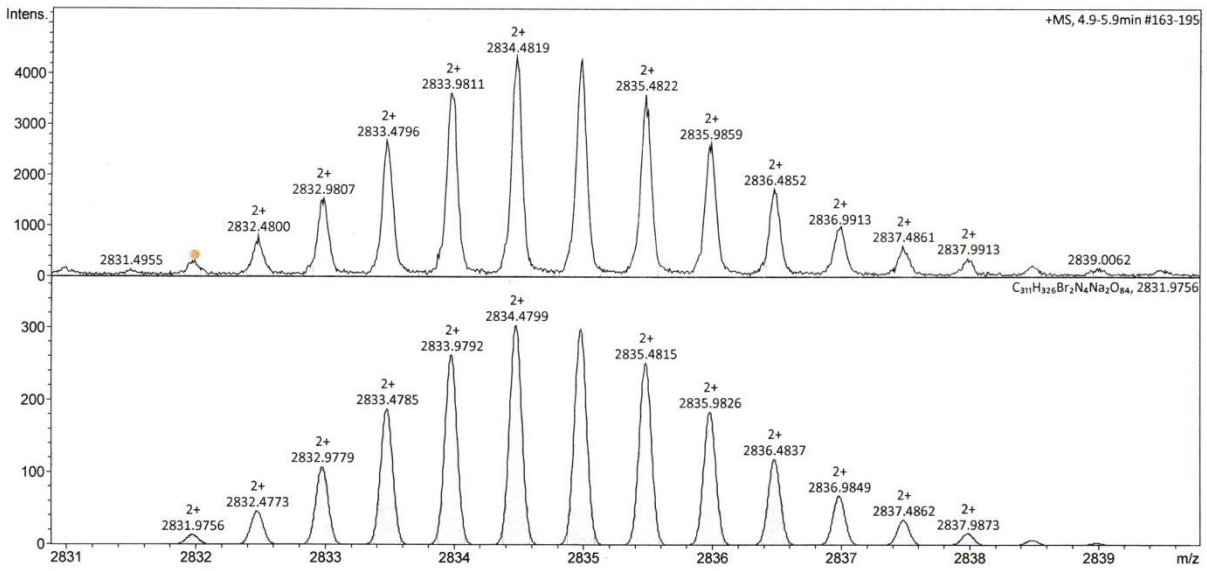

Figure S37. APPI HRMS spectrum of side product **P2F1$_{TEG}$**.

8. UV-Vis absorption spectroscopy

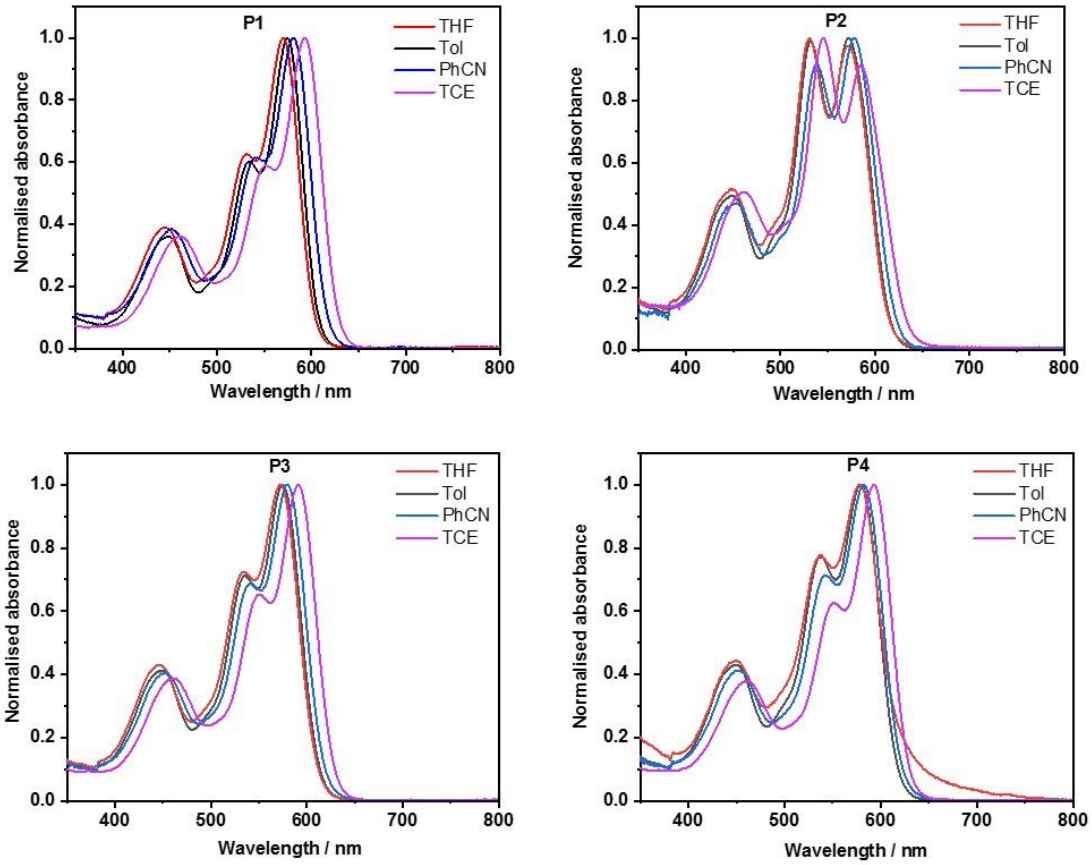

Figure S38. Normalized absorption spectra of **P1**, **P2**, **P3**, and **P4** in tetrahydrofuran, toluene, benzonitrile, and 1,1,2,2-tetrachloroethane measured at room temperature.

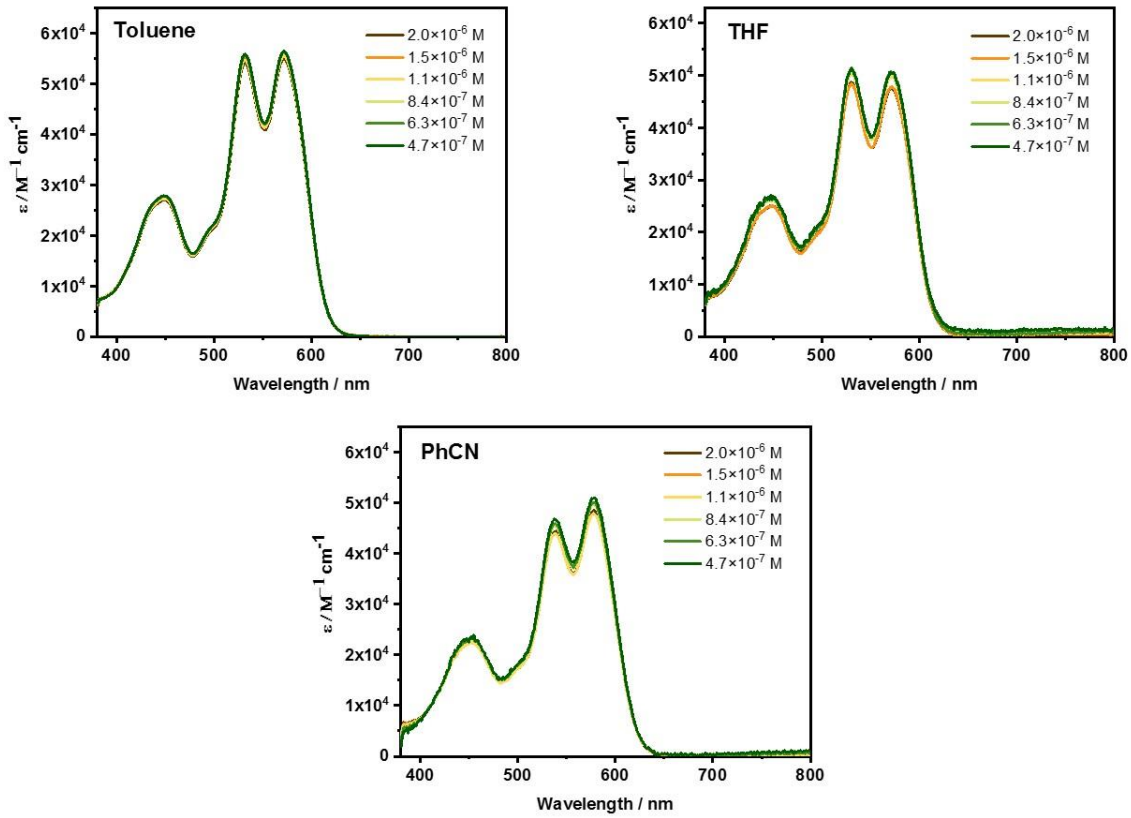

Figure S39. Absorption spectra of cyclophane **P2** at different concentrations in toluene, tetrahydrofuran and benzonitrile measured at room temperature.

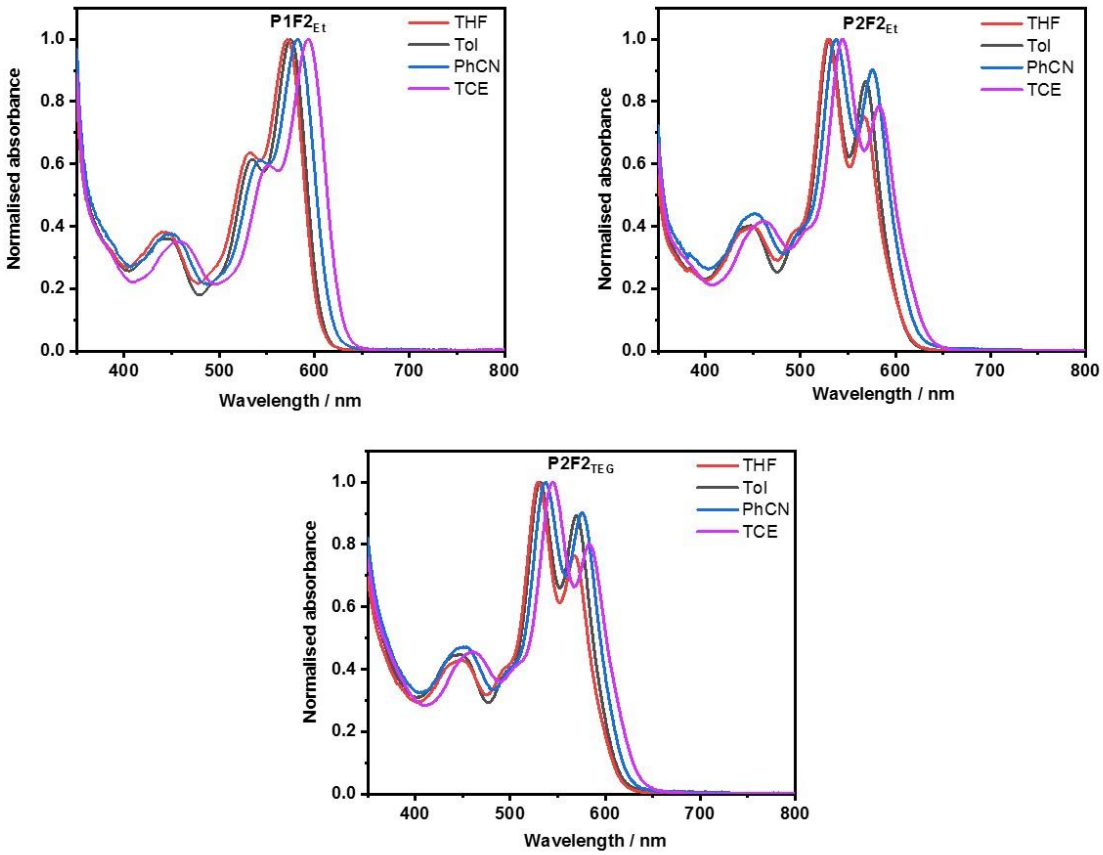

Figure S40. Normalized absorption spectra of **P1F2$_{Et}$**, **P2F2$_{Et}$**, and **P2F2$_{TEG}$** in tetrahydrofuran, toluene, benzonitrile, and 1,1,2,2-tetrachloroethane measured at room temperature.

Table S2. The peak wavelengths (in nm) for 0–*0 and 0–*1 vibrational transitions, molar extinction coefficient at the peak positions (in M^{-1} cm^{-1}) and the 0–*1 : 0–*0 transition intensity ratios for all the samples in different solvents, measured at room temperature.

Sample		Toluene		THF		Benzonitrile		5% THF/water	
		0–*1	0–*0	0–*1	0–*0	0–*1	0–*0	0–*1	0–*0
P1	Peak position (nm)	534	575	531	570	541	580		
	ε (M^{-1} cm^{-1})	2.6×10^4	4.4×10^4	2.4×10^4	3.8×10^4	2.4×10^4	3.8×10^4		
	0 – *1 : 0 – *0	0.60 : 1		0.63 : 1		0.62 : 1			
P2	Peak position (nm)	532	572	530.5	571.5	539	578		
	ε (M^{-1} cm^{-1})	5.6×10^4	5.6×10^4	4.8×10^4	4.7×10^4	4.4×10^4	4.8×10^4		
	0 – *1 : 0 – *0	0.99 : 1		1.03 : 1		0.92 : 1			
P3	Peak position (nm)	535.5	574.5	534	572	541.5	579.5		
	ε (M^{-1} cm^{-1})	3.4×10^4	4.8×10^4	1.1×10^5	1.5×10^5	8.2×10^4	1.2×10^5		
	0 – *1 : 0 – *0	0.71 : 1		0.72 : 1		0.69 : 1			
P4	Peak position (nm)	538	579.5	538	577.5	543	582		
	ε (M^{-1} cm^{-1})	2.6×10^4	3.3×10^4	3.4×10^4	4.4×10^4	4.7×10^4	6.6×10^4		
	0 – *1 : 0 – *0	0.77 : 1		0.79 : 1		0.71 : 1			
$P1F2_{Et}$	Peak position (nm)	534	575	531.5	571.5	543	582.5		
	ε (M^{-1} cm^{-1})	2.1×10^4	3.5×10^4	2.5×10^4	4.0×10^4	2.2×10^4	3.5×10^4		
	0 – *1 : 0 – *0	0.61 : 1		0.54 : 1		0.62 : 1			
$P2F2_{Et}$	Peak position (nm)	530.5	568.5	529	567	537.5	576		
	ε (M^{-1} cm^{-1})	6.8×10^4	5.9×10^4	8.0×10^4	6.0×10^4	6.3×10^4	5.7×10^4		
	0 – *1 : 0 – *0	1.16 : 1		1.33 : 1		1.11 : 1			
$P2F2_{TEG}$	Peak position (nm)	531	569	530	568	538	576	537	577
	ε (M^{-1} cm^{-1})	4.6×10^4	4.2×10^4	5.5×10^4	4.2×10^4	4.2×10^4	3.8×10^4	4.6×10^4	3.6×10^4
	0 – *1 : 0 – *0	1.12 : 1		1.30 : 1		1.10 : 1		1.30 : 1	

9. Fluorescence spectroscopy

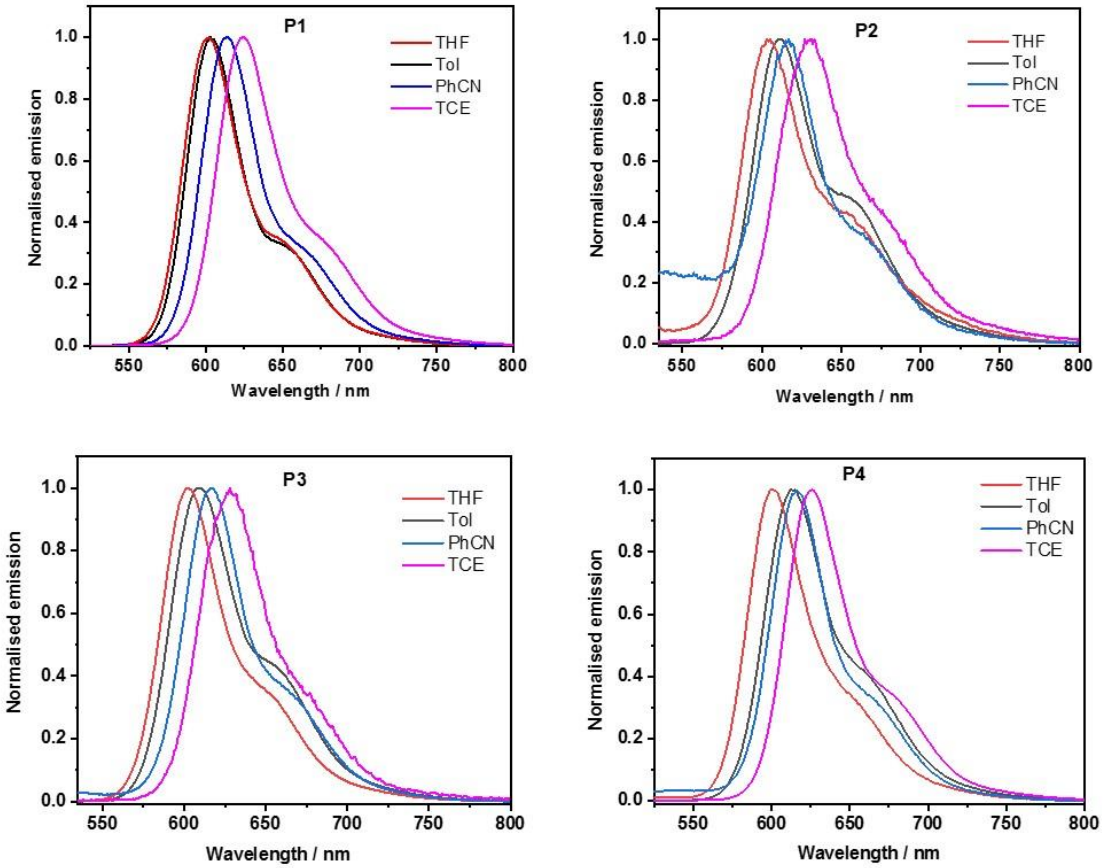

Figure S41. Normalized fluorescence spectra of **P1**, **P2**, **P3**, and **P4** in tetrahydrofuran, toluene, benzonitrile, and 1,1,2,2-tetrachloroethane obtained upon photo-excitation at 510 nm at room temperature.

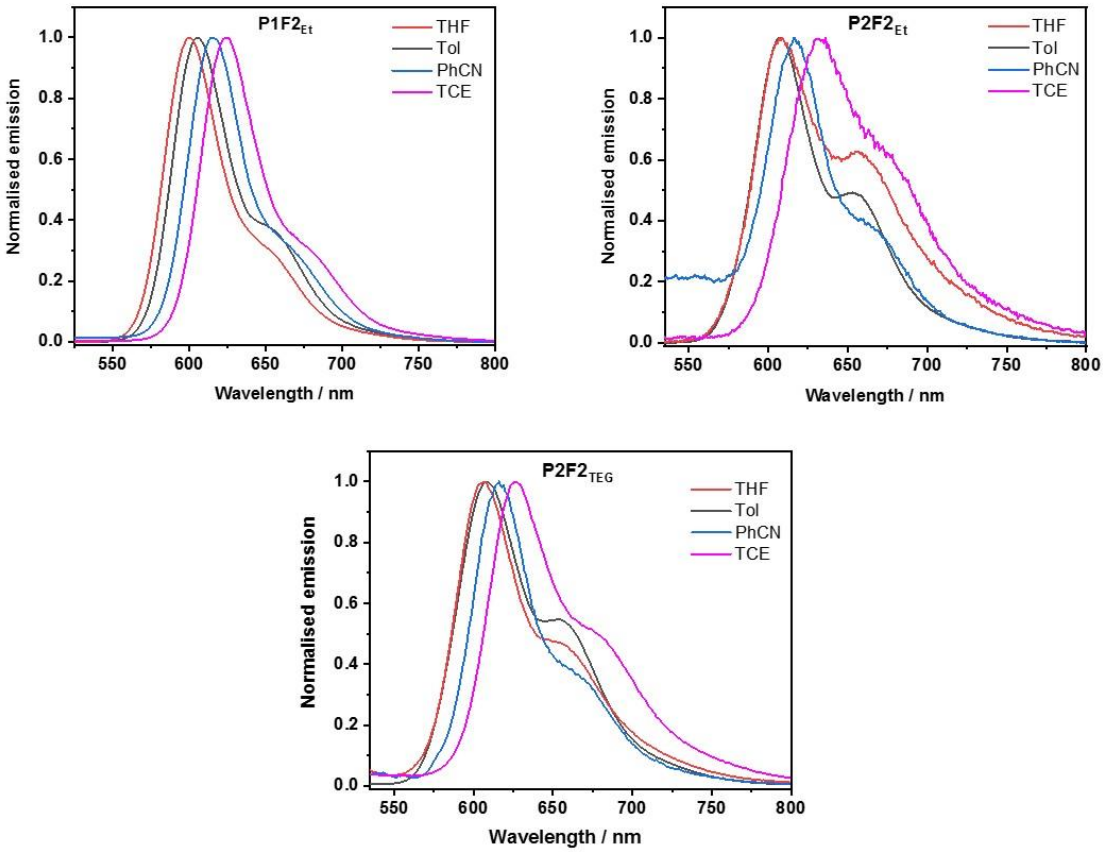

Figure S42. Normalized fluorescence spectra of **P1F2$_{Et}$**, **P2F2$_{Et}$**, and **P2F2$_{TEG}$** in tetrahydrofuran, toluene, benzonitrile, and 1,1,2,2-tetrachloroethane obtained upon photo-excitation at 510 nm at room temperature.

Table S3. Fluorescence quantum yields measured in different solvents at room temperature (Rhodamine B in ethanol used as reference).

Emission quantum yield	Toluene	THF	Benzonitrile	5% THF/water
P1	0.904	0.792	0.722	-
P2	0.176	0.015	0.016	-
P3	0.254	0.085	0.118	-
P4	0.183	0.058	0.104	-
P1F2$_{Et}$	0.391	0.536	0.531	-
P2F2$_{Et}$	0.152	0.007	0.012	-
P2F2$_{TEG}$	0.234	0.025	0.027	0.007

10. Temperature-dependent absorption and fluorescence spectra

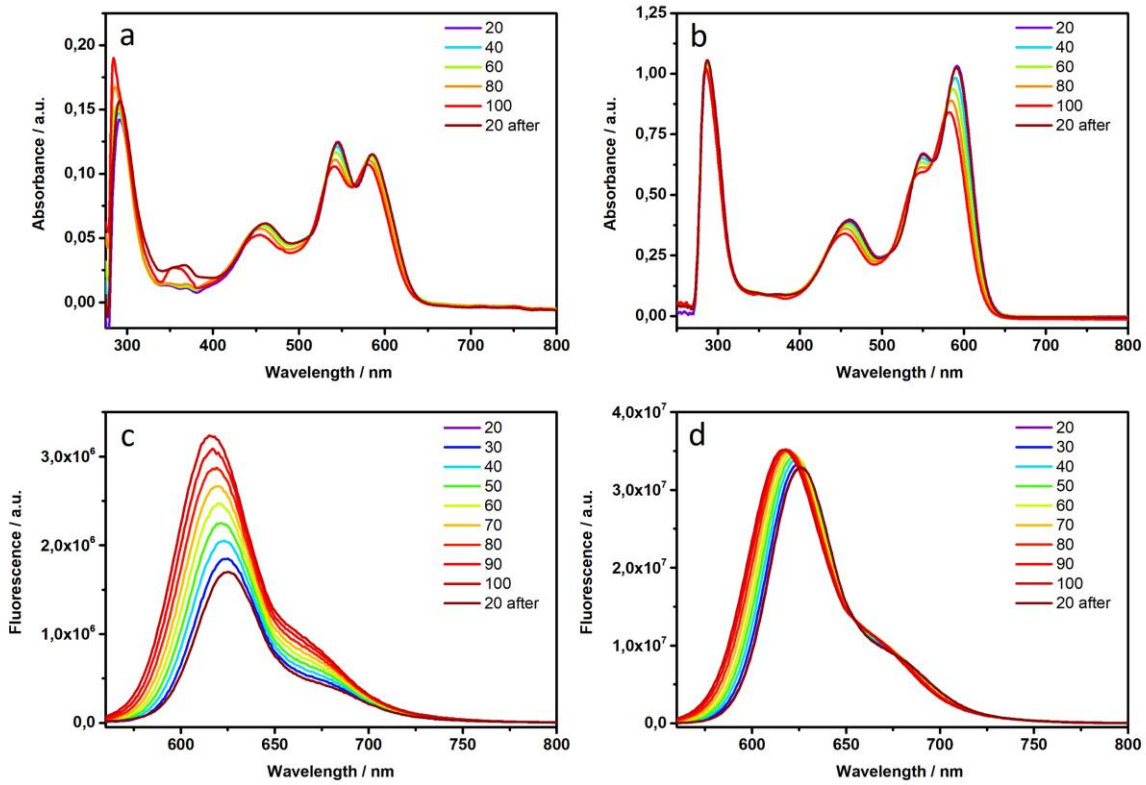

Figure S43. Temperature-dependent absorptions of **P2** (a) and **P3** (b) as well as fluorescence of **P2** (c) and **P3** (d) in 1,1,2,2-tetrachloroethane.

11. Spectroelectrochemistry

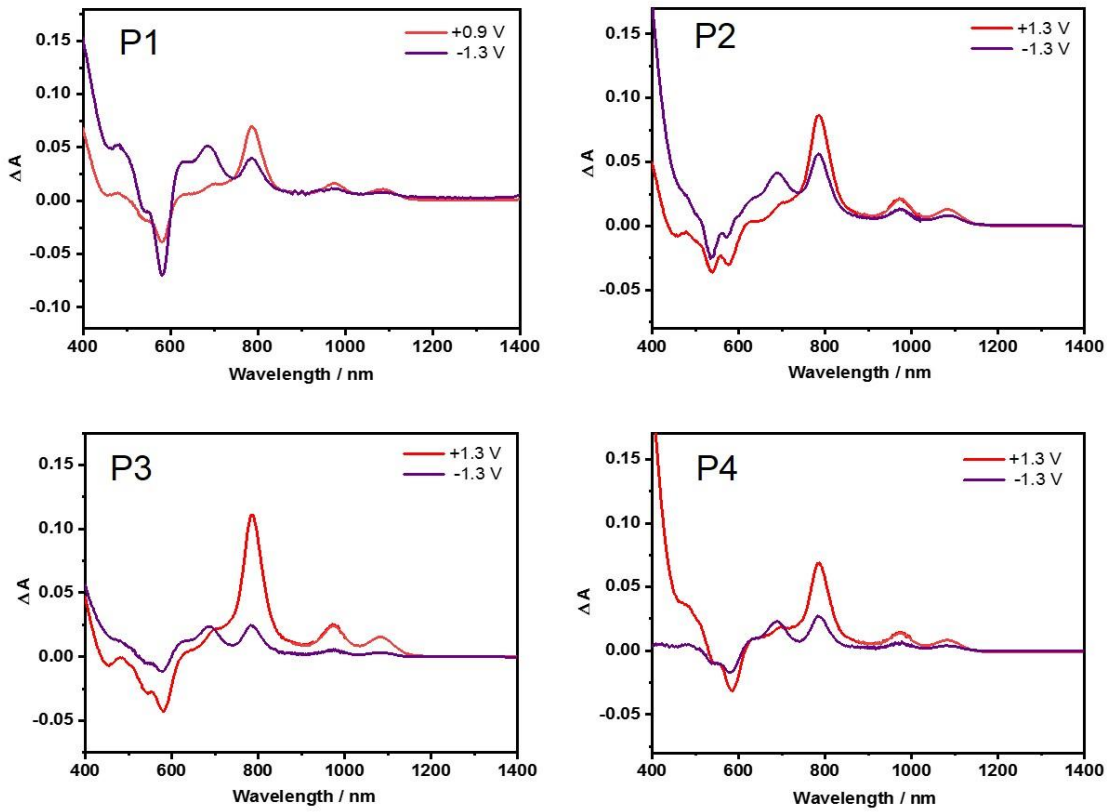

Figure S44. Differential absorption spectra of **P1**, **P2**, **P3**, and **P4** in argon-saturated benzonitrile containing 0.1 M $TBAPF_6$ supporting electrolyte, obtained upon electrochemical oxidation and reduction using Ag wire as reference electrode.

12. Transient absorption measurements

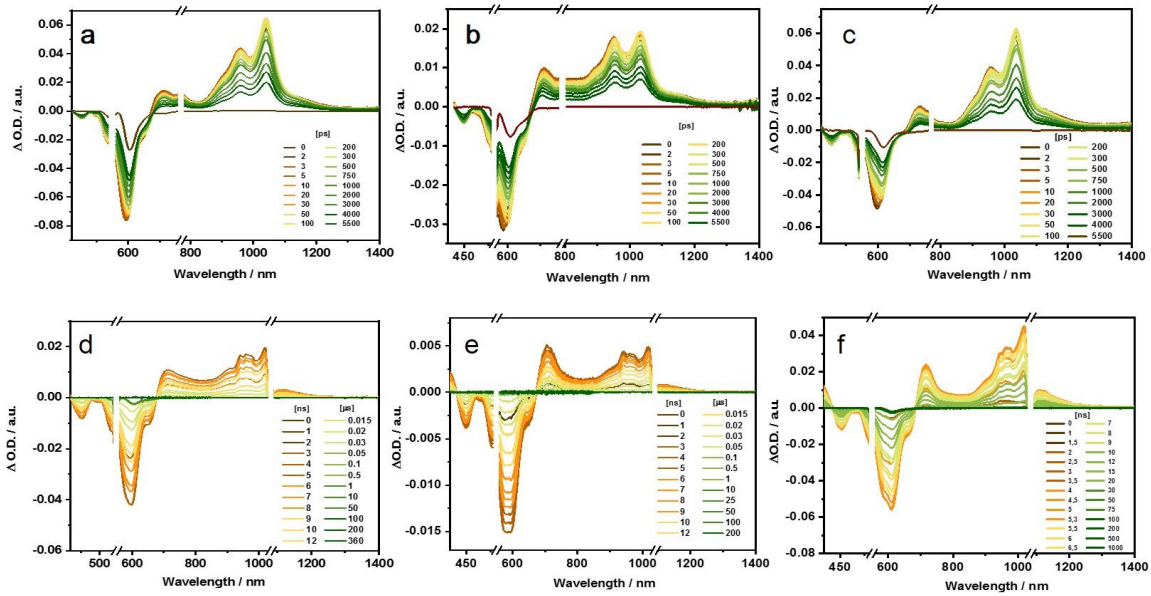

Figure S45. Femtosecond differential absorption spectra of **P1** in argon-purged toluene (a), THF (b), and PhCN (c), at time delays between 0 and 5500 ps after 550 nm photo-excitation at rt. Nanosecond differential absorption spectra of **P1** in argon-purged toluene (d), THF (e), and PhCN (f), at time delays between 1 ns and >100 μs after 550 nm photo-excitation at rt.

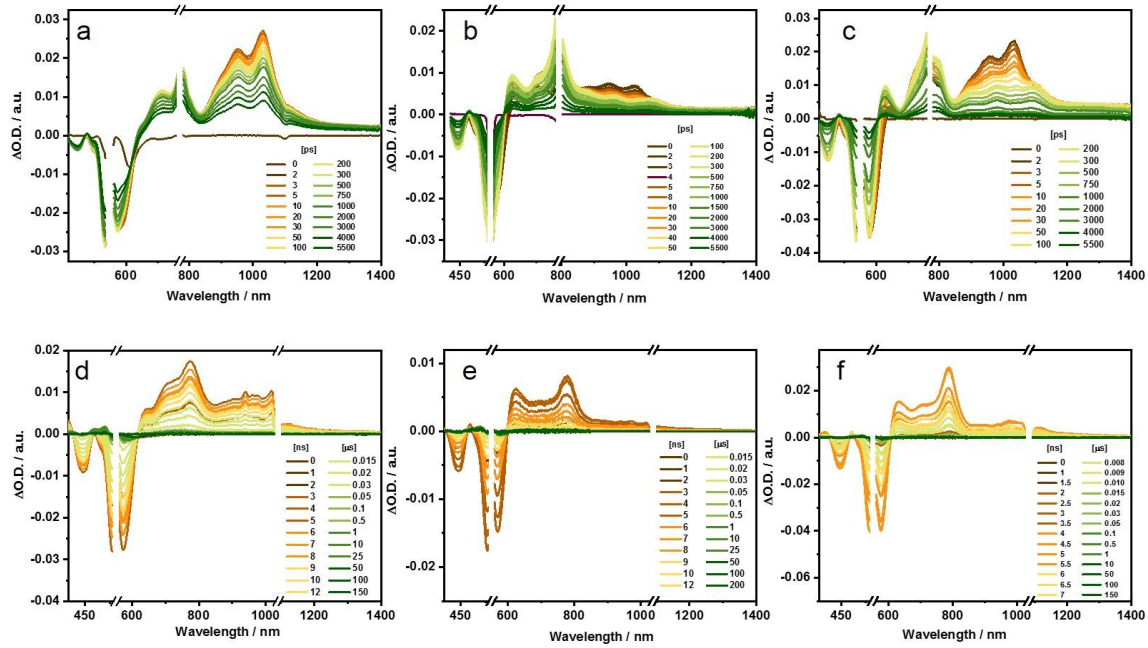

Figure S46. Femtosecond differential absorption spectra of **P2** in argon-purged toluene (a), THF (b), and PhCN (c), at time delays between 0 and 5500 ps after 550 nm photo-excitation at rt. Nanosecond differential absorption spectra of **P2** in argon-purged toluene (d), THF (e), and PhCN (f), at time delays between 1 ns and >100 µs after 550 nm photo-excitation at rt.

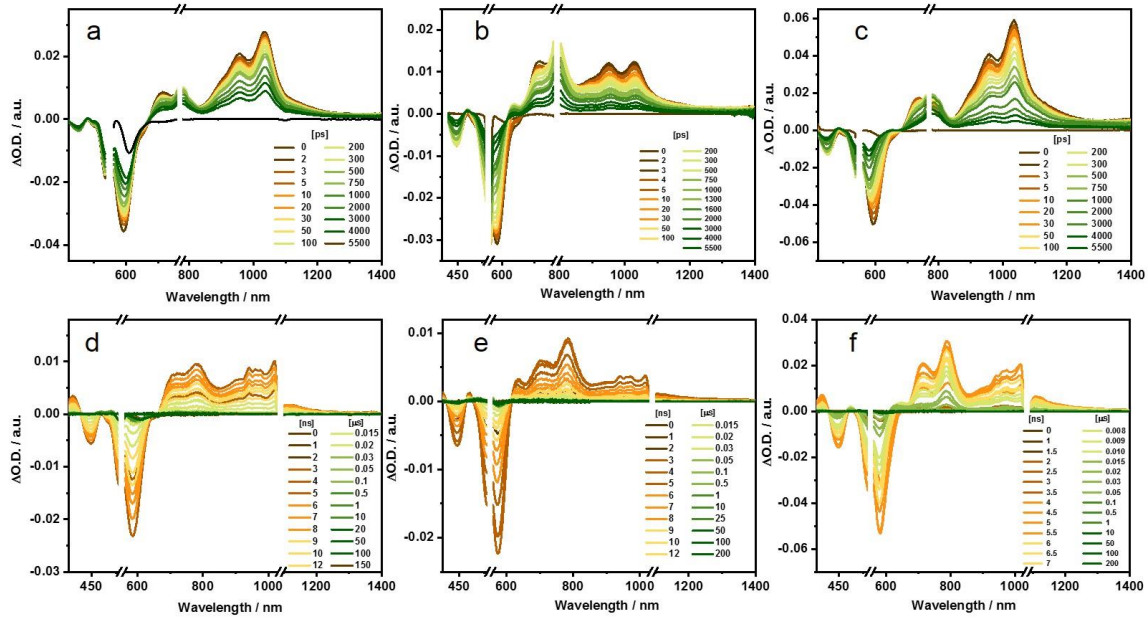

Figure S47. Femtosecond differential absorption spectra of **P3** in argon-purged toluene (a), THF (b), and PhCN (c), at time delays between 0 and 5500 ps after 550 nm photo-excitation at rt. Nanosecond differential absorption spectra of **P3** in argon-purged toluene (d), THF (e), and PhCN (f), at time delays between 1 ns and >100 μs after 550 nm photo-excitation at rt.

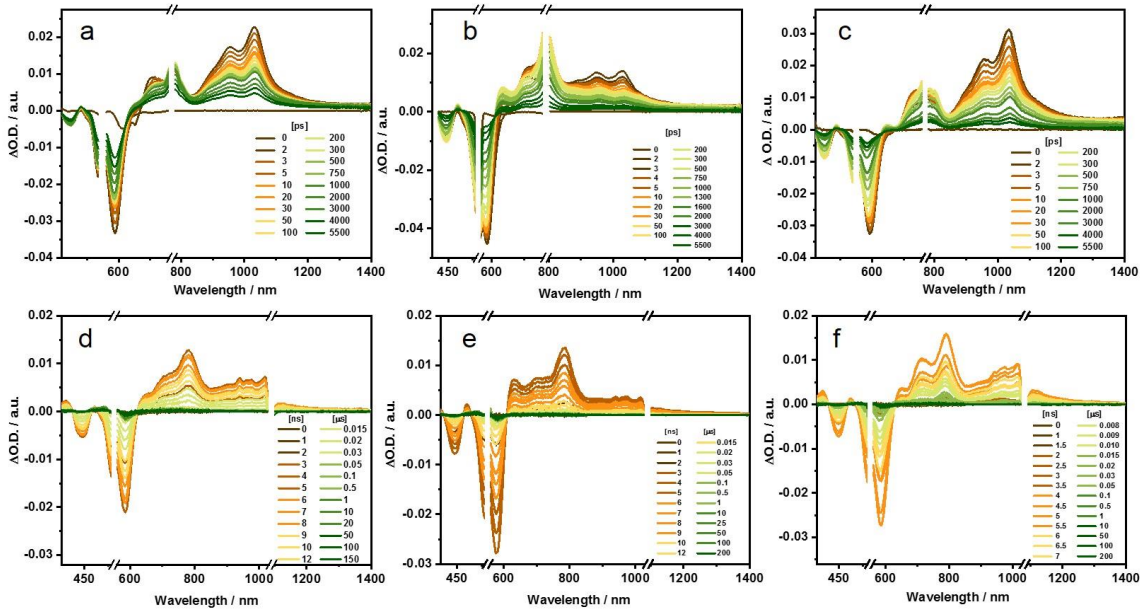

Figure S48. Femtosecond differential absorption spectra of **P4** in argon-purged toluene (a), THF (b), and PhCN (c), at time delays between 0 and 5500 ps after 550 nm photo-excitation at rt. Nanosecond differential absorption spectra of **P4** in argon-purged toluene (d), THF (e), and PhCN (f), at time delays between 1 ns and >100 µs after 550 nm photo-excitation at rt.

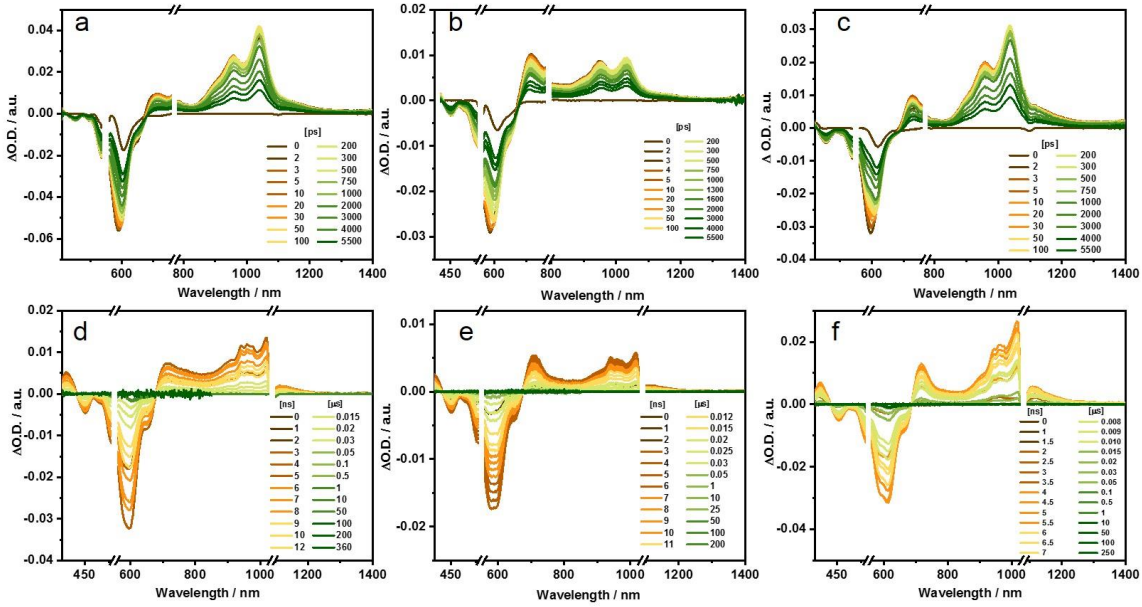

Figure S49. Femtosecond differential absorption spectra of **P1F2$_{Et}$** in argon-purged toluene (a), THF (b), and PhCN (c), at time delays between 0 and 5500 ps after 550 nm photo-excitation at rt. Nanosecond differential absorption spectra of **P1F2$_{Et}$** in argon-purged toluene (d), THF (e), and PhCN (f), at time delays between 1 ns and >100 µs after 550 nm photo-excitation at rt.

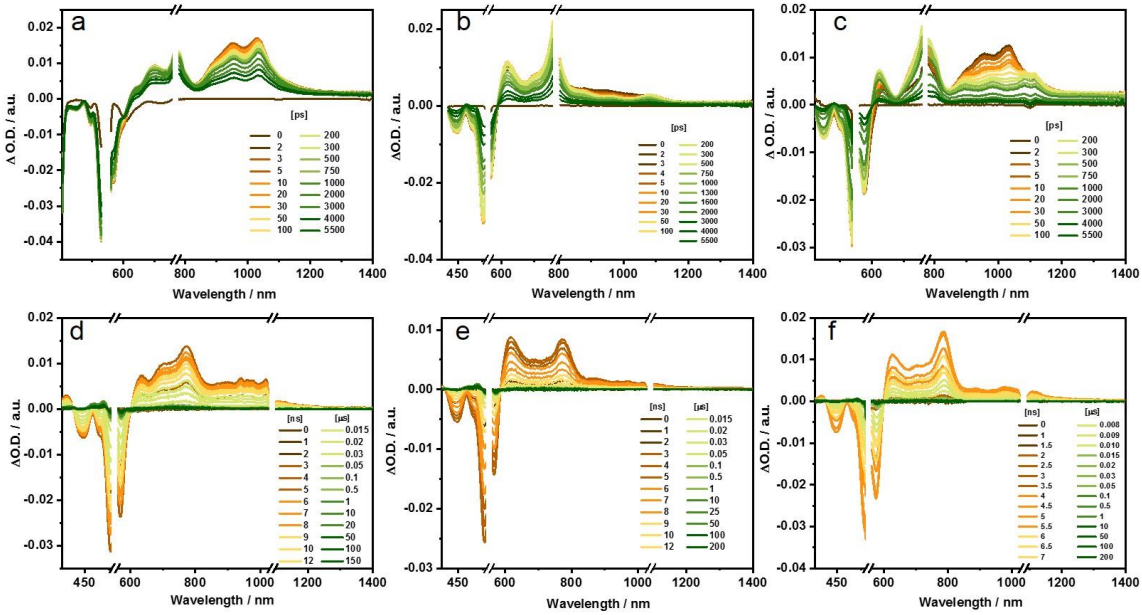

Figure S50. Femtosecond differential absorption spectra of **P2F2$_{Et}$** in argon-purged toluene (a), THF (b), and PhCN (c), at time delays between 0 and 5500 ps after 550 nm photo-excitation at rt. Nanosecond differential absorption spectra of **P2F2$_{Et}$** in argon-purged toluene (d), THF (e), and PhCN (f), at time delays between 1 ns and >100 µs after 550 nm photo-excitation at rt.

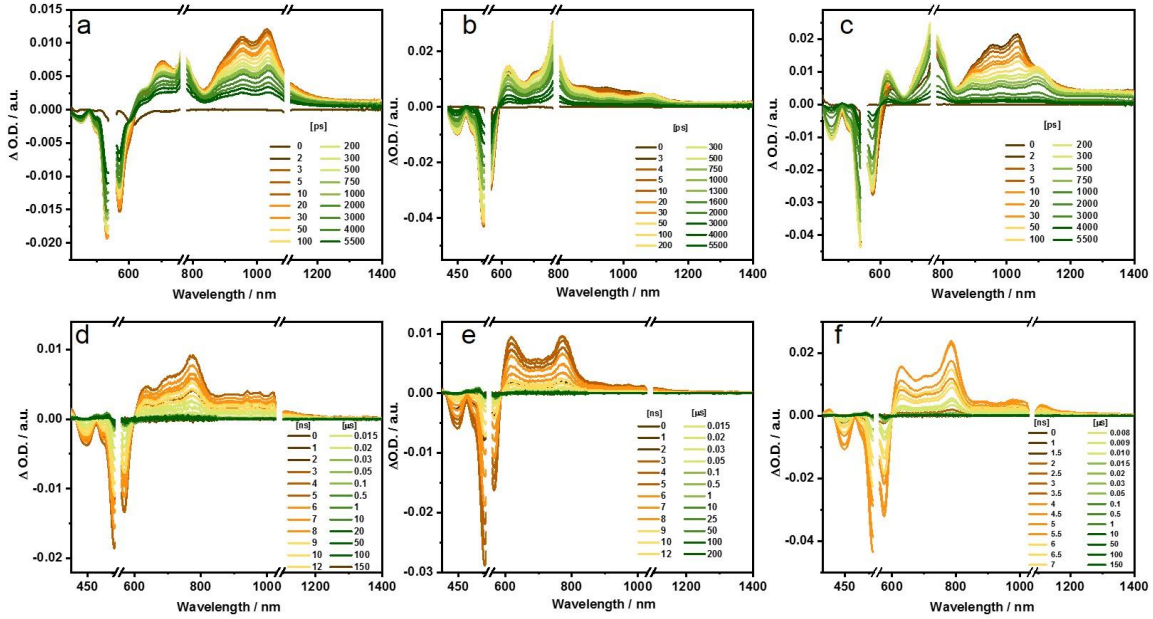

Figure S51. Femtosecond differential absorption spectra of **P2F2$_{TEG}$** in argon-purged toluene (a), THF (b), and PhCN (c), at time delays between 0 and 5500 ps after 550 nm photo-excitation at rt. Nanosecond differential absorption spectra of **P2F2$_{TEG}$** in argon-purged toluene (d), THF (e), and PhCN (f), at time delays between 1 ns and >100 µs after 550 nm photo-excitation at rt.

13. Global analysis of transient absorption spectra

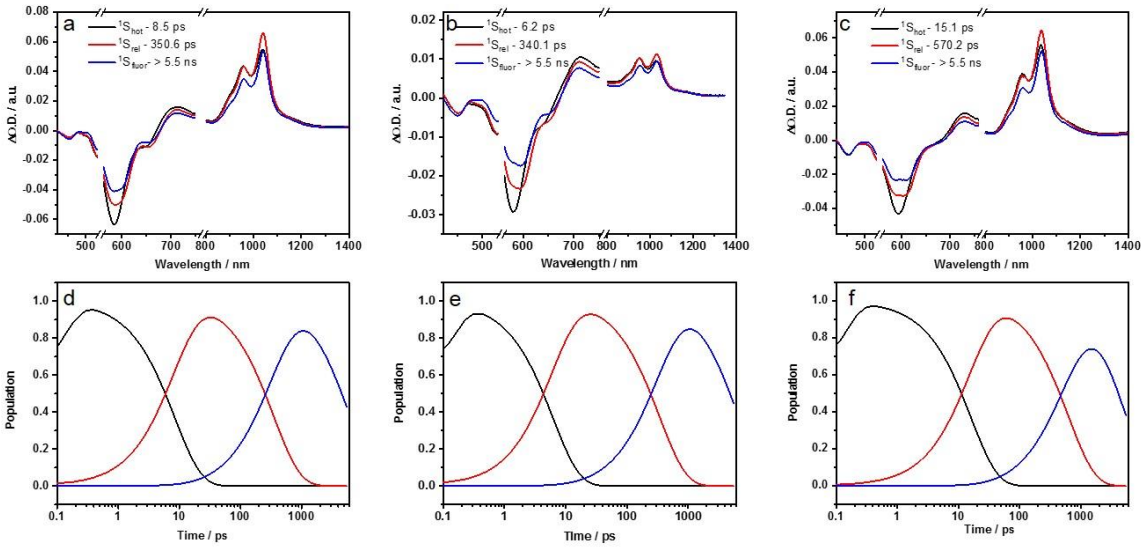

Figure S52. Evolution associated spectra reconstructed from the sequential global analysis of fs-TA spectra of **P1** in toluene (a), THF (b), PhCN (c) and the corresponding population kinetics in toluene (d), THF (e), and PhCN (f).

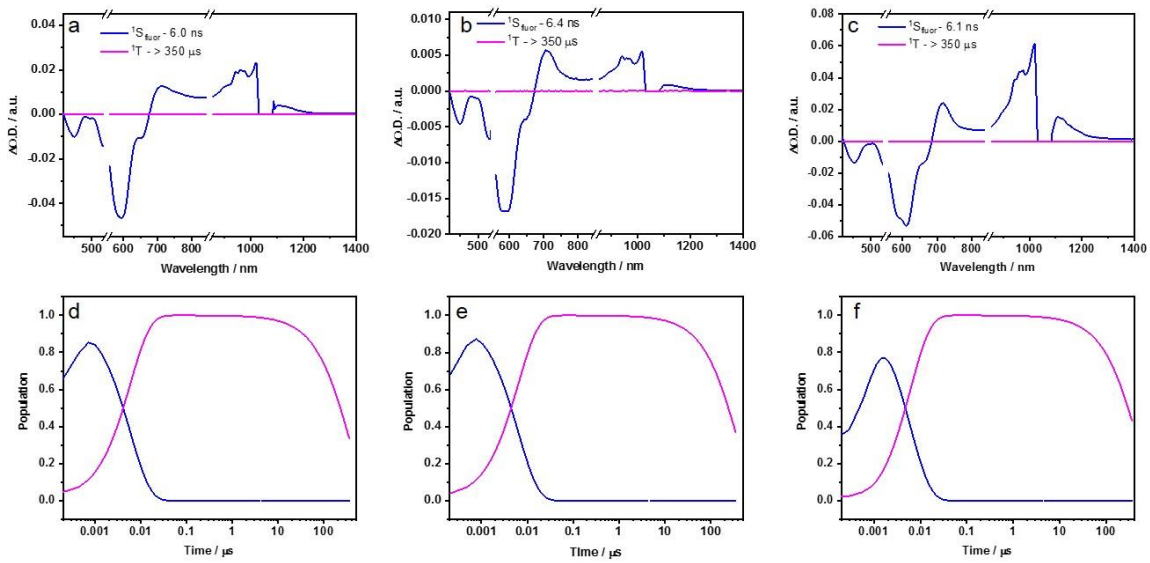

Figure S53. Evolution associated spectra reconstructed from the sequential global analysis of ns-TA spectra of **P1** in toluene (a), THF (b), PhCN (c) and the corresponding population kinetics in toluene (d), THF (e), and PhCN (f).

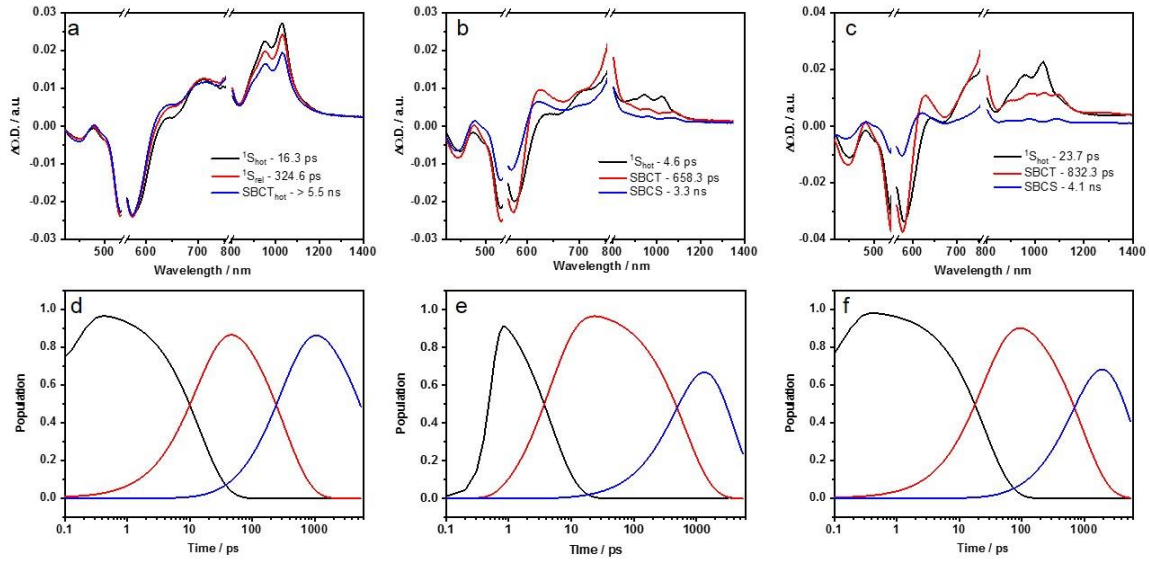

Figure S54. Evolution associated spectra reconstructed from the sequential global analysis of fs-TA spectra of **P2** in toluene (a), THF (b), PhCN (c) and the corresponding population kinetics in toluene (d), THF (e), and PhCN (f).

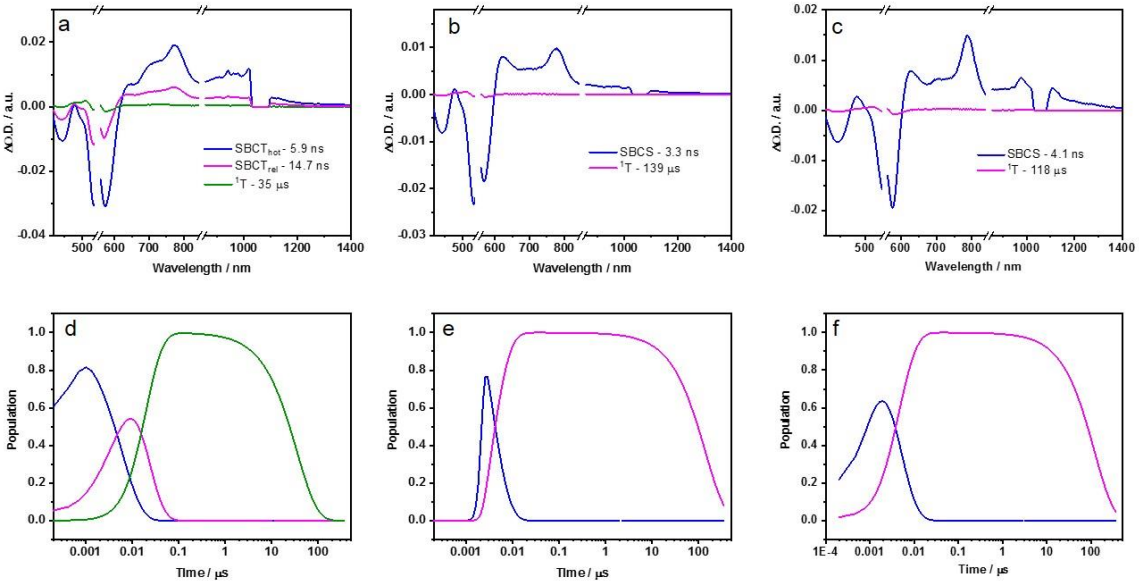

Figure S55. Evolution associated spectra reconstructed from the sequential global analysis of ns-TA spectra of **P2** in toluene (a), THF (b), PhCN (c) and the corresponding population kinetics in toluene (d), THF (e), and PhCN (f).

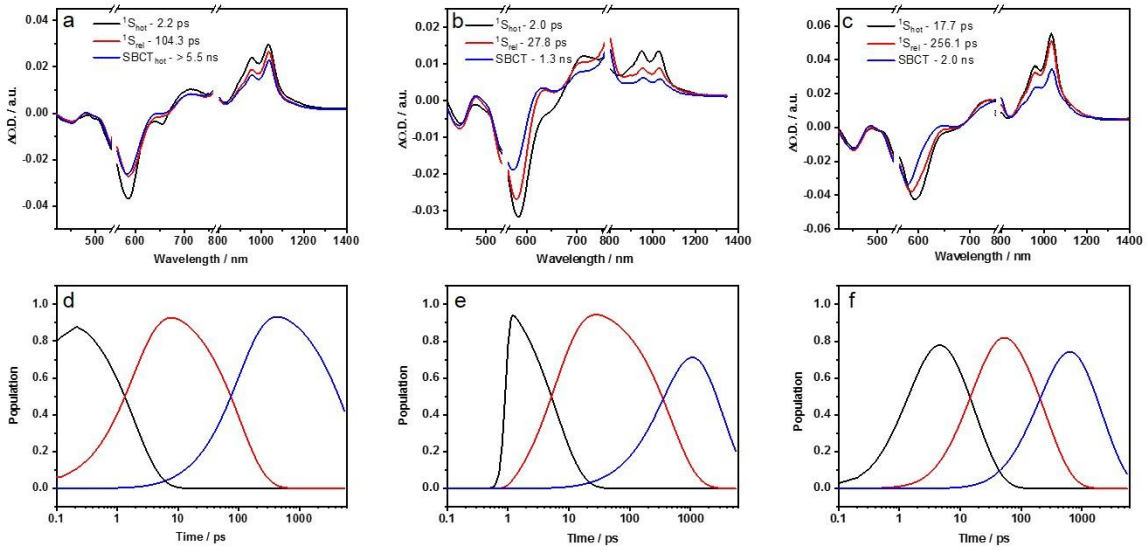

Figure S56. Evolution associated spectra reconstructed from the sequential global analysis of fs-TA spectra of **P3** in toluene (a), THF (b), PhCN (c) and the corresponding population kinetics in toluene (d), THF (e), and PhCN (f).

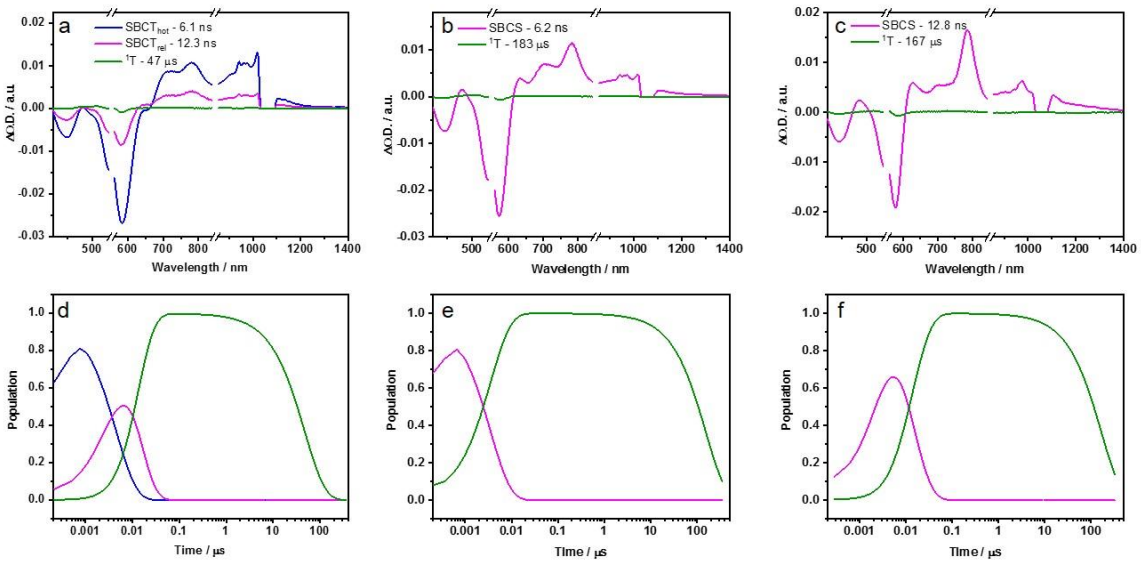

Figure S57. Evolution associated spectra reconstructed from the sequential global analysis of ns-TA spectra of **P3** in toluene (a), THF (b), PhCN (c) and the corresponding population kinetics in toluene (d), THF (e), and PhCN (f).

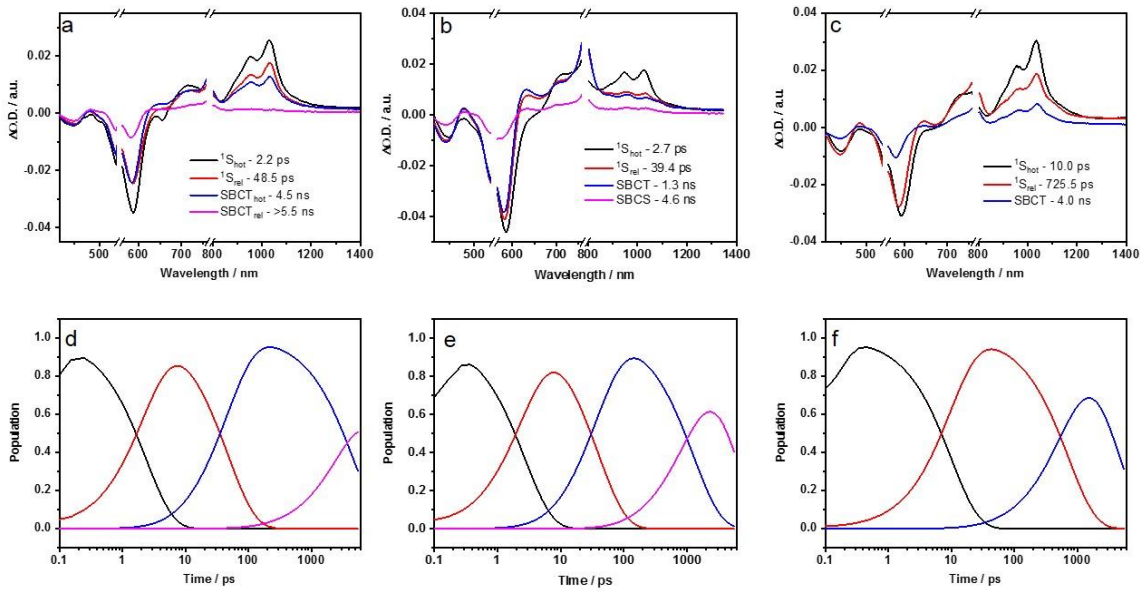

Figure S58. Evolution associated spectra reconstructed from the sequential global analysis of fs-TA spectra of **P4** in toluene (a), THF (b), PhCN (c) and the corresponding population kinetics in toluene (d), THF (e), and PhCN (f).

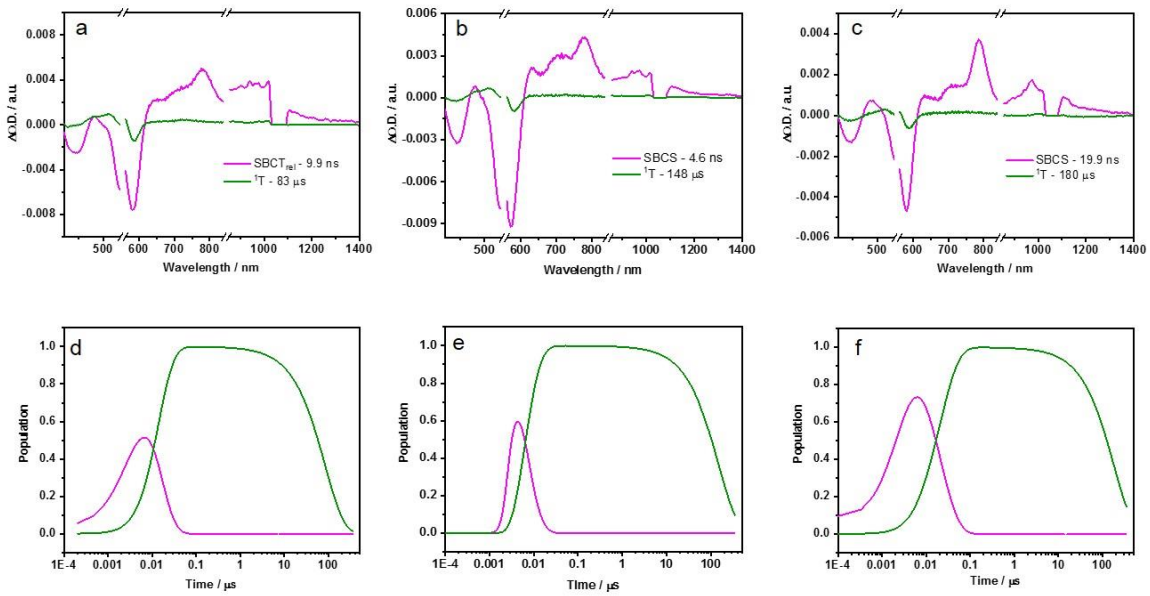

Figure S59. Evolution associated spectra reconstructed from the sequential global analysis of ns-TA spectra of **P4** in toluene (a), THF (b), PhCN (c) and the corresponding population kinetics in toluene (d), THF (e), and PhCN (f).

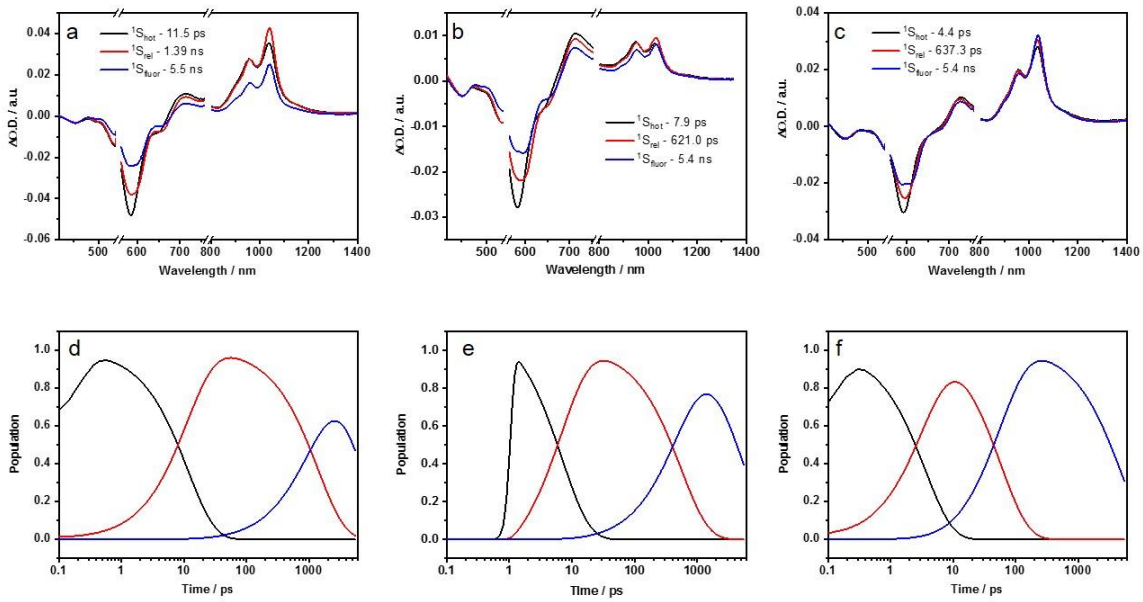

Figure S60. Evolution associated spectra reconstructed from the sequential global analysis of fs-TA spectra of **P1F2$_{Et}$** in toluene (a), THF (b), PhCN (c) and the corresponding population kinetics in toluene (d), THF (e), and PhCN (f).

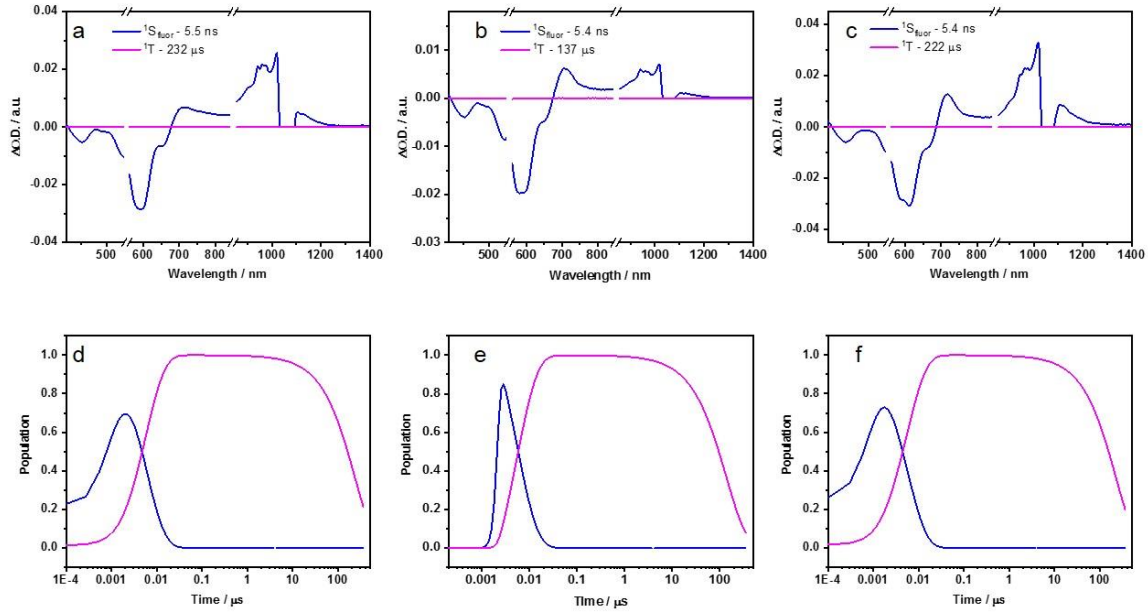

Figure S61. Evolution associated spectra reconstructed from the sequential global analysis of ns-TA spectra of **P1F2$_{Et}$** in toluene (a), THF (b), PhCN (c) and the corresponding population kinetics in toluene (d), THF (e), and PhCN (f).

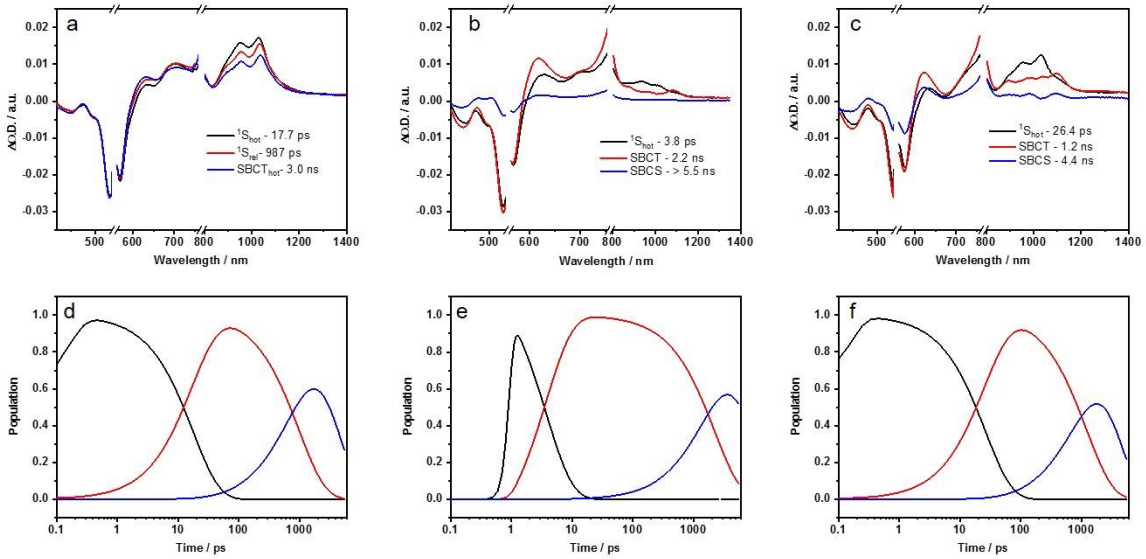

Figure S62. Evolution associated spectra reconstructed from the sequential global analysis of fs-TA spectra of **P2F2$_{Et}$** in toluene (a), THF (b), PhCN (c) and the corresponding population kinetics in toluene (d), THF (e), and PhCN (f).

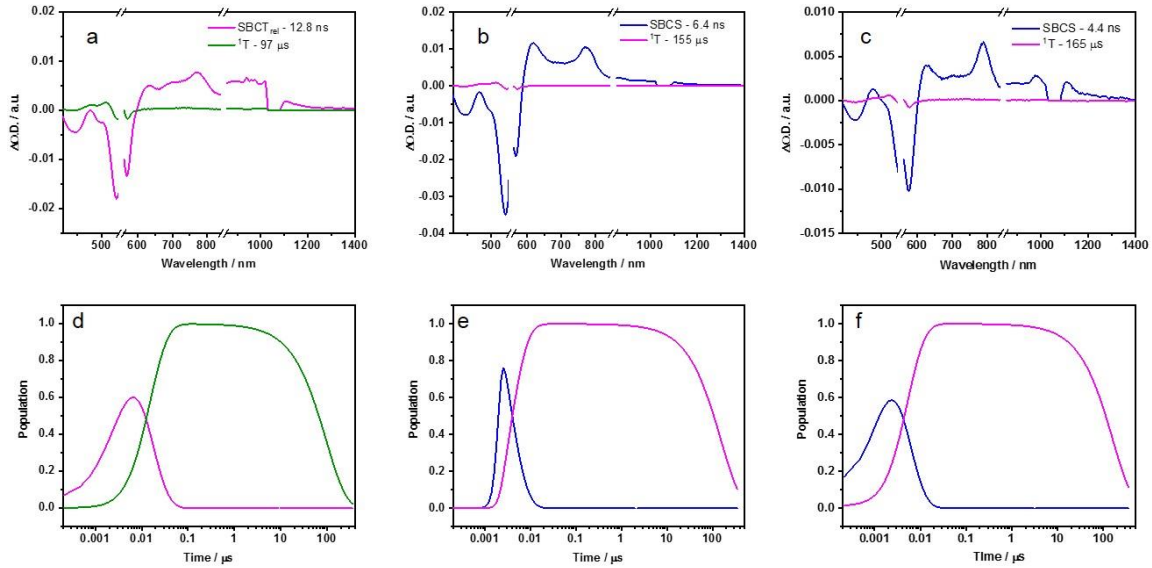

Figure S63. Evolution associated spectra reconstructed from the sequential global analysis of ns-TA spectra of **P2F2$_{Et}$** in toluene (a), THF (b), PhCN (c) and the corresponding population kinetics in toluene (d), THF (e) and PhCN (f).

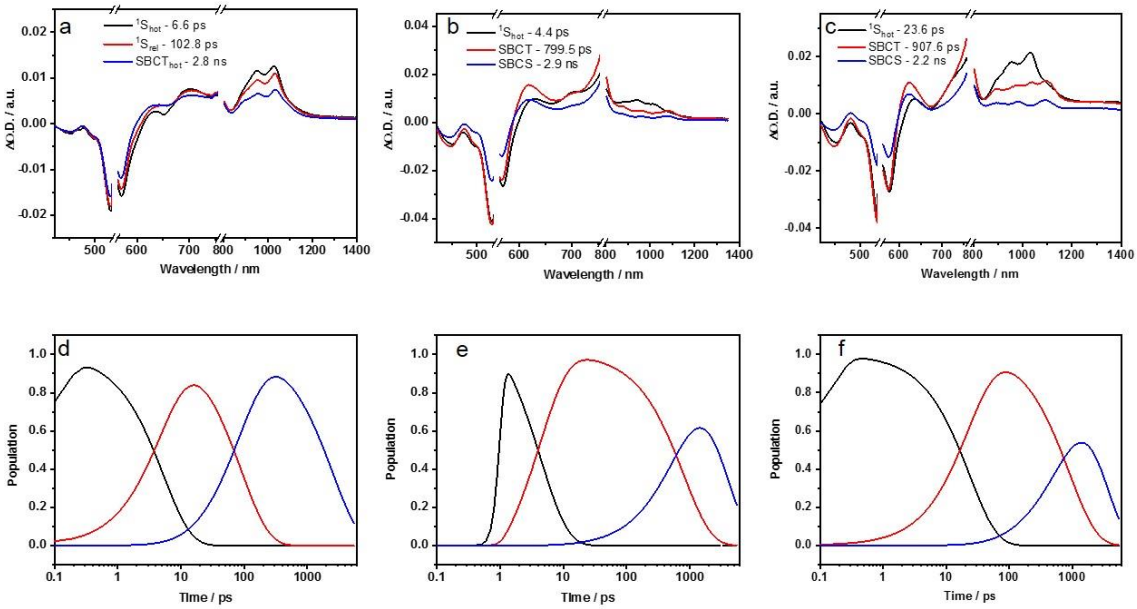

Figure S64. Evolution associated spectra reconstructed from the sequential global analysis of fs-TA spectra of **P2F2$_{TEG}$** in toluene (a), THF (b), PhCN (c) and the corresponding population kinetics in toluene (d), THF (e), and PhCN (f).

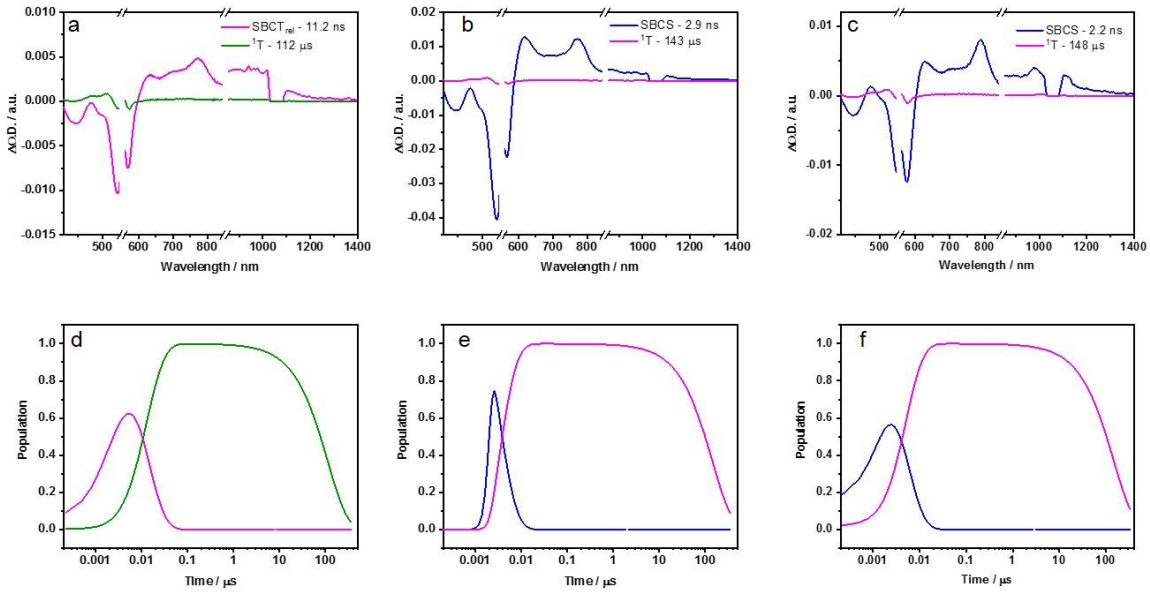

Figure S65. Evolution associated spectra reconstructed from the sequential global analysis of ns-TA spectra of **P2F2$_{TEG}$** in toluene (a), THF (b), PhCN (c) and the corresponding population kinetics in toluene (d), THF (e), and PhCN (f).

Table S4. Lifetimes of different species involved in the excited state decay dynamics of **P1** and **P1F2$_{Et}$**, determined from the global sequential analysis of fs-TA and ns-TA measurements.

		$^1S_{hot}$ (ps)	$^1S_{rel}$ (ps)	$^1S_{fluor}$ (ns)	^1T (µs)
P1	Tol	8.5	350.6	6.0	> 350
	THF	6.2	340.1	6.4	> 350
	PhCN	15.1	570.2	6.1	> 350
P1F2$_{Et}$	Tol	11.5	1397.9	5.5	232
	THF	7.9	621.0	5.4	137
	PhCN	4.4	637.3	5.4	222

Table S5. Lifetimes of different species involved in the excited state decay dynamics determined from the global sequential analysis of fs-TA and ns-TA measurements for **P2**, **P3**, **P4** as well as **P2F2$_{Et}$** and **P2F2$_{TEG}$**.

		$^1S_{hot}$ (ps)	$^1S_{rel}$ (ps)	$SBCT_{hot}$ (ns)	$SBCT_{rel}$ (ns)	SBCS (ns)	^1T (µs)
P2	Tol	16.3	324.6	5.9	14.7	-	35
	THF	4.6	-	0.6	-	3.3	139
	PhCN	23.7	-	0.8	-	4.1	118
P3	Tol	2.2	104.3	6.1	12.3	-	47
	THF	2.0	27.8	1.3	-	6.2	183
	PhCN	17.7	256.1	2.0	-	12.8	167
P4	Tol	2.2	48.5	4.5	9.9	-	83
	THF	2.7	39.4	1.3	-	4.6	148
	PhCN	10.0	725.5	4.0	-	19.9	180
P2F2$_{Et}$	Tol	17.7	987.0	3.0	12.8	-	97
	THF	3.8	-	2.2	-	6.4	155
	PhCN	26.4	-	1.2	-	4.4	165
P2F2$_{TEG}$	Tol	6.6	102.8	2.8	11.2	-	112
	THF	4.4	-	0.8	-	2.9	143
	PhCN	23.6	-	0.9	-	2.2	148

14. Singlet oxygen quantum yield measurements

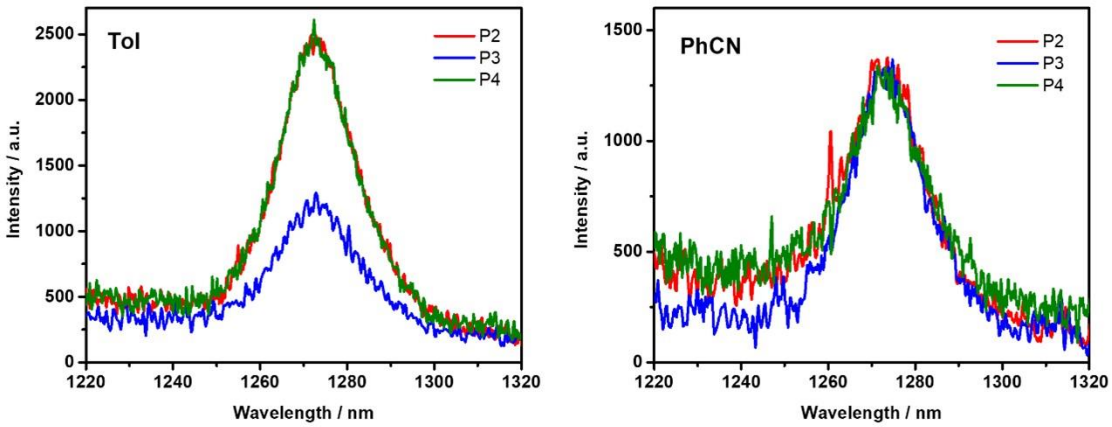

Figure S66. Singlet oxygen phosphorescence of **P2**, **P3** and **P4** measured in oxygen saturated toluene and benzonitrile after 532 nm photo-excitation (OD = 0.08).

Table S6. Singlet oxygen quantum yields of **P2**, **P3,** and **P4** in toluene and benzonitrile, measured using C_{60} in air-equilibrated toluene as reference ($\Phi_{\Delta}^{ref} = 0.98 \pm 0.05$).

Compound	Solvent	Φ_{Δ}
P2	Tol	0.67 ± 0.08
	PhCN	0.53 ± 0.07
P3	Tol	0.37 ± 0.08
	PhCN	0.43 ± 0.07
P4	Tol	0.76 ± 0.07
	PhCN	0.44 ± 0.06

15. 3D Fluorescence heat map

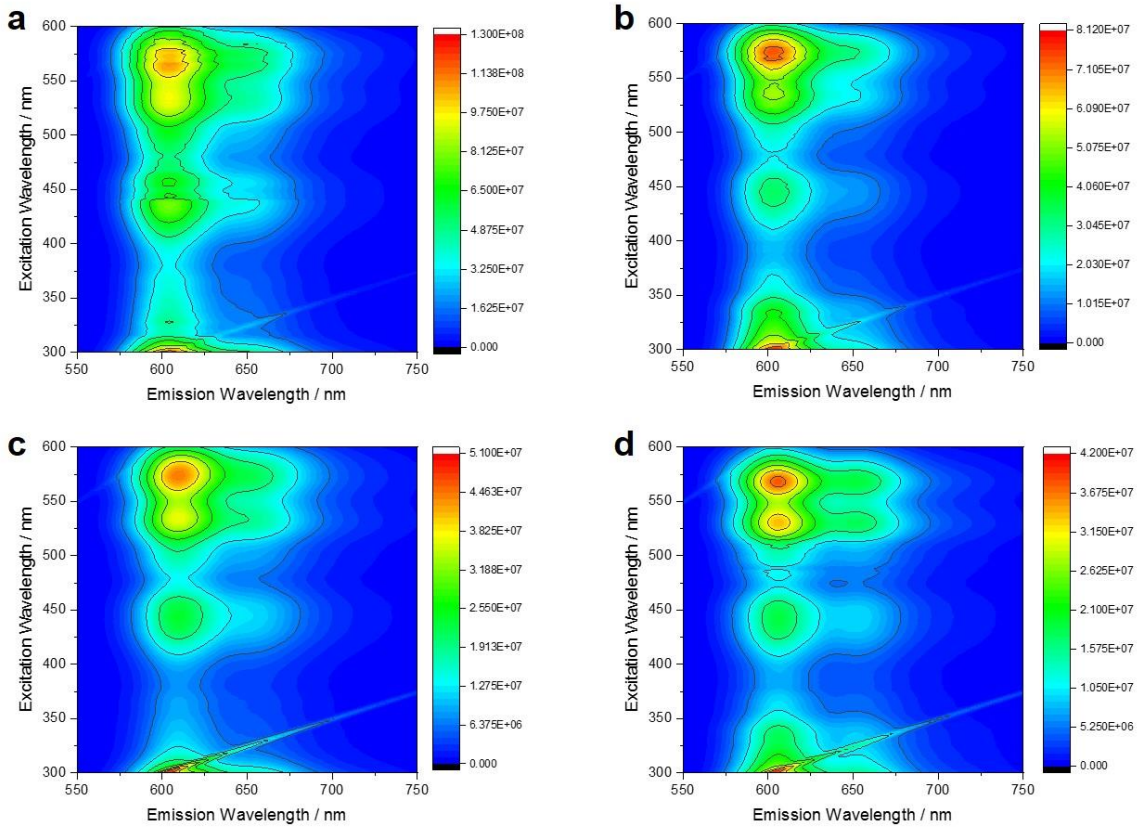

Figure S67. 3D fluorescence heat map of (a) **P1**, (b) **P1F2$_{Et}$**, (c) **P2**, and (d) **P2F2$_{Et}$** in toluene at room temperature.

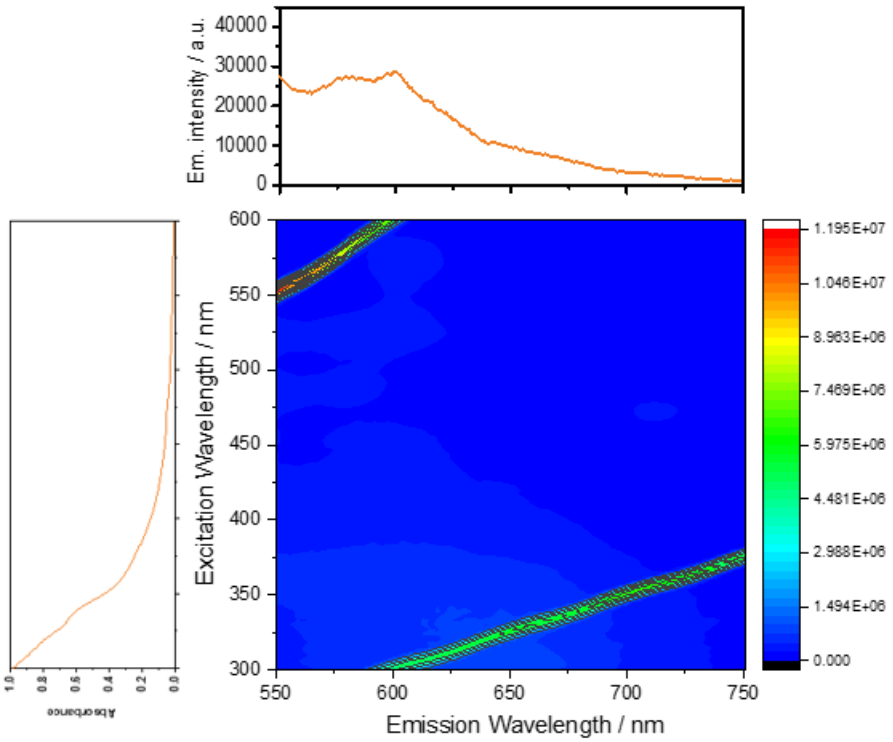

Figure S68. 3D fluorescence heat map along with the absorption and emission spectra of fullerene hexakisadduct in toluene at room temperature.

16. Literature

[1] J. J. Snellenburg, S. P. Laptenok, R. Seger, K. M. Mullen, I. H. van Stokkum, *J. Stat. Softw.* **2012**, *49*, 1-22.

[2] M. Hesse, H. Meier, B. Zeeh, *Spektroskopische Methoden in der organischen Chemie*, Georg Thieme Verlag, **2005**.